

Georgia State University

ScholarWorks @ Georgia State University

Neuroscience Institute Dissertations

Neuroscience Institute

8-12-2016

Adipose Sensory Nerves: Functional and Neuroanatomical Evidence for Their Emerging Role in Energy Balance

John Garretson

Follow this and additional works at: https://scholarworks.gsu.edu/neurosci_diss

Recommended Citation

Garretson, John, "Adipose Sensory Nerves: Functional and Neuroanatomical Evidence for Their Emerging Role in Energy Balance." Dissertation, Georgia State University, 2016.
doi: <https://doi.org/10.57709/8872423>

This Dissertation is brought to you for free and open access by the Neuroscience Institute at ScholarWorks @ Georgia State University. It has been accepted for inclusion in Neuroscience Institute Dissertations by an authorized administrator of ScholarWorks @ Georgia State University. For more information, please contact scholarworks@gsu.edu.

ADIPOSE SENSORY NERVES: FUNCTIONAL AND NEUROANATOMICAL EVIDENCE
FOR THEIR EMERGING ROLE IN ENERGY BALANCE

by

John Thomas Garretson Jr.

Under the Direction of Geert J. de Vries, PhD

ABSTRACT

White adipose tissue (WAT) lipolysis is initiated via direct sympathetic nervous system (SNS) innervation and activation. SNS control to WAT is vital to maintaining homeostasis in response to metabolic challenges such as food deprivation and cold exposure. Using transneuronal viral tract tracers, we have identified sensory nerves from WAT that project to brainstem and forebrain areas critical to metabolic function. In addition, these sensory circuits from fat communicate with SNS outflow neurons that project back to fat—forming neural feedback loops throughout the CNS—providing neuroanatomical evidence for sensory WAT-SNS crosstalk. It is unclear, however, what role these WAT-specific sensory nerves serve to inform the CNS of acute and dynamic metabolic challenges to which it can then respond. Here we tested mechanisms of activation of WAT sensory nerves and present a working model to deepen our understanding of why these neural circuits act as conduits for acute metabolic feedback signals from WAT. Neurochemical, neuroanatomical, and neurophysiological evidence supports the presence of: 1) WAT lipolytic sensors from a neural population known to be capable of controlling SNS outflow; and 2) functional neural links among fat depots mediated via the peripheral and central nervous systems.

INDEX WORDS: SS-SNS crosstalk, adipose afferent reflex, free fatty acids

ADIPOSE SENSORY NERVES: FUNCTIONAL AND NEUROANATOMICAL EVIDENCE
FOR THEIR EMERGING ROLE IN ENERGY BALANCE

by

John T. Garretson Jr.

A Dissertation Submitted in Partial Fulfillment of the Requirements for the Degree of

Doctor of Philosophy

in the College of Arts and Sciences

Georgia State University

2016

Copyright by
J. T. Garretson, Jr.
2016

ADIPOSE SENSORY NERVES: FUNCTIONAL AND NEUROANATOMICAL EVIDENCE
FOR THEIR EMERGING ROLE IN ENERGY BALANCE

by

John T. Garretson, Jr.

Committee Chair: Geert J. de Vries

Committee: Aaron G. Roseberry

Gary J. Schwartz

Charles D. Derby

Electronic Version Approved:

Office of Graduate Studies

College of Arts and Sciences

Georgia State University

August 2016

DEDICATION

This document is dedicated to Tim Bartness and all those like him. As an accomplished Regents' Professor, a revered mentor, and a loving friend, he touched many lives with his enthusiastic creativity and discipline. His influence will persist.

ACKNOWLEDGEMENTS

This body of work could not have been compiled without the immense network of people who have helped directly with the work, supported the work financially, and/or personally helped me during my time at Georgia State University. Firstly, I thank Dr. Vitaly Ryu, Alex Thomas, Ngoc Ly Nguyen, Sierra Williams, Dr. Emily Bruggeman, and Richard Campbell for their friendship and collaboration throughout. Working with them has improved my technical skills, generated important critical feedback, and personally encouraged me to persevere after the saddening loss of our dear mentor. I can state outright that I could not have completed this work without their support. With this in mind, I broadly acknowledge GSU administrators in the College of Arts and Sciences for allowing our research to persist despite our loss. In addition, I thank Emily Hardy and Elizabeth Weaver for always ensuring my success in any way possible as well as their personal support and enthusiasm throughout. Special thanks to Dr. Aras Petrulis and Dr. Luis Martinez for sharing their passion for research with me and countless others. I also thank my committee members Chuck Derby, Aaron Roseberry, Gary Schwartz, and my committee chair Geert de Vries for continually encouraging me by challenging my experiments even to the final steps. Finally, my friends and family. Particularly Hillary Doyle for her selfless support, her humble generosity, and her very durable enthusiasm. I believe that astonishingly little is ever accomplished by a solitary person. Any achievements I have made, I owe to the foundations and inspirations I've gained from others. At the very onset of all of my accomplishments and the foundation for all my future goals, is my parents Linda Breheim and Jack Garretson and my siblings Chris, Katie, and Mark. Every thanks I can possibly give begins with you.

TABLE OF CONTENTS

ACKNOWLEDGEMENTS		ii
LIST OF TABLES		vii
LIST OF FIGURES		viii
LIST OF ABBREVIATIONS		x
1 INTRODUCTION		1
1.1 Global obesity and its reversal		1
1.2 Introduction to adipose tissue		2
<i>1.2.1 Brown adipose tissue (BAT) physiology</i>		3
<i>1.2.2 White adipose tissue (WAT) physiology</i>		7
1.3 Communication from adipose tissue to the brain		8
<i>1.3.1 Circulating factors as adipose communication</i>		9
<i>1.3.2 Peripheral innervation of adipose tissue</i>		11
<i>1.3.3 Central innervation of adipose tissue</i>		13
1.4 Sensation and functions of adipose afferent nerves inferred by denervation experiments		15
<i>1.4.1 Technical approaches to denervation</i>		16
<i>1.4.2 Adipose afferent sensation and function inferred by denervation experiments</i>		18
<i>1.4.3 Technical approach to neurophysiological recordings</i>		19

1.4.4	<i>Adipose afferent sensation and function demonstrated by neurophysiological recording experiments</i>	20
1.5	Purpose of this dissertation	23
2	BROWN ADIPOSE TISSUE HAS SYMPATHETIC-SENSORY FEEDBACK CIRCUITS	26
2.1	Abstract	26
2.2	Introduction	27
2.3	Methods and Materials	29
2.3.1	<i>Animals</i>	29
2.3.2	<i>Experiment 1: Viral injections</i>	30
2.3.3	<i>Experiment 2: Fast Blue (FB) labeling and CL316,243 administration</i>	31
2.3.4	<i>Experiment 3: Electrophysiological recordings of IBAT afferent nerve activity</i>	34
2.4	Results	37
2.4.1	<i>Experiment 1: Viral infections in the brain</i>	38
2.4.2	<i>Experiment 2: IBAT thermogenesis, DRG c-Fos immunostaining of FB-labeled neurons after intra-IBAT CL316,243 administration</i>	42
2.4.3	<i>Experiment 3: Electrophysiological recordings of IBAT afferent nerve activity</i>	44

2.5	Discussion	44
2.6	Author contributions	53
3	LIPOLYSIS SENSATION BY WHITE ADIPOSE TISSUE AFFERENTS TRIGGERS BROWN FAT THERMOGENESIS.....	55
3.1	Abstract	55
3.2	Introduction	56
3.3	Methods and Materials	59
3.3.1	<i>Animals.....</i>	<i>59</i>
3.3.2	<i>Neurophysiological recordings of IWAT afferent nerve activity</i>	<i>59</i>
3.3.3	<i>Western blot analysis of lipolysis induced by CL.....</i>	<i>62</i>
3.3.4	<i>Fast Blue (FB) labeling and CL administration</i>	<i>63</i>
3.3.5	<i>Tissue fixation and c-Fos immunostaining on DRGs</i>	<i>64</i>
3.3.6	<i>Brown fat transponder implantation, temperature recordings, and acute surgical denervation of IWAT.....</i>	<i>65</i>
3.3.7	<i>Data analysis.....</i>	<i>66</i>
3.4	Results	68
3.5	Discussion	73
3.6	Author contributions	77
3.7	Acknowledgements.....	77

4	CHEMOGENETIC CONTROL OF ADIPOSE AFFERENT NERVES	78
	4.1 Introduction	78
	4.2 Method and Results	80
	4.2.1 Pilot experiment using AAV2 transduction of excitatory	
	<i>DREADDs</i>	80
	4.2.2 Experiment 1: Chemogenetic control of WAT afferents 2	
	<i>weeks after AAV2 injection into IWAT.</i>	83
	4.2.3 Experiment 2: Chemogenetic control of WAT afferents 6	
	<i>weeks after AAV8 injection into IWAT and GWAT.</i>	86
	4.3 Discussion.....	94
	4.4 Author contributions	95
5	CONCLUSIONS AND FUTURE DIRECTIONS.....	96
	REFERENCES	98

LIST OF TABLES

Table 1. Distribution of sympathetic (PRV152) and sensory (H129) neurons across the neuraxis.....	49
--	----

LIST OF FIGURES

Figure 1. Adipose distribution (Tchkonia et al., 2013) and cellular ultrastructure of WAT and BAT (Cinti, 1999).	4
Figure 2. Representative viral tract tracing images of BAT SS-SNS feedback loops.	39
Figure 3. Quantification of viral tract tracing of BAT SS-SNS feedback loops.	41
Figure 4. BAT and core temperature after intra-BAT β 3-agonist injections.	43
Figure 5. Activation of spinal afferents innervating BAT.	45
Figure 6. Diagram of BAT SS-SNS feedback loops.	47
Figure 7. Glucoprivation increases IWAT multiunit nerve spiking in a β -AR dependent fashion.	68
Figure 8. Intra-adipose β 3-AR agonism increases IWAT multiunit nerve activity.	69
Figure 9. Intra-adipose CL increases pHSL/HSL indicating β 3-AR induced lipolysis.	70
Figure 10. Intra-adipose β 3-AR agonism increases c-Fos-ir in DRG neurons connected to IWAT.	71
Figure 11. Intra-IWAT eicosopentanoic acid (EPA) and arachidonic acid (AA) increases IWAT multiunit nerve activity.	72
Figure 12. CL-induced IWAT afferent stimulation is sufficient to increase BAT thermogenesis.	73
Figure 13. <i>AVIL</i> ^{cre+} expression in mouse (from Zurborg et al.,2011).	79
Figure 14. Pilot experiment demonstrating probable DREADD control of IWAT afferents.	82

Figure 15. Timeline for metabolic chamber experiments using AAV2 transfection of DREADDs.	83
Figure 16. Experiment 1: Metabolic consequences of hm3d(q) activation of IWAT afferent nerves.	84
Figure 17. Experiment 1: hm4d(i) inhibition of IWAT afferent nerves does not produce a robust phenotype.	84
Figure 18. AAV2 translation of mCherry and c-Fos response to CNO.	85
Figure 19. Timeline for Experiment 2a-f using AAV8 DREADD 6wks after infection.	88
Figure 20. Experiment 2a: AAV8-hm3d(q) activation of IWAT and GWAT afferent nerves does not produce a food intake differences after food deprivation.	89
Figure 21. Experiment 2b: AAV8-hm3d(q) activation of IWAT and GWAT afferent nerves does not produce robust differences in metabolic measures.	90
Figure 22. Experiment 2d: AAV8-hm3d(q) activation of IWAT and GWAT afferent nerves does not produce a differences in BAT or body temperature.	91
Figure 23. Experiment 2c: AAV8-hm3d(q) activation or AAV8-hm4d(i) inhibition of IWAT and GWAT afferent nerves does not produce a differences in blood glucose. ..	92
Figure 24. Experiment 2e: CNO applied to dissociated mCherry-positive DRG neurons from <i>AVIL^{cre+}</i> mice increases intracellular calcium.	92
Figure 25. Experiment 2e: CNO applied to dissociated mCherry-positive DRG neurons from wild type mice injected with hm3d(q) increases intracellular calcium.	93

LIST OF ABBREVIATIONS

2DG, 2-deoxyglucose

AA, arachidonic acid

AAR, adipose afferent reflex

AAV, adeno-associated virus

ATGL, adipose triglyceride lipase

AVIL^{cre+}, transgenic mouse expressing *cre-recombinase* in advillin neurons

BAT, brown adipose tissue

BMI, body mass index

CGRP, calcitonin-gene related peptide

CL, CL 316,243 (β 3-adrenoreceptor agonist)

CNO, clozapine-n-oxide

DIO, double-floxed inverted open reading frame

DMP, dimethylpyrazole

EPA, eicosopentanoic acid

FB, fast blue

FFA, free fatty acids

GWAT, gonadal white adipose tissue

H129, herpes-simplex virus strain 129

HSL, hormone sensitive lipase

IBAT, interscapular brown adipose tissue

IHC, immunohistochemistry

IML, intermedio-lateral horn of the spinal cord

ir, immunoreactivity

IWAT, inguinal white adipose tissue

NEFA, non-esterified fatty acids

PBS, phosphate buffered saline

PRV, pseudorabies virus

PSHS, parasympathetic nervous system

PUFA, polyunsaturated fatty acids

PVH, paraventricular nucleus of the hypothalamus

RER, respiratory exchange ratio

SNS, sympathetic nervous system

SS, sensory system

T, Thomas

TAG, triacylglycerol

TAG, triglycerides

Tb, body temperature

Tg, transgenic mouse

WAT, white adipose tissue

WT, wild type mouse

1 INTRODUCTION

The U.S. census reports that 67% of Americans are overweight or obese, creating a healthcare-related economic burden that exceeds \$140 billion annually ("Centers for Disease Control and Prevention ", 2009). Complications of obesity include hypertension, cardiovascular disease, type II diabetes, stroke and some cancers ("Centers for Disease Control and Prevention ", 2009) and contribute to up to 26.8% of U.S. deaths annually (Masters et al., 2013). Clearly, uncovering effective obesity reversal strategies will improve the health of millions of people, reduce obesity-related deaths, and decrease healthcare costs associated with increased body fat. A relatively unstudied facet of obesity reversal is the investigation of neural circuits that emanate from fat tissue and are networked to brain regions capable of controlling energy balance via the sympathetic nervous system (SNS). With the exception of the largely unsuccessful efforts to reverse so-called 'leptin resistance' to the adipose-derived satiety hormone (Myers et al., 2012), few studies have examined the functional connectedness of fat tissue to the brain as a means to counteract obesity. Therefore, the purpose of this dissertation is to review our current knowledge of adipose afferent nerve sensitivities and functions, demonstrate new and physiologically relevant functions of these nerves, and consolidate this new information into a synthetic working model in order to generate testable hypothesis regarding the emerging role of adipose afferent nerves in energy balance.

1.1 Global obesity and its reversal

People who are overweight (BMI = 25 through 30) or obese (BMI > 30) are at risk for deleterious comorbidities, many of which are associated with the ectopic and overabundant storage of white adipose tissue (WAT). As of 2014, this includes

approximately 1.9 billion individuals around the globe: 39% of all adults worldwide; and this number has more than doubled since 1980 (W.H.O., 2014). Thankfully, body mass reduction by diet and exercise can attenuate or even resolve symptoms of obesity-induced hypertension, type 2 diabetes (Lewis, 2013), respiratory distress (Dattani, Swerner, Stradling, & Manuel, 2016), infertility (Dag & Dilbaz, 2015), and sleep apnea (Quintas-Neves, Preto, & Drummond, 2016). This shift in healthiness by fat reduction may be due to many factors associated with better diet and exercise (Dankel, Loenneke, & Loprinzi, 2016); however, surgical removal of white fat also rapidly alleviates comorbidity symptoms such as insulin insensitivity and hyperlipidemia (Crahay & Nizet, 2016). This suggests that the presence of fat itself produces negative consequences. Clearly, WAT mass reduction by better diet and exercise is healthful and therefore a variety of obesity reversal strategies have been employed. In order to discover the many possible ways permanent obesity reversal may be accomplished, we must know how fat depot size is regulated and functionally how to control this regulation.

1.2 Introduction to adipose tissue

Adipocytes, or fat cells, vary in size and structure and perform a variety of specialized functions throughout the body. Two primary types of adipocytes each comprise large depots throughout the body known as WAT and brown adipose tissue (BAT) (Fig. 1), whose similarities and differences will be discussed in detail here. However, other types of fat are not trivial and exist in bone, joints, ectopically within other organs, and are reviewed elsewhere (Grundy, 2016; Mace, Bhatti, & Anand, 2016; Scheller, Cawthorn, Burr, Horowitz, & MacDougald, 2016). In general, WAT adipocytes store excess energy in the form of triglycerides (TAG) and BAT adipocytes expends

energy by burning lipid during nonshivering thermogenesis. This broad dichotomy often brings one to assume WAT is bad and BAT is good; however, this conclusion is somewhat flawed. White fat mobilization is engaged when glucose stores have been depleted, thus fuel utilization after the exhaustion of or beyond the rate provided by WAT reflect a state of extreme depletion. This results in wasting and associated consequences (Kyle & Pichard, 2006)—with obesity being a possible evolutionary survival strategy to prevent wasting (Prentice, 2005). Lipodystrophy—a disorder characterized by the inability to store fat at appropriate sites—is associated with a spectrum of disorders including insatiable appetite, insulin resistance, and cardio myopathies (Seip & Trygstad, 1996). WAT, conversely, becomes extremely unhealthy after unregulated accumulation that inevitably leads to its sometimes fatal comorbidities (Lewis, 2013). BAT, on the other hand, is primarily considered beneficial and performs thermogenic and glucoregulatory functions (van Marken, 2012). Its energy consumption often correlates with fat loss and the general reversal of obesity (Cannon & Nedergaard, 2004b; Carey & Kingwell, 2013; Nedergaard, Bengtsson, & Cannon, 2011). Although WAT and BAT are both types of adipose tissues, their metabolic functions, regulatory mechanisms, and even cell lineages are remarkably distinct (Carey & Kingwell, 2013; Wu et al., 2012).

1.2.1 Brown adipose tissue (BAT) physiology

Largely studied in rodents but also shown to be active in humans (Nedergaard, Bengtsson, & Cannon, 2007), BAT is a thermogenic tissue that expends energy and is thus an important contributor to the energy balance equation (Carey & Kingwell, 2013). Human BAT is more active in winter months (Au-Yong, Thorn, Ganatra, Perkins, &

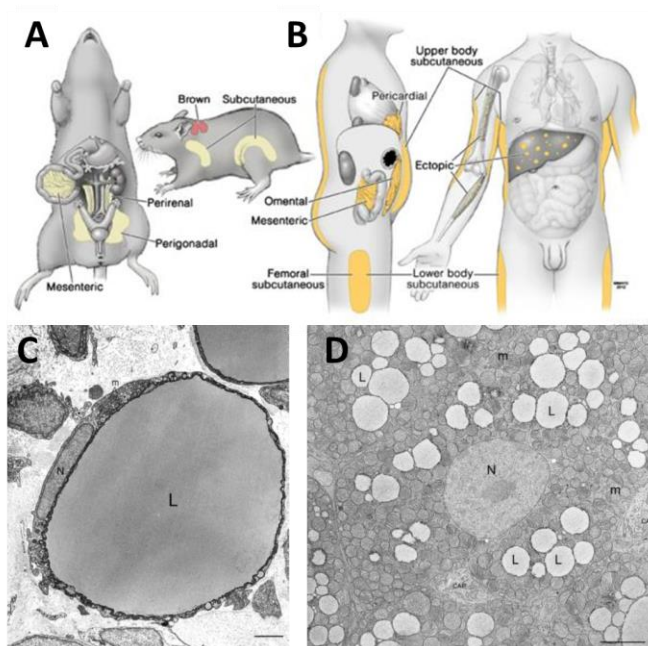


Figure 1. Adipose distribution (Tchkonia et al., 2013) and cellular ultrastructure of WAT and BAT (Cinti, 1999).

a-b) Figure from (Tchkonia et al., 2013). a) Rodent and b) human distribution of WAT and BAT. c-d) Figure from (Cinti, 1999). Electron microscopy of c) epididymal white and d) interscapular brown adipocytes: n, nucleus; m, mitochondria; L, lipid droplet; CAP, capillary.

Symonds, 2009) and is acutely activated by cold (Sacks et al., 2013). Its activity also contributes to better glucose regulation and reduced risk for type 2 diabetes (Cannon & Nedergaard, 2004a). In rodents, BAT is localized primarily in the interscapular region (Tchkonia et al., 2013) but also in pericardial, subclavical, and supraspinal regions; whereas, human primary BAT depots are pericardial, subclavical, supraspinal and are absent from the interscapular region in adulthood (Tchkonia et al., 2013) (Fig. 1a, b). Indeed, animals with higher BAT activity tend to be thinner, more glucose tolerant, and illustrate a healthier inflammatory profile than their counterparts with low BAT activity (Krief, Bazin, Dupuy, & Lavau, 1989; Stanford et al., 2013; Vijgen et al., 2012). In addition, many clinical investments target BAT activation as a strategy to treat human obesity. Therefore, recent research initiatives have focused on BAT growth, BAT activity, BAT transplantation in BAT deficient animals, and the browning of WAT to resemble

BAT all to test how this tissue contributes to better metabolic health (Carey & Kingwell, 2013).

BAT adipocytes generate heat using their numerous mitochondria and (Fig. 1d) specialized thermogenic gene expression profile. When glucose is insufficient, then either BAT intracellular TAG stores, gluconeogenesis, and circulating lipids released by WAT fuel are capable of fueling BAT thermogenesis (Labbé et al., 2015). In brief, fatty acids and glucose are usually used to generate ATP; however, BAT cells produce uncoupling-protein 1 (UCP1) which creates a mitochondrial protein leak that dissipates heat (Fedorenko, Lishko, & Kirichok, 2012). This heat production by BAT is increased during cold exposure, becomes more efficient and robust when animals are chronically exposed to cold, and is triggered by SNS activity (Festuccia, Blanchard, Richard, & Deshaies, 2010). Astonishingly, BAT itself contributes to approximately one half of all energy expended by cold-acclimated small rodents despite comprising less than one percent of total body mass (Cannon & Nedergaard, 2004a). In obese rodents and humans, BAT is less active and has a lower capacity for cold-induced activity than lean counterparts (Lidell & Enerback, 2010). This demonstrates that reduced BAT function is either caused by or contributes to the development of obesity. Therapeutic intervention by enhancing BAT function may therefore prevent or reverse obesity development by improving metabolic health in individuals at risk.

Results from studies using transplantation of BAT into BAT-deficient rodent models tests the potential for non-native BAT to rescue rodent models of obesity and glucose-intolerance. Autologous BAT transplant into the visceral cavity restores glucose sensitivity in streptozotocin-induced diabetic mice, suggesting that BAT glucose utilization is sufficiently high to rescue pancreatic islet cell destruction (Gunawardana &

Piston, 2012). To illustrate the potentially versatile benefits of enhanced BAT function, BAT implantation also rescues menstrual irregularity in rodent models of polycystic ovarian syndrome (Yuan et al., 2016). These data together illustrate that a greater amount of BAT, and theoretically enhanced activity of native BAT, may improve dysregulated functions across several organ systems. Sympathomimetics that increase BAT activity in rodents have little to no effect in humans (Cypess et al., 2012). However, recent advances in BAT transplantation methodology (Tharp et al., 2015) established that human BAT transplantation is approaching a clinical possibility.

Inspired by the advantages of targeting BAT to achieve better metabolic health, many researchers are using this strategy to enhance the BAT-like functional characteristics of WAT: known colloquially as 'browning' or 'beiging.' Indeed, some WAT adipocytes are capable of transitioning from a lipid storage cell across an adipocyte continuum to instead burn lipid by the induction of a somewhat brown or 'beige' state, a transition brought on almost exclusively by chronic stimulation by the sympathetic nervous system (SNS) (Cannon & Nedergaard, 2004a). Not all WAT adipocytes are capable of browning, and importantly, beige adipocytes are not identical to classical brown adipocytes most notably due to their divergence from different cell lineages (Wu et al., 2012). These distinctions, however, do not prevent browned WAT depots from generating measureable heat during cold exposure and thereby contribute to enhanced energy expenditure when stimulated (Wu, Cohen, & Spiegelman, 2013). Thus, WAT browning is poised to mediate obesity reversal by both generating heat to expend energy, and by reducing the amount of classical WAT mass (Ishibashi & Seale, 2010).

1.2.2 White adipose tissue (WAT) physiology

Classical WAT adipocytes store large vacuoles of lipid as TAG and have relatively few mitochondria (Figure 1a). In addition to its role as a secretory organ (Scherer, 2006), a primary function of this tissue is to store excess lipid during periods of energy surplus and release lipid as fuel during periods of energy deficit. During energy surplus, WAT accumulates lipid by hypertrophy (*i.e.* growing in size) and by hyperplasia (*i.e.* becoming more numerous in cell number) to accommodate more TAG (Bourgeois, Alexiu, & Lemonnier, 1983). In rodents, WAT depots are stored in five stereotypically identified regions (Fig. 1c) with three being subcutaneous (*e.g.* dorsal, inguinal), others abdominal (*e.g.* perigonadal, retroperitoneal) and one visceral fat pad (*e.g.* mesenteric) defined by its venous draining directly into hepatic portal circulation (Tchkonia et al., 2013). Humans, however, store subcutaneous fat more homogeneously across the body and, in the case of visceral obesity, have a large visceral omental fat depot under the greater curvature of the stomach (Tchkonia et al., 2013). In rodents, individual control of WAT depot size is accomplished by direct SNS outflow capable of delivering NE to distinct depots in differential degrees (Brito, Brito, Baro, Song, & Bartness, 2007; Brito, Brito, & Bartness, 2008).

Indeed, stimulated WAT lipolysis and BAT thermogenesis are triggered by SNS stimulation. This notion is supported by broad expression of $\alpha_{1, 2}$ and $\beta_{1, 2, 3}$ adrenergic receptors (β -ARs) on adipocytes (Lafontan & Berlan, 1993), NE content within the tissue, and *ex vivo* responses of cultured adipocytes to NE. WAT lipolysis is stimulated when norepinephrine released by axon terminals of post ganglionic SNS neurons binds to β -adrenoreceptors (β -ARs)—present on adipocytes (Lafontan et al., 1997)—initiating a lipolytic cascade that is dependent on the phosphorylation of hormone sensitive lipase

(HSL) leading to the preferential release of long-chain free-fatty acids (FFAs) and glycerol from TAG stores (Bartness & Song, 2007a; Belfrage, Fredrikson, Nilsson, & Stralfors, 1981). WAT lipid droplets contain an array of saturated and unsaturated species of fatty acids in the form of TAG, spanning from characteristically short to long carbon chain species (Raclot, Mioskowski, Bach, & Groscolas, 1995). Although all FFAs are released during WAT lipolysis, polyunsaturated fatty acids with longer carbon chains are mobilized to a higher degree (Raclot & Groscolas, 1993). Direct efferent innervation of the tissue, instead of circulating NE, is thought to stimulate WAT lipolysis and BAT thermogenesis because of the preserved SNS control of these functions after adrenalectomy (Edens, Moshirfar, Potter, Fried, & Castonguay, 1999; Holt, Wheal, & York, 1988).

1.3 Communication from adipose tissue to the brain

Adipose communication by neurohumoral factors was first described directly with the discovery of leptin (Zhang et al., 1994); however more recent studies also define an additional robust and interconnected sensory neural component of this tissue (Bartness, Liu, Shrestha, & Ryu, 2014a; Giordano, Morroni, Santone, Marchesi, & Cinti, 1996). Adipose sensory nerve activity is an emerging contributor to blood pressure regulation and likely other metabolic processes via broadly triggering SNS activation (Nijjima, 1998), this is despite any demonstration that WAT or BAT can generate signals that communicate to the sensory nerves innervating the tissue. Because of the potential for sensory innervation of WAT and BAT to affect SNS outflow, uncovering mechanisms by which WAT and BAT activate their afferents may reveal key strategies for how adipocyte function is integrated with many organ systems.

To assess candidate activators of adipose afferents and targets of endocrine communication, we begin with listing the probable types of messages fat may be sending regarding its state and functions. WAT and BAT activity can be generally refined to several distinct roles such that identifying these basic functions makes clear several likely outgoing messages from fat to adipose afferents. 1) Lipogenesis is a crucial ongoing process to animal survival preparing for unforeseen physiological challenges (*e.g.* cold exposure, periods of famine); 2) Lipolysis is the breakdown and release of lipid as fuel, which is rapidly triggered when glucose is insufficient and energy demand is high; 3) BAT and 'browned' WAT thermogenesis also is a context-dependent rapidly triggered process that is vital to rodent survival in a cold environment. These three general functions of WAT and BAT occur during specific physiological states wherein lipolysis and thermogenesis are high during energy challenge; lipogenesis occurs primarily during energy surplus. Consequently, lipolysis and thermogenesis are vital to survival during scarcity of food and warmth whereas lipogenesis occurs largely during abundance of food and states of rest (Ng, 1990). It is unclear, however, if or how the state of these adipose processes are signaled to other organs; but by the nature of their design, endocrine signaling likely favors tonic messages while local paracrine fat to neural signaling most likely favors acutely relevant adipocyte functions.

1.3.1 Circulating factors as adipose communication

Signaling polyproteins secreted by adipocytes, or adipokines, are a diverse pool of molecules and contribute to a wide variety of physiological processes including but not limited to energy expenditure, insulin sensitivity (Dyck, Heigenhauser, & Bruce, 2006; Mullen et al., 2009), cardiovascular function (Salazar et al., 2016), immune function

(Odegaard & Chawla, 2013), hunger, and even reproduction (Reverchon, Ram, Bertoldo, & Dupont, 2014). Among the over hundreds of adipokines identified (Halberg, Wernstedt-Asterholm, & Scherer, 2008; Scherer, 2006), leptin and adiponectin are perhaps the most highly studied. Leptin is secreted by fat based on the amount of accumulated lipid evidenced by serum levels proportional to the amount of stored WAT. It is colloquially referred to as the 'adiposity hormone.' Adiponectin, which is present in serum inversely proportional to fat mass, precedes insulin insensitivity by its diminished levels in blood (Lee & Shao, 2014). As with other adipokines, leptin exerts its effects at many targets (*e.g.* brain, peripheral nervous system, liver, bone, heart, gastrointestinal tract) and is thought to inform the body of the general amount of adipose tissue. Mechanisms of leptin resistance, a term that describes the insufficiency for exogenous leptin to inhibit appetite and reduce body mass in the case of diet-induced obesity, are sought after by many and believed to be driven by leptin receptor sensitization, downregulation, and/or diminished permeability of leptin into the brains of obese animals. However, leptin resistance as a phenomenon may be misguided due to the apparent hyperphagia induced by leptin absence compared with little to no effect on feeding after exogenous administration and/or exaggerated levels during an obese state (Allison & Myers, 2014). A more reasonable explanation is the impaired functioning of downstream signaling in metabolic neuronal populations because of enhanced suppressor of cytokine 3 or an otherwise enhanced inflammatory profile (Myers, 2015). Clearly, leptin as well as adipokines are examples of adipocytes signaling to other tissues and can become dysregulated during disease conditions (*e.g.* obesity and diabetes).

1.3.2 Peripheral innervation of adipose tissue

In addition to endocrine signaling by adipokines, it is clear that local paracrine communication between adipocytes and neurons within fat depots occurs on a rapid scale. Efferent, or motor, innervation of fat was clearly defined with the first observance of direct efferent connectivity in 1898 by Dogiel (Dogiel, 1898), and many have demonstrated functional integration of SNS into fat tissue (for review see (Bartness et al., 2014a). Afferent, sensory innervation of fat, however, was not anatomically identified until 1987 by Fishman and Dark (Fishman & Dark, 1987) and has been studied to a relatively underwhelming degree.

1.3.2.1 Sensory nerve phenotype

First identified using the true blue neurotracer directly into WAT (Fishman & Dark, 1987), WAT and BAT afferents share a common neurochemical profile with nociceptive free nerve endings throughout the body. Immunohistochemical identification of WAT afferents in the tissue reveals expression of sensory nerve markers calcitonin-gene related peptide (CGRP) and substance P indicating the presence—or the absence—of sensory innervation (Giordano et al., 1996). Electron microscopy of WAT afferents using these markers reveals a mix of both myelinated and unmyelinated fibers that are congregated predominately around vasculature of the innervated tissue (De, Ricquier, & Cinti, 1998).

These afferents, like other afferents innervating skin, muscle, and liver, are pseudo-unipolar neurons, with a single axon bifurcating where one arm extends to the sensory organ and the other arm projecting into the spinal cord to synapse with dorsal horn neurons at the level of spinal entry (Tandrup, 1995). Tracing studies suggest that

WAT and BAT afferents are spinal neurons, in that their cell bodies are located together among a group of cell bodies outside the spinal cord known collectively as the dorsal root ganglion (DRG) (Fishman & Dark, 1987). To understand the functional roles of WAT sensory innervation, DRGs are extracted post-mortem to characterize neuro-traced adipose afferents using immunohistochemistry (Murphy et al., 2013) and *in situ* hybridization (Oliveira et al., 2003). DRG analysis of WAT afferent nerves is often preferred to tissue level analysis due to cell body access and possible occlusion of afferent fibers by adipocytes that make distinguishing WAT from afferent nerve receptor protein expression difficult; further, immediate early genes (*e.g.* c-Fos, pERK) are common proxies for neuronal activity and are only present in cell bodies (Hoffman, Smith, & Verbalis, 1993). Using this method together with immunohistochemistry for the long form leptin receptors (ObRb), we have demonstrated that WAT afferents are activated by injection of leptin into WAT (Murphy et al., 2013). Functional evidence described in depth below also suggests that WAT afferents express adenosine receptors and capsaicin-sensitive transient potential vallinoid receptors (TrpVRs) (Shi et al., 2012).

1.3.2.2 Motor nerve phenotype

As with other SNS fibers that send output to organs (*e.g.* liver, pancreas, heart), WAT efferent/motor nerves are neurochemically homogenous in that most are identified by catecholaminergic markers (*e.g.* dopamine β -hydroxylase, tyrosine hydroxylase) and neuropeptide Y (NPY). Transneuronal viral neurotracing of WAT reveals broad neuronal populations in brain and spinal regions discussed in detail below; however, neurotracing to WAT pads whose catecholaminergic innervation has

been depleted by a SNS-specific neurotoxin—6-hydroxy-dopamine—results in no apparent innervation across the peripheral and central neuraxis (Giordano et al., 2006). The finding that parasympathetic nervous system (PSNS) innervation of fat has been described as well (Kreier et al., 2002). This is controversial, however, because classical markers of PSNS are not present in adipose tissue (Ballantyne, 1968; Giordano et al., 2006). Thus, evidence that adipose motor nerves are entirely catecholaminergic suggest that PSNS innervation is trivial at best (Giordano et al., 2005; Giordano et al., 2007; Lundberg, Terenius, Hokfelt, & Goldstein, 1983).

Control of SNS WAT and BAT efferent nerves drives lipolysis and thermogenesis of WAT and BAT, respectively (Bartness et al., 2014a); therefore, mechanisms of WAT and BAT efferent control are those which coincide with energy expenditure to a large degree. Although many attempts have been made to pharmacologically mimic SNS output to promote fat loss in humans (Omran, 2016), most therapies include concomitantly increased cardiovascular risk (Siebenhofer et al., 2016). To this end, specific SNS activation of adipose efferents is a primary goal to achieve safe obesity reversal in humans.

1.3.3 Central innervation of adipose tissue

We have established efferent and afferent neural circuits of BAT and WAT by using transneuronal viral tract tracers (Bamshad, Song, & Bartness, 1999; Bartness, Song, Shi, Bowers, & Foster, 2005; Bowers et al., 2004; Ryu, Garretson, Liu, Vaughan, & Bartness, 2015b; Song, Schwartz, & Bartness, 2009). These methods rely on infection of neural tissue after parenchymal viral injection into single or multiple tissue depots. Bartha K Pseudorabies virus strains (PRV) that express green (PRV152) or red (PRV614)

fluorescent proteins specifically infect neurons from the ends of their circuit to the beginning, infecting neuronal pathways in a retrograde fashion with viral uptake occurring at the nerve terminals (Strack & Loewy, 1990). These two viruses have been used to trace differences in efferent innervation between multiple fat pads (Nguyen, Randall, Banfield, & Bartness, 2014) and elucidated shared and divergent neural pathways to individual depots. Herpes simplex virus strain 129 (HSV129) infects neuronal pathways in an anterograde fashion (Barnett, Evans, Sun, Perlman, & Cassell, 1995), traveling from the beginning of neural circuits to the end with viral uptake occurring at dendritic processes. Viral infection of PRVs and HSV129 occurs when viral attachment molecules bind to neuronal glycoproteins. These are amplified by the infected cells, and then transmitted to connected neurons (Curanovic & Enquist, 2009; Ekstrand, Enquist, & Pomeranz, 2008). Although PRVs and H129 seem to infect all first order neurons despite their role as sensory or motor neurons in the tissue (Rinaman & Schwartz, 2004), viral transmission to the next neuron in the circuit occurs via distinct differences in their axonal transport and synaptic transmission. Therefore, these viruses have been key tools to illustrate the central efferent and afferent neural circuits connected to adipose tissue.

Using both PRV152 and HSV129 in the same animal, we have illustrated individual neurons that both receive sensory input from and project SNS outflow to WAT (Bartness & Song, 2007b) and to BAT (Ryu et al., 2015b). These double labeled neurons throughout the neuraxis are presumably each capable of relaying sensory input from fat into SNS outflow to fat. We find that most double-labeled neurons reside in the mid and hindbrain (Bartness et al., 2014a). Based on the accumulating evidence that WAT afferent activation increases in SNS activity (Li et al., 2013; Niiijima, 1998), these

relay neurons likely propagate a feed-forward WAT-brain-SNS circuit meaning afferent activation leads to efferent activation. Indeed, adipose-initiated SNS reflexes that do not require cortical function are supported by the neuroanatomical localization of midbrain and brainstem WAT-BAT circuits sufficient to drive BAT thermogenesis in the absence of neural connectivity with structures rostral to the midbrain. For example, cooling of the skin increases BAT thermogenesis in decorticated but not decerebrated rats (Osaka, 2004), a reflex action believed to originate by BAT afferent activation.

1.4 Sensation and functions of adipose afferent nerves inferred by denervation experiments

WAT and BAT afferents have been demonstrated to contribute to distinct biological functions such as SNS feedback regulation to multiple tissues (Niiijima, 1998, 1999), SNS-induced hypertension (Xiong, Chen, & Zhu, 2014), regulation of fat deposition throughout the body (Shi & Bartness, 2005), and food intake regulation (Yamada et al., 2006). These functions have been elucidated by two primary approaches to date. First, loss of function experiments using surgical denervation or excitotoxic chemical denervation by high dose capsaicin (Jancso et al., 1984) or resinerfertoxin (Acs, Biro, Acs, Modarres, & Blumberg, 1997) infused into adipose tissue of anesthetized rodents. The second approach to test WAT and BAT afferent function is accomplished by recording extracellular neurophysiological activity in anesthetized animals beginning with Niiijima's discovery that leptin activates WAT afferents (Niiijima, 1999) and more recently with understanding mechanisms of the adipose afferent reflex (AAR) (Shi et al., 2012; Xiong et al., 2012; Xiong et al., 2014). This section will discuss technical details of these approaches as well as their advantages and disadvantages to interrogate adipose

afferent neurophysiological stimulators and physiological processes engaged by increased adipose afferent activity.

1.4.1 Technical approaches to denervation

Surgical or chemical destruction of peripheral nerves innervating tissues are exclusion experiments designed to test the role of neural connectivity by categorically comparing intact with denervated animals to infer chronic neural function. These experiments, although quite useful for establishing necessity of WAT and BAT afferent connectivity, have two critical flaws in that both 1) lack specificity and 2) rely on a surgical recovery period of weeks during which some degree of reinnervation of the tissue and/or other physiological compensation will likely occur. Both surgical and chemical methods consistently reduce or abolish sensory nerve markers (*e.g.* substance P, CGRP) within fat tissue compared with control animals suggesting that despite these shortcomings each technique is adequate for testing the necessity of WAT and BAT afferent functions. Tissues that are specifically targeted by these methods are the interscapular BAT, perigonadal (GWAT), or the subcutaneous inguinal WAT (IWAT). Whole animal deafferentation by capsaicin, although non-specific to adipose afferents, is relevant to this discussion and will be referenced in regard to adipose functions controlled by afferents.

Surgical denervation of WAT and BAT is completed by physically removing a portion of all nerves innervating each tissue, which prevents adipose tissue from emitting sensory neural signals (Vaughan, Zarebidaki, Ehlen, & Bartness, 2014). During this procedure, a small section of each nerve is removed using two precise cuts—instead—of a single cut to reduce the likelihood of nerve regrowth by a neural system

unknown in its regenerative capacity. This type of denervation is performed while the animal is anesthetized, typically takes 2-3 min per fat pad, has only been completed in rodents. To successfully accomplish this task and completely destroy all innervation of the target fat pad, the surgeon must non-specifically destroy nerves innervating overlying skin—subcutaneous fat—or nearby organs possibly innervated by shared nerve bundles. The nonspecific denervation of other organs more likely occurs with GWAT surgical denervation compared with IWAT and IBAT due to their relative proximities to other organs (*e.g.* gonads) (Cinti, 1999). By definition, surgical denervation mutes bidirectional communication of both sensory signals arising from fat and, importantly, motor signals communicated by the brain to fat. Thus, despite surgical denervation being the most complete method to abolish adipose sensory signals, its equal removal of SNS outflow to fat often excludes it as an independent tool to investigate the role of sensory specific innervation. Consequently, surgical denervation is often accompanied with more chemically specific approaches when adipose afferent function is considered.

Chemical denervation by high doses of capsaicin (Jancso et al., 1984) or resinerfertoxin (Acs et al., 1997) infusion into fat involves controlled surgical microinjections throughout the target tissue (Vaughan et al., 2014) to cause excitotoxicity of sensory neurons specifically. During this procedure, sub-microliter volumes of fluid are infused into as many as 20 loci across the entire fat pad to produce the most robust decreases in sensory innervation—as measured by CGRP protein content in homogenized tissue 3-6 weeks after recovery (Vaughan & Bartness, 2012). For each locus of injection, the microsyringe needle is held in place for 1 min to minimize efflux of fluid outside the pad and reduce the spread to non-specific tissues;

thus this surgery takes up to 20 min per fat pad and therefore requires a considerably longer duration of anesthesia than with surgical denervation. Due to the duration of time spent injecting the fat pad and the surgical recovery period thereafter, acute conclusions from adipose afferent destruction studies are often avoided.

The most profound flaw of chemical denervation is that it does not completely abolish sensory innervation within the tissue. Typically, successful chemical denervation results in a reduction in total CGRP protein of as little as ~40-50% less than vehicle-injected control tissues (Vaughan & Bartness, 2012). This is either due to the excitotoxin not reaching all adipose afferents in the fat pad or that both capsaicin and resiniferatoxin target transient receptor potential cation channel subfamily V member 1 (TrpV1) receptors which may be present on some but not all CGRP-positive sensory neurons (Koltzenburg, 2004). Although this sensory nerve destruction is clearly not as complete as surgical destruction of afferents, its specificity to sensory not motor neurons is paramount. The physiological effects it produces marks this as the most useful tool to test metabolic processes that require functionally intact adipose afferents.

1.4.2 Adipose afferent sensation and function inferred by denervation experiments

These loss of function studies describe the variety of physiological functions that required adipose afferent innervation. Surgical removal of fat from one specific depot causes increased lipid accumulation in other fat depots, we demonstrated that this compensation exists in Siberian hamsters (Mauer & Bartness, 1994). It also can be mimicked by WAT afferent chemical destruction (Shi, Song, Giordano, Cinti, & Bartness, 2005), suggesting that WAT afferents provide 'inventory' data to the CNS

which then compensates for the loss of fat by adding more elsewhere (Mauer, Harris, & Bartness, 2001). In addition, chemical denervation of IWAT or EWAT afferents contributes to a regulation of fat cell proliferation (Shi et al., 2005).

General connectivity between WAT afferents and BAT has been investigated following chemical deafferentation of rats by systemic capsaicin (Cui & Himms-Hagen, 1992a; Cui, Zaror-Behrens, & Himms-Hagen, 1990; Melnyk & Himms-Hagen, 1994). After systemic capsaicin treatment, rats have diminished BAT thermogenic capacity (Giordano et al., 1998) and atrophy of the IBAT tissue depot (Cui & Himms-Hagen, 1992b; Cui et al., 1990). These studies suggest that afferent nerve throughout the body functionality contributes to healthy BAT function and provokes curiosity into the specific location of the afferents that control of BAT.

Only one study demonstrates that adipose afferents exert effects on the innervated tissue by the local release of neuropeptides. This signaling mechanism is well defined in other innervated tissues [*e.g.* muscle (Dvorakova, Kruzliak, & Rabkin, 2014)] but otherwise novel to adipocyte afferent innervation. CGRP released by BAT afferent nerves reduces sensitivity of BAT adipocytes to NE thus attenuating SNS-induced thermogenesis (Osaka et al., 1998). Neuropeptide release by WAT afferents may perform similar functions although this has yet to be investigated. As a potent vasodilator (Tippins, 1986), CGRP's release by adipose afferents may increase adipose blood flow to enhance the reception or extravasation of lipid by the adipose organs.

1.4.3 Technical approach to neurophysiological recordings

Extracellular nerve recordings of adipose innervation are a targeted surgical approach to test for the control of afferent or efferent function of these nerves in an

anesthetized rodent. To date, adipose afferent recordings have only been accomplished in rats and Siberian hamsters, the former due to their larger relative size and the latter because of the detailed illustrations of adipose innervation revealed by tract tracing studies (Bamshad et al., 1999; Bartness et al., 2005; Bowers et al., 2004; Ryu et al., 2015b; Song et al., 2009). Critical to this technique is effective surgical isolation of anatomically connected nerves innervating the tissue and electrical isolation of the desired signal (*i.e.* afferent or efferent). When examining adipose afferent function, this technique involves infusing the target fat depot with a candidate chemical to test for the sufficiency to activate sensory fibers monitored by the recording electrode. Each of these strategies, however, must be performed under urethane or ketamine/xylazine anesthesia wherein the rodents' temperature regulation, metabolic rate, respiration, and blood pressure are all unlike that of an awake animal. Because of these limitations, experiments using this method explicitly exclude behavioral measures and perhaps are solely capable to identify acute perturbations that mechanistically control adipose afferents and efferent activity.

1.4.4 Adipose afferent sensation and function demonstrated by neurophysiological recording experiments

Nijijima was the first to demonstrate experimental activation of WAT afferents by measuring increased afferent spiking after leptin infusion into epididymal WAT (GWAT) (Nijijima, 1998). Adipose activation induced by leptin is repeated in a series of studies (Nijijima, 1998, 1999; Shi et al., 2012), it occurs within minutes after the onset of infusion, and is also apparent in neurons arising from inguinal WAT (Murphy et al., 2013; Shi et al., 2012; Xiong et al., 2012; Xiong et al., 2014). In addition, Nijijima was the

first to demonstrate that neurophysiological recordings of adipose nerves was possible, and served as the principal exploration into a new method by which WAT afferent sensitivity can be established. Niiijima further discovered leptin-induced GWAT afferent activation reflexively increases in SNS outflow to GWAT and broadly dampens vagal nerve PSNS outflow (Niiijima, 1999), also serving as the first identification that efferent outflow could be triggered by WAT afferent activation.

WAT afferent-induced SNS outflow, later termed the 'adipose afferent reflex' (AAR), has been extended by Zhu and colleagues into an apparent sufficiency of IWAT afferent activity to trigger renal SNS outflow thereby increasing blood pressure. This positive reflex is initiated by IWAT activation which can be induced by leptin but also by bradykinin, adenosine, and the indiscriminate activator of sensory nerves, capsaicin. The WAT afferent activators not included by Niiijima (*e.g.* bradykinin, adenosine) further extend the role of WAT afferents to monitor the release of a variety of ligands from adipocytes and implicate WAT afferents in organ systems. Overall, Zhu and colleagues argue that WAT afferents sensitive to leptin are involved in SNS increases causing hypertension. This positive feedback may be responsible for the high comorbidity between obesity and hypertension in humans. Adenosine receptors A1 and A2 on adipocytes regulate fat lipolysis as well (Johansson, Lindgren, Yang, Herling, & Fredholm, 2008); thus, sensation of adenosine by WAT afferents vaguely suggests lipolysis is an event that stimulates their activity. Bradykinin, however, is primarily released by the kidneys in response to increased blood pressure and therefore may serve as a message to WAT afferents regarding the status of circulation. Thus, this serves as a conduit that is important to adipose tissue for released lipolytic products to be circulated throughout the body as fuel. Overall, WAT afferent activation causes

increases in SNS outflow to multiple targets and these data highlight this neural circuit as mediator of SNS function overall.

Despite the broad and seemingly redundant distribution of adipose afferent and efferent neural circuitry (Bartness & Song, 2007c; Song et al., 2009), the paraventricular nucleus of the hypothalamus (PVH) is a required brain region through which WAT afferent-induced hypertension occurs. Excitotoxic lesion of the PVH disrupts the AAR by attenuating increased renal SNS activity (Cui et al., 2013). Several lines of evidence have been proposed for the mechanism by which the PVH converts adipose afferent stimulation to SNS outflow. Indeed, blockade of PVH melanocortin 3 and 4 receptors produces similar AAR inhibition as PVH lesion, as also is the case for GABA_A receptor antagonism (Ding et al., 2015a) and depletion of PVH supraoxide anions by the scavenger tempol (Ding et al., 2013). All of these explorations of the PVH involvement use capsaicin infusions into IWAT or GWAT as an AAR trigger which increases PVH field potentials; however, it is unclear if PVH disruption by any of these means prevents excited adipose afferents from causing SNS increases, or if central disruption of this pathway reduces excitability of adipose afferents by capsaicin. This shortcoming demonstrates fundamental questions that still exist in adipose afferent physiology because of the difficulty to capture the synchrony of organ systems using techniques currently available.

The apparent increased SNS outflow has been of key interest among labs studying adipose afferent physiology; however, only we have produced a physiological challenge for the animal and measured subsequent adipose afferent responses (Song et al., 2009). Peripheral administration of 2-deoxy-glucose (2DG), a sympathomimetic that causes the β -adrenergic dependent breakdown of adipose tissue, also causes a

correlational increase in WAT afferent activity suggesting again that lipolysis, as also hinted by direct adenosine infusion into IWAT, causes WAT afferent stimulation. This suggests either that adipose afferents are stimulated by circulating products of lipolysis (*e.g.* FFAs and glycerol) or that they sense local secretions by their receptive fields within fat parenchyma. In order to dissociate these two possibilities, improved methods are needed to site specifically cause lipolysis and capture site specific afferent responses.

1.5 Purpose of this dissertation

After synthesis of the known characteristics of adipose afferents and their downstream functions, many inferences suggest activation by and interconnectedness of these fibers with other organ systems. Adipose afferents potentially control body fat deposition, general SNS outflow, and do so by their collective patterns of nerve activity that somehow drive coordinated organ level responses. Of the evidence provided, the research themes by others are focused on SNS-outflow produced by general adipose afferent activation; however, it is largely unclear under what physiological settings these nerves are activated. Indeed, correlational exploration of glucoprivation-induced afferent activation is the only study that demonstrates adipose afferents respond to adipocyte-derived signals based on a physiological reaction to enhanced SNS drive (Song et al., 2009). Instead, others have injected exogenous substances into WAT or BAT as *in vivo* pharmacological experiments by testing the capability of their ligand of choice to affect the adipose afferents hidden within the depot. To this effect, injecting leptin into WAT—at a dose not justified to be physiologically relevant—to stimulate WAT afferents ignores the context in which adipocytes may release leptin to activate

these afferents *in vivo*. These tests essentially neglect the notion that specific functions of adipocytes cause afferent activation.

Thus, we seek to understand what signals BAT and WAT adipocytes are capable of producing that control the activity of the afferent nerves residing within. We accomplish this by testing the hypothesis that SNS-outflow to BAT and WAT results in increased adipose afferent nerve activity; specifically, BAT afferents are thermosensors and WAT afferents are lipid sensors. We do so by using the β_3 -AR agonist CL 316,243 to target adipocytes within each depot then measuring subsequent reactions of BAT and WAT afferents. Measurements of afferent activity include neurophysiological recordings and neurotracing combined with c-Fos immunohistochemistry as a molecular marker of activation within connected DRGs. We continue this work by demonstrating neuroanatomical feedback loops comprised of BAT sensory and sympathetic nerves using transneuronal viral tract tracing. In addition, we establish a functional neural connection between WAT and BAT whereby WAT afferent activity drives BAT thermogenesis. Finally, we explore a novel chemogenetic strategy that permits measurement of the behavioral and metabolic consequences of adipose afferent activity in awake-behaving animals for the first time. Progress in developing this approach is discussed and additionally, we propose improvements based on this work for future studies.

2 BROWN ADIPOSE TISSUE HAS SYMPATHETIC-SENSORY FEEDBACK CIRCUITS

Vitaly Ryu, John T. Garretson, Yang Liu, Cheryl H. Vaughan, and Timothy J. Bartness

Department of Biology, Center for Obesity Reversal, Neuroscience Institute, Georgia
State University, Atlanta, Georgia, 30302-4010

Published in *The Journal of Neuroscience* on February 4th 2015

2.1 Abstract

Brown adipose tissue (BAT) is an important source of thermogenesis which is nearly exclusively dependent on its sympathetic nervous system (SNS) innervation. We previously demonstrated the SNS outflow from brain to BAT using the retrograde SNS-specific transneuronal viral tract tracer, pseudorabies virus (PRV152) and demonstrated the sensory system (SS) inflow from BAT to brain using the anterograde SS-specific transneuronal viral tract tracer, H129 strain of herpes simplex virus-1. Several brain areas were part of both the SNS outflow to, and receive SS inflow from, interscapular BAT (IBAT) in these separate studies suggesting SNS-SS feedback loops. Therefore, we tested whether individual neurons participated in SNS-SS crosstalk by injecting both PRV152 and H129 into IBAT of Siberian hamsters. To define which dorsal root ganglia (DRG) are activated by BAT SNS stimulation, indicated by c-Fos immunoreactivity (ir), we pre-labeled IBAT DRG innervating neurons by injecting the retrograde tracer Fast Blue (FB) followed 1 wk later by intra-BAT injections of the specific β_3 -adrenoceptor

agonist CL316,243 in one pad and the vehicle in the contralateral pad. There were PRV152+H129 dually-infected neurons across the neuroaxis with highest densities in the raphe pallidus nucleus, nucleus of the solitary tract, periaqueductal gray, hypothalamic paraventricular nucleus and medial preoptic area, sites strongly implicated in the control of BAT thermogenesis. CL316,243 significantly increased IBAT temperature, afferent nerve activity and c-Fos-ir in C2-C4 DRG neurons ipsilateral to the CL316,243 injections versus the contralateral side. The neuroanatomical reality of the SNS-SS feedback loops suggests coordinated and/or multiple redundant control of BAT thermogenesis.

2.2 Introduction

Brown adipose tissue (BAT) is a critical for non-shivering thermogenesis in rodents and its physiological function is directly controlled by its sympathetic nervous system (SNS) innervation (Bartness, Vaughan, & Song, 2010; Richard & Picard, 2011). Rodent BAT has parasympathetic nervous system (PSNS) innervation of two minor BAT depots -- pericardial (Schafer, Eiden, & Weihe, 1998) and mediastinal (Giordano, Frontini, Castellucci, & Cinti, 2004), but not interscapular BAT (IBAT), the major rodent BAT depot (Giordano et al., 2004). Absence of BAT PSNS permits use of the viral transneuronal tracer pseudorabies virus (PRV; Bartha's K strain) to define the origins of the SNS outflow innervating peripheral tissues [for review see: (Enquist, 2002; Song, Enquist, & Bartness, 2005)] including IBAT (Bamshad et al., 1999; Oldfield et al., 2002). Increases in BAT SNS drive lead to release of norepinephrine (NE) from its SNS postganglionic nerve terminals thereby stimulating brown adipocyte β_3 -adrenoceptors [*e.g.*, (Zhao, Unelius, Bengtsson, Cannon, & Nedergaard, 1994)] that ultimately activate

uncoupling protein-1 resulting in thermogenesis increases [for review see: (Cannon & Nedergaard, 2004b)]. This NE effect is mimicked by CL316,243, a highly selective β_3 -adrenoceptor agonist both *in vivo* (Atgie, Faintrenie, Carpene, Bukowiecki, & Geloën, 1998a; Himms-Hagen et al., 1994) and *in vitro* (Gabaldón, McDonald, & Horwitz, 1998)

BAT also has sensory system (SS) innervation. At the tissue level, IBAT has immunoreactivity (-ir) for two proven SS neuropeptides, substance P and calcitonin gene-related peptide (De et al., 1998; Norman, Mukherjee, Symons, Jung, & Lever, 1988). Furthermore, with intra-IBAT injection of an anterograde transneuronal viral tract tracer, the H129 strain of herpes simplex virus 1 (HSV-1), we identified the central SS circuits from this tissue (Vaughan & Bartness, 2012). Many of the sites receiving SS input from IBAT (Vaughan & Bartness, 2012) also are part of the SNS outflow from the CNS to IBAT revealed by our PRV studies. Thus, this SNS-SS overlap between studies suggests the possibility of individual neurons that are part of the SNS outflow from brain to BAT that also receive SS input from the tissue – that is, potential SNS-SS feedback loops serving an anatomical basis for crosstalk between BAT SNS and SS innervations. Although the exact role of the BAT SS is unknown, the impairment of the thermogenic response of BAT to acute cold exposure due to sensory denervation accomplished via intra-IBAT injection of the sensory-specific neurotoxin capsaicin (Jansco, Kiraly, & Jansco-Gabor, 1980; Jansco, Kiraly, Joo, Such, & Nagy, 1985), strongly suggests BAT SS innervation is necessary for its optimal physiological functioning (Vaughan & Bartness, 2012). Therefore, we hypothesized that BAT SNS-SS feedback loops might exist and tested this as well as identifying which dorsal root ganglia (DRG) receive sensory input when IBAT is adrenergically-activated by: 1)

injecting both the SS-specific transneuronal tract tracer, H129, and the SNS-specific transneuronal tract tracer, PRV, intra-IBAT to test for dually-infected SNS-SS neurons, 2) injecting CL316,243 intra-IBAT using c-Fos-ir to reveal activation (Hoffman et al., 1993) of pseudounipolar neurons within the DRG pre-labeled with Fast Blue (FB) thereby identifying IBAT afferent neurons activated by IBAT adrenergic stimulation, and 3) measuring IBAT sensory nerve activity electrophysiologically after intra-IBAT CL316,243 injection.

2.3 Methods and Materials

In this study we used Siberian hamsters (*Phodopus sungorus*) because these animals provide an irreplaceable model over other rodent models to study a naturally-occurring seasonal obesity as well as foraging and hoarding. Using this model, we established the origins of the efferent sympathetic (SNS) outflow from brain to WAT and BAT pads utilizing SNS-specific viral tract tracer PRV152. Moreover, we identified the central sensory centers innervating those fat pads using sensory-specific viral tract tracer H129 which altogether prepared neuroanatomical background for identification of SNS-SS circuits to characterize specific fat pads.

2.3.1 Animals

Adult male Siberian hamsters (*Phodopus sungorus*; ~3-4 mo old) from our breeding colony were single-housed in a long day photoperiod (16h:8h light:dark cycle; at 22 ± 2 °C) with free access to water and regular chow for 1 wk before viral injections. All procedures were approved by the Georgia State University Institutional Animal Care and Use Committee and are in accordance with Public Health Service and United States Department of Agriculture guidelines.

2.3.2 Experiment 1: Viral injections

All virus injections were performed according to Biosafety Level 2 standards. Hamsters (n=8) were anesthetized with isoflurane (2.0-3.0 % in oxygen; Baxter Healthcare, Deerfield, IL) and the left IBAT pad was exposed for a series of PRV152 (gift from Dr. Enquist, Princeton University) microinjections (7.5×10^7 pfu/ml) into five loci (150 nl/locus) evenly distributed across one IBAT pad. After 24 h, the same IBAT pad received five H129 (gift from Dr. Richard Dix, Georgia State University) microinjections (7.5×10^7 pfu/ml; 150 nl/locus). The syringe was held in place for 60 s to prevent efflux of virus after each injection. Finally, the incision was closed with sterile sutures and wound clips. Nitrofurazone powder (nfz Puffer; Hess & Clark, Lexington, KY) was applied locally to minimize the risk of bacterial infection. Note that previously we demonstrated that surgical isolation of the fat pad from the surrounding tissues before H129 injections results in a pattern of infection indistinguishable from that of pads injected in their natural *in situ* position suggesting the infections came directly from sensory nerves innervating the fat pad, but not the surrounding tissues [Song, C.K. and Bartness, T.J., unpublished observations]. As a control for possible viral diffusion, we also demonstrated that the same virus titer of PRV152 or of H129 and volume placed on the surface of the exposed IBAT pad resulted in no infection in the sympathetic ganglia or DRG, spinal cord, and brain as opposed to intra-IBAT pad viral infections (Ryu V and Bartness TJ, unpublished observations). In addition, we found both PRV152 and H129-infected neurons in the intermediolateral cell column (IML) of the spinal cords (data not shown), respectively, suggesting specific IBAT-SNS ganglia and IBAT-SS DRG-spinal cord-brain routes of infection which are in concordance with our previous findings where PRV152 and H129 individually infected the classic SNS and SS spinal cord

neurons (Bamshad et al., 1999; Vaughan & Bartness, 2012). Finally, we have not noticed left-right pad differences in brain infections with injections of either PRV152 or H129. Note that pilot studies indicated no left-right IBAT differences (Vaughan, C.H. and Bartness, T. J.; and Song, C. K. and Bartness, T. J., unpublished observations) nor in our published work (Bamshad et al., 1999; Leitner & Bartness, 2009; Song et al., 2008; Vaughan & Bartness, 2012).

2.3.3 Experiment 2: Fast Blue (FB) labeling and CL316,243 administration

One week before CL316,243 microinjections, Siberian hamsters (n=12) were deeply anesthetized with ketamine/xylazine (100 mg/kg, 10 mg/kg; i.p.) and a dorsal 2 cm interscapular incision was made to expose IBAT. The retrograde tracer FB (1.0 %; EMS-CHEMIE GmbH, Gross-Umstadt, Germany) was injected with a microsyringe into five separate loci (1 μ l/locus) of the left IBAT. After the last injection, the incision was closed with sterile wound clips and ketofen [5 mg/kg; s.c.; Fort Dodge Animal Health, Fort Dodge, IA] was administered for 3 d postinjection to minimize postoperative discomfort.

For CL316,243 administration, two electronic transponders (Bio Medic Data Systems Inc., Seaford, were connected to BAT-10 Thermometer Physitemp (Physitemp Instruments Inc., Clifton, NJ). CL316,243 (0.2 ng/kg in 0.9 % saline), a highly selective β_3 -adrenoceptor agonist that stimulates facultative thermogenesis [*e.g.*, (Himms-Hagen et al., 1994)], was injected intra-left IBAT at five loci (2 μ l/locus for a total of 10 μ l) while nearly simultaneous intra-right IBAT injections of CL) each with a built-in temperature sensor were gently implanted under each IBAT pad, the output of which

was read with a hand-held DAS-7007R scanner (Bio Medic Data Systems Inc.) for IBAT temperature (T_{IBAT}) acquisition as we have used successfully previously (Brito et al., 2007; Leitner & Bartness, 2009; Nautiyal et al., 2008; Song et al., 2008; Vaughan & Bartness, 2012; Vaughan, Shrestha, & Bartness, 2011). This system provides an opportunity to program the transponder with a unique identification code to distinguish between left and right IBAT pad temperatures. Core body temperature (T_b) in these anesthetized animals was measured using a rectal temperature sensor. The saline vehicle (2 μ l/locus for a total of 10 μ l) served as a within animal control. In preliminary studies, we determined that s.c. CL316,243 injections at 0.2 ng/kg failed to elevate T_{IBAT} and therefore this dose was selected for IBAT microinjections [Ryu, V. and Bartness, T.J., unpublished observations]. Following each injection, the microsyringe needle was held in place for at least 1 min to minimize efflux. The incision was immediately closed with sterile wound clips and parallel temperature recordings from both IBAT pads as well as T_b were monitored every 5 min for 1 h post injection (observation time based on pilot studies showing little or, most often, no change in temperatures after that time [Ryu, V. and Bartness, T. J., unpublished observations]).

2.3.3.1 Histology

Animals were terminated 6 d after the last PRV152 injections (5 d after the last H129 injections) based on progression of both viruses to the brain in pilot studies (Ryu, V. and Bartness, T. J, unpublished observations). Hamsters were overdosed with pentobarbital sodium (Sleep Away; 300 mg/kg) and transcardially perfused with 0.9 % heparinized saline followed by 4.0 % paraformaldehyde in 0.1 M phosphate buffered saline (PBS; pH 7.4). The brains were collected and post-fixed in the same fixative for 3-

4 h at 4 °C, then transferred to a 30.0 % sucrose solution in 0.1 M PBS with 0.1 % sodium azide and stored at 4 °C until they were sectioned on a freezing stage sliding microtome at 30 µm. Sections were stored in 0.1 M PBS solution with 0.1 % sodium azide until processed for double immunofluorescence.

For the CL316,243 experiment, the hamsters were euthanized with pentobarbital sodium (Sleep Away; 300 mg/kg) immediately after individual temperature recordings and transcardially perfused (see above). DRG associated with vertebral levels C1-T5 were extracted bilaterally, the epineurium debrided from the ganglia, post-fixed in the same fixative for 15 min and transferred to an 18.0 % sucrose solution in 0.1 M PBS with 0.1 % sodium azide at 4 °C overnight. DRG were sectioned longitudinally at 20 µm and directly mounted onto slides (Superfrost Plus; VWR International, West Chester, PA) in three series with every fourth section on the same slide. This procedure yielded ~24 sections with each slide containing eight sections. Therefore, multiplying the number per section by 24 will give an estimated total neuronal number per ganglion.

For the double-label fluorescent immunohistochemistry, free-floating brain sections were rinsed in 0.1 M PBS (2 x 15 min) followed by a 30 min blocking in 10.0 % normal goat serum (NGS; Vector Laboratories, Burlingame, CA) and 0.4 % Triton X-100 in 0.1 M PBS. Next, sections were incubated with a mixture of primary rabbit anti-HSV-1 antibody (1:2000; DakoCytomation, Carpinteria, CA) and mouse anti-GFP antibody (1:700; Abcam, Cambridge, MA) for 18 h. Sections were then incubated in the mixture of the secondary goat anti-rabbit (1:700; Jackson ImmunoResearch, West Grove, PA) and goat anti-mouse Alexa-488 (1:700; Jackson ImmunoResearch) antibodies with 2.0 % NGS and 0.4 % Triton X-100 in 0.1 M PBS for 2 h at room temperature. For immunohistochemical controls, the primary antibody was either omitted or

preadsorbed with the immunizing peptide overnight at 4 °C resulting in no immunoreactive staining. Sections were mounted onto slides (Superfrost Plus) and coverslipped using ProLong Gold Antifade Reagent (Life Technologies, Grand Island, NY).

After rehydration, DRG sections were processed for detection of H129 (anti-HSV-1 antibody, 1:100 dilution; DakoCytomation) and PRV152 (anti-GFP antibody, 1:500 dilution; Abcam) directly on the slides using the same immunohistochemical protocol as above.

For DRG c-Fos immunostaining on the slides, sections were rinsed in 0.1 M PBS (2 x 15 min) followed by 1 h blocking in 5.0 % normal horse serum (NHS; Vector Laboratories) and 0.3 % Triton X-100 in 0.1 M PBS. Sections were then incubated in the primary rabbit anti-c-Fos (1:500; sc-52; Santa Cruz Biotech, Santa Cruz, CA) antibody with 10.0 % NHS and 0.3 % Triton X-100 in 0.1 M PBS overnight. Next, the sections were incubated in the secondary donkey anti-rabbit Cy3 (1:200; Jackson Immunoresearch) for 3 h, rinsed with 0.1 M PBS (3 x 15 min) and coverslipped with ProLong Gold Antifade Reagent (Life Technologies). All steps were performed at room temperature.

2.3.4 Experiment 3: Electrophysiological recordings of IBAT afferent nerve activity

Siberian hamsters (n=10) were anesthetized with ketamine/xylazine (100 mg/kg, 10 mg/kg; i.p.), a 2 cm dorsal interscapular incision made, IBAT and connective tissue resected exposing nerves innervating right IBAT lobe. Single nerves were isolated with a petroleum jelly barrier, severed, then the decentralized nerve placed on silver (32-

guage) hook electrodes to measure afferent activity. A petroleum jelly mineral oil mixture (1:1) was applied to the site completely enveloping the electrode/nerve connection, and then warm mineral oil was pooled into the recording area to insulate electrical noise, secure the nerve on the electrode, and reduce drying of tissue. A steady anesthetic plane was maintained with supplemental ketamine by examining toe pinch repeatedly on all four paws and testing the eye blink response throughout the recording. Three stainless steel needles connected with silastic tubing to microsyringes affixed to a microsyringe infusion pump were inserted into right IBAT along the lateral-coronal plane spaced 4-5 mm apart at a depth of 4 mm each. In a pilot experiment, we used this delivery system for intra-IBAT application of Evan's blue dye as a visual surrogate for CL316,243 and found that the whole ventral IBAT pad turned blue showing excellent distribution of fluid across the pad by this method (Garretson, J. T. and Bartness, T. J., unpublished observations). Ten minutes of basal electrical activity was measured and served as baseline. At that point, 15 μ l of CL316,243 (0.2 ng/kg) or the saline vehicle was infused at a rate of 3.0 μ l/min and recording continued.

Extracellular signals were amplified 10,000 times with a differential AC amplifier set to low pass filter 100 Hz and high pass filter 1000 Hz (Model 1700; A-M Systems, Sequim, WA). The analog signal was visualized using an oscilloscope (2530, BK Precision, Yorba Linda, CA) to optimize signal-to-noise ratio and concurrently identified via an audio analyzer (74-30-1; FHC, Bowdoin, ME). Data were digitized through Digidata 1440a data acquisition system (1440a; Molecular Devices, Sunnyvale, CA), recorded with accompanying Clampex 10.3 software at a 20,000 Hz sampling rate, then analyzed for number of spikes based on a voltage threshold two standard deviations above mean non-signal noise via the Clampfit 10.2 data analysis software package. All

identified waveforms were visually screened whereby any aberrant signals counted by the software were easily identified and removed from the analyses.

2.3.4.1 Quantitative and statistical analysis

Images were viewed and captured using 100x and 200x magnification with an Olympus DP73 imaging photomicroscope (Olympus, Tokyo, Japan) with appropriate filters for Cy3 and Alexa-488. The single-labeled PRV152 and H129, c-Fos and FB images were evaluated and overlaid with the aid of CellSens (Olympus) and the Adobe Photoshop CS5 (Adobe Systems, San Jose, CA) software. In every sixth brain section, we counted cells showing SNS PRV152+SS H129-ir, single cells with PRV152- or H129-ir as well as c-Fos-ir and FB labeling in every fourth DRG section using the manual tag feature of the Adobe Photoshop CS5 software thus eliminating the likelihood of counting the same neurons more than once. Absolute neuronal numbers as well as their corresponding percentages in the brain and DRG were averaged across each examined region/nucleus/ganglion from all animals. A mouse brain atlas (Paxinos & Franklin, 2007) was used to identify brain areas because no Siberian hamster brain atlas is available and because of the similarity in size and shape of most of the brain structures between Siberian hamsters and mice. For the preparation of the photomicrographs, we used Adobe Photoshop CS5 (Adobe Systems) only to adjust the brightness, contrast and sharpness, to remove artifactual obstacles (*i.e.*, obscuring bubbles) and to make the composite plates.

Temperature data were analyzed by one-way repeated measures analysis of variance (ANOVA) followed by Holm-Sidak's or Bonferroni's least significant difference (PLSD) post-hoc tests using NCSS (version 2007, Kaysville, UT). For

electrophysiological analysis, spike number across time was quantified by collapsing the spikes into 10 min bins from the onset of infusion up to 20 min post infusion. The percent change of mean nerve activity from baseline was compared using a 2 x 2 analysis ANOVA (time x drug), and post hoc analysis of drug effects at individual time points using Student's t-test with Bonferroni's correction. Significance was set at $P < 0.05$. For simplicity and clarity, exact test results and exact P values are not presented.

2.4 Results

Following viral infections, hamsters remained asymptomatic until Day 5 after PRV152 and Day 4 after H129 inoculation, whereupon many began to display some symptoms of infection including occasional slight loss of body weight and decreased mobility, but most often an ungroomed coat. All hamsters were euthanized the next day for histological analyses when such symptoms became apparent. Five out of 8 animals were equally infected by both PRV152 and H129 viral tracers throughout the neuroaxis from the hindbrain to the forebrain and therefore were included in the analyses. Three other animals exhibited over-infection of the CNS either by PRV152 and/or H129 indicated by widespread 'cloudy plaques' around the over-infected neurons and were excluded from the analysis. We noticed both PRV152- and H129-labeled (-infected) neurons in the IML of the spinal cord (data not shown) with the latter SS innervation of the IML in accordance with studies showing SS presence in the IML of amphibians (Horn & Stofer, 1989), prenatal laboratory mice (Funakoshi et al., 2003), laboratory rats (Yamamoto, Senba, Matsunaga, & Tohyama, 1989) and Djungarian (Siberian) hamsters (Reuss, 1993).

2.4.1 Experiment 1: Viral infections in the brain

The dual injections of the SNS nerve tract tracer PRV152 and the SS nerve tract tracer H129 unilaterally into the same (left) IBAT pad appeared bilaterally in the brain with slightly ipsilateral domination to the side of inoculation for both viruses.

Both single- and double-labeled neurons were notably present in the hindbrain. Some of the hindbrain areas with the highest percentages of double-labeled PRV152- and H129-ir cells included the lateral paragigantocellular nucleus (LPGi; 13.0 ± 1.2 %; Table 1), raphe obscurus nucleus (ROb; 12.9 ± 1.4 %; Table 1 and Fig. 2A, B), medial parabrachial nucleus (MPB; 12.7 ± 1.1 %; Table 1), raphe pallidus nucleus (RPa; 12.6 ± 1.1 %; Table 1 and Fig. 2A) and superior vestibular nucleus (SuVe; 12.1 ± 1.8 %; Table 1). The RPa and ROb also were among the regions with the highest absolute numbers of infected neurons (Table 1 and Figs. 2A, B; 3A). Overall, the percentage of double-labeled hindbrain neurons was ~ 10.0 % (Fig. 3B).

The midbrain areas with the highest percentages of double-labeled PRV152- and H129-ir cells were the lateral periaqueductal gray (LPAG; 11.5 ± 2.1 %; Table 1) and ventrolateral periaqueductal gray (VLPAG; 10.3 ± 1.8 %; Table 1). Among the brain sites with a predominantly SNS efferent output to IBAT, as compared with a SS afferent input from the same IBAT pad, were the LPAG ($F_{(1,9)}=7.76$; $P<0.05$; Table 1 and Fig. 1C, D), dorsolateral periaqueductal gray (DLPAG; $F_{(1,9)}=42.91$; $P<0.05$; Table 1 and Fig. 2C) and dorsal raphe nucleus (DR; $F_{(1,9)}=5.35$; $P<0.05$; Table 1 and Fig. 2C). As in the hindbrain, the overall percentage of midbrain double-labeled neurons was ~ 10.0 % (Fig. 3B).

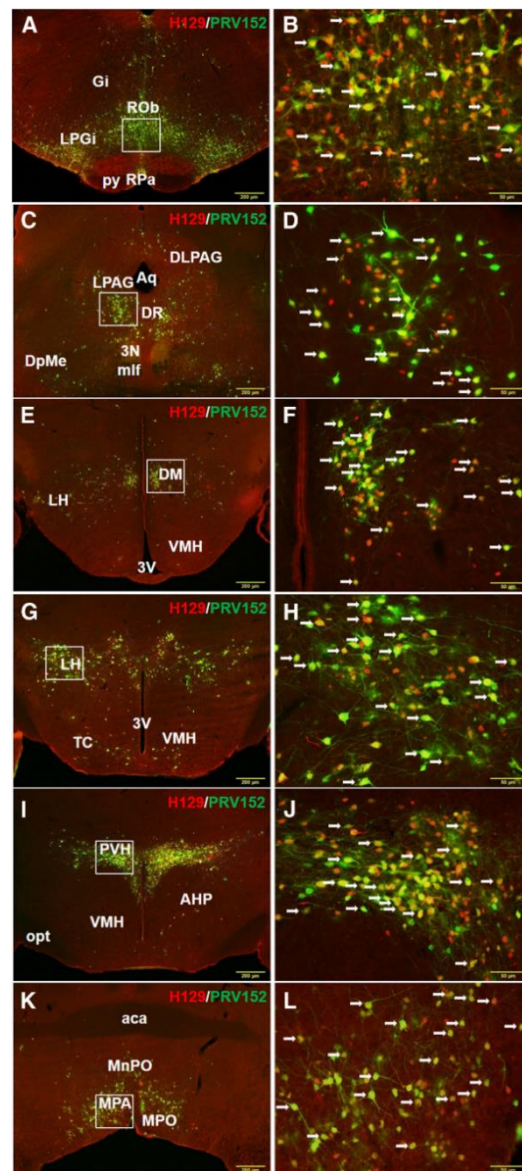


Figure 2. Representative viral tract tracing images of BAT SS-SNS feedback loops.

(A) Low and (B) high magnification of the microphotographs illustrating single PRV152 (green), single H129 (red) and double PRV152+H129 (arrows) immunolabeling in the RPa and ROb following viral injections into IBAT. Gi, gigantocellular reticular nucleus; LPGi, lateral paragigantocellular nucleus; py, pyramidal tract. $n=5$. (C) Low and (D) high magnification of the microphotographs illustrating single PRV152 (green), single H129 (red) and double PRV152+H129 (arrows) immunolabeling in the PAG following viral injections into IBAT. 3N, oculomotor nucleus; Aq, aqueduct; DLPAG, dorsolateral periaqueductal gray; DpMe, deep mesencephalic nucleus; DR, dorsal raphe nucleus; LPAG, lateral periaqueductal gray; mlf, medial longitudinal fasciculus. (E) Low and (F) high magnification of the microphotographs illustrating single PRV152 (green), single H129 (red) and double PRV152+H129 (arrows) immunolabeling in the DM following viral injections into IBAT. 3V, third ventricle; LH, lateral hypothalamus; VMH, ventromedial hypothalamic nucleus. (G) Low and (H) high magnification of the microphotographs illustrating single PRV152 (green), single H129 (red) and double PRV152+H129 (arrows) immunolabeling in the LH following viral injections into IBAT. 3V, third ventricle; TC, tuber cinereum area; VMH, ventromedial hypothalamic nucleus. (I) Low and (J) high magnification of the microphotographs illustrating single PRV152 (green), single H129 (red) and double PRV152+H129 (arrows) immunolabeling in the PVH following viral injections into IBAT. AHP, anterior hypothalamic area, posterior part; opt, optic tract; VMH, ventromedial hypothalamic nucleus. (K) Low and (L) high magnification of the microphotographs illustrating single PRV152 (green), single H129 (red) and double PRV152+H129 (arrows) immunolabeling in the MPA following viral injections into IBAT. aca, anterior commissure; MnPO, median preoptic nucleus; MPO, medial preoptic nucleus. Scale bar=200 μm in (A, C, E, G, I and K) and 50 μm in (B, D, F, H, J and L).

extensive percentages of double-infected neurons included the sub zona incerta (SubZI; 13.5 ± 3.9 %; Table 1), posterior hypothalamic nucleus (PH; 11.1 ± 1.5 %; Table 1), dorsomedial hypothalamic nucleus (DM; 9.8 ± 2.3 %; Table 1 and Fig. 1E, F), lateral hypothalamic area (LH; 9.3 ± 0.6 %; Table 1 and Fig. 2G, H), paraventricular hypothalamic nucleus (PVH; 11.2 ± 1.8 %; Table 1 and Fig. 2I, J) and anterior hypothalamic area (AHA; 9.2 ± 4.3 %; Table 1). The infected neurons were more heavily represented in the medial parvicellular (PaMP) subnucleus within the PVH (absolute numbers: 137.8 ± 22.1 for PRV152-ir neurons and 129.8 ± 32.8 for H129-ir neurons; Table 1). The ventromedial hypothalamic nucleus (VMH) was scarcely represented only by a few PRV152-ir neurons by comparison with other forebrain regions (Table 1 and Figs. 2G; 2I) as we have seen previous (Bamshad et al., 1999; Leitner & Bartness, 2009; Song et al., 2008). The overall percentage of PRV152- and H129-ir posterior hypothalamus and thalamus double-labeled neurons was ~ 9.0 % (Fig. 3B).

In the anterior hypothalamus of the forebrain, the medial preoptic area (MPA), medial preoptic nucleus (MPO) and median preoptic nucleus (MnPO) had significantly higher absolute numbers of PRV152-ir neurons as compared with those infected with H129 ($F_{(1,9)}=60.88$; $P<0.05$ for MPA; $F_{(1,9)}=5.67$; $P<0.05$ for MPO and $F_{(1,9)}=9.81$; $P<0.05$ for MnPO; Table 1 and Figs. 2K, L; 3B). The H129 immunostaining was suggestively decreased compared to PRV152 immunostaining in other forebrain areas such as the lateral preoptic area (LPO), anteroventral preoptic nucleus (AVPO) and anteroventral periventricular nucleus (AVPe) ($F_{(1,9)}=3.96$; $P=0.081$ for LPO, $F_{(1,9)}=4.89$; $P=0.058$ for AVPO and $F_{(1,9)}=5.38$; $P=0.057$ for AVPe; Table 1). The percentage of

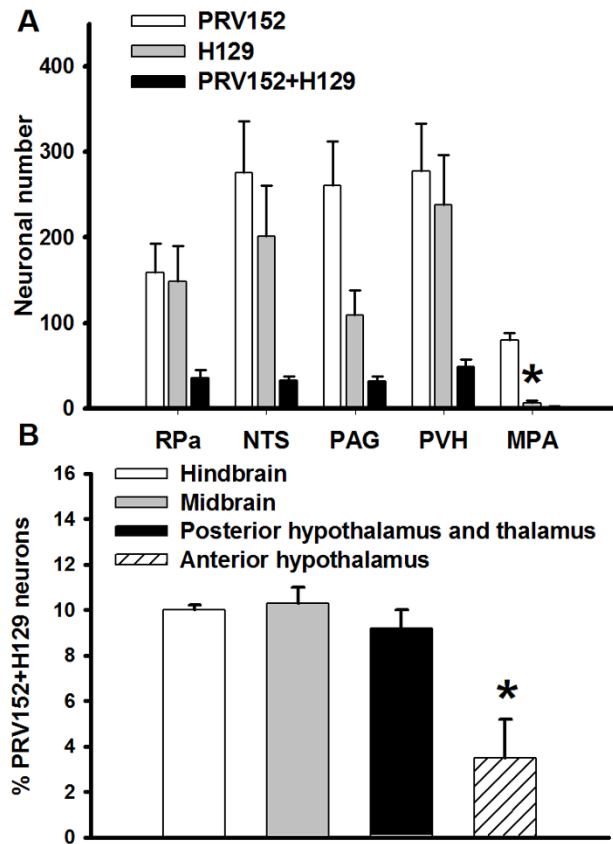


Figure 3. Quantification of viral tract tracing of BAT SS-SNS feedback loops.

(A) Brain areas with highest absolute numbers of PRV152- and H129-ir neurons. Note that the MPA contained predominantly SNS (PRV152) efferent output to IBAT as compared to a SS (H129) afferent input from the same fat pad. MPA, medial preoptic area; NTS, nucleus of the solitary tract; PAG, periaqueductal gray; PVH, paraventricular hypothalamic nucleus; RPa, raphe pallidus nucleus. $n=5$; $*P<0.05$ vs. PRV152. (B) Percentile quantification of PRV152 and H129 double-labeled (-infected) in the hindbrain, midbrain, posterior hypothalamus and thalamus, and anterior hypothalamus. $n=5$; $*P<0.05$ vs. hindbrain, midbrain and posterior hypothalamus and thalamus.

anterior hypothalamus double-labeled neurons (~3.5 %) was significantly lower than those in the posterior hypothalamus and thalamus, midbrain and hindbrain

($F_{(3,19)}=9.61$; $P<0.05$; Fig. 3B), where there was no statistical difference between the numbers of PRV152/H129 colocalized neurons (Fig. 3B).

The RPa and NTS of the hindbrain, the PAG of the midbrain, and the PVH of the forebrain contained the highest absolute numbers of both single- and double-labeled virally-infected neurons (Fig. 3A). The MPA of the forebrain had the highest absolute number only for PRV152 single-labeled neurons ($F_{(1,9)}=60.88$; $P<0.05$ vs. H129; Fig. 3A).

2.4.2 Experiment 2: IBAT thermogenesis, DRG c-Fos

immunostaining of FB-labeled neurons after intra-IBAT

CL316,243 administration

One aim of this study was to test whether a highly selective β_3 -adrenoceptor agonist, CL316,243, stimulated facultative thermogenesis in IBAT. Compared with saline vehicle-treated right IBAT, intra-left IBAT CL316,243 injections significantly increased T_{IBAT} within 10 min and this effect remained significant up to 60 min post-injections ($t_{(21)}=11.73$; $P<0.05$; Fig. 4A;). The difference in T_{IBAT} between CL316,243- and saline-treated fat pads steadily increased to 0.8 °C by 10 min, then slightly dropped to 0.56 °C by 20 min and stabilized to 0.53 °C by 60 min (Fig. 4B). T_b did not undergo significant fluctuations over 60 min; however, it was significantly lower compared with CL316,243-induced temperature increases ($t_{(21)}=26.89$; $P<0.05$; Fig. 4A;).

To define which DRG were activated by BAT SNS stimulation, we pre-labeled DRG neurons innervating IBAT by injecting a conventional retrograde tracer FB followed 1 wk later by intra-IBAT injections of β_3 -adrenoceptor agonist CL316,243 into the left and saline into the right IBAT pad. c-Fos immunostaining and FB labeling in the DRG pseudounipolar neurons appeared largely at vertebral C1-T5 levels (Figs. 5A-H). CL316,243 intra-IBAT injections significantly activated C2-C4 DRG neurons ipsilateral to the CL316,243 injections compared with the contralateral control side ($F_{(1,17)}=4.51$; $P<0.05$ for C2; $F_{(1,23)}=5.63$; $P<0.05$ for C3 and $F_{(1,23)}=4.85$; $P<0.05$ for C4; Figs. 5G, H). The c-Fos baseline level before the CL316,243 injections was approximately 4-fold lower

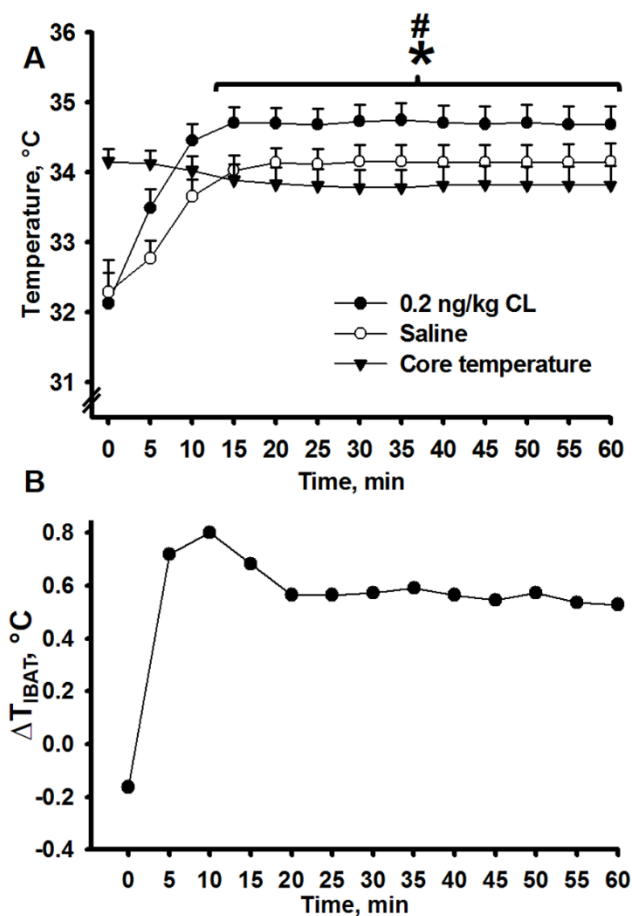


Figure 4. BAT and core temperature after intra-BAT β_3 -agonist injections.

(A) The activation of IBAT thermogenesis produced by selective β_3 -adrenoceptor agonist CL316,243 microinjections intra-left IBAT in comparison with core body temperature and T_{IBAT} after saline microinjections intra-right IBAT. (B) Changes in T_{IBAT} after CL316,243 microinjections intra-left IBAT and saline intra-right IBAT over a 60-min period. $n=12$; * $P<0.05$ vs. saline, # $P<0.05$ vs. core body temperature.

in aforementioned DRG. C4, C5 and T2 DRG contained the highest absolute numbers of FB-labeled neurons innervating IBAT compared with the contralateral side ($F_{(1,23)}=9.06$; $P<0.05$ for C4; $F_{(1,23)}=9.48$; $P<0.05$ for C5 and $F_{(1,23)}=6.36$; $P<0.05$ for T2; Figs. 5G, H). The numbers of FB-labeled DRG neurons were significantly increased at C1-T2 ipsilateral to the FB injections compared with those of the contralaterally FB-labeled neurons ($F_{(1,11)}=10.21$; $P<0.05$ for C1; $F_{(1,17)}=8.30$; $P<0.05$ for C2; $F_{(1,23)}=30.98$; $P<0.05$ for C3; $F_{(1,23)}=9.06$; $P<0.05$ for C4; $F_{(1,23)}=9.48$; $P<0.05$ for C5; $F_{(1,23)}=4.91$; $P<0.05$ for C6; $F_{(1,23)}=4.81$; $P<0.05$ for C7; $F_{(1,23)}=5.67$; $P<0.05$ for T1 and $F_{(1,23)}=6.36$; $P<0.05$ for T2; Figs. 5G, H). C3-C6 DRG had significantly more c-Fos+FB colocalized neurons as

compared with corresponding counter-DRG ($F_{(1,23)}=11.66$; $P<0.05$ for C3; $F_{(1,23)}=12.40$; $P<0.05$ for C4; $F_{(1,23)}=9.76$; $P<0.05$ for C5 and $F_{(1,23)}=4.66$; $P<0.05$ for C6; Figs. 5G, H).

2.4.3 Experiment 3: Electrophysiological recordings of IBAT afferent nerve activity

Three simultaneous infusions of saline vehicle along the lateral-coronal plane of IBAT resulted in no significant change in the rate of IBAT sensory nerve activity above baseline levels at 10 min or 20 min post-infusions. By contrast, three simultaneous intra-IBAT infusions of CL316,243 (0.2 ng/kg; same dose as used for T_{IBAT} measures) significantly elevated mean IBAT sensory nerve activity within 10 min ($t_{(19)}=10.43$; $P<0.05$), with peak activity at 20 min post-infusions ($t_{(19)}=12.03$; $P<0.05$; Fig. 5I) and a significant interaction between drug and time post-injection ($F_{(2,29)}=42.69$; $P<0.05$).

2.5 Discussion

We report here the presence of crosstalk between the SNS and SS neural innervation of the IBAT evidenced by the co-localization of both PRV152 and H129 neural tract tracers especially predominately in the RPa, NTS, PAG, PVH, and MPA brain regions. In addition, we demonstrated for the first time that intra-IBAT CL316,243-triggered β_3 -adrenoceptor stimulation significantly increased T_{IBAT} and directly activated IBAT-associated DRG neurons. Lastly, intra-IBAT CL316,243-triggered β_3 -adrenoceptor stimulation also significantly elevated afferent nerve activity. Collectively, these data provide important insight into the distributed neural system integrating SNS and SS neural circuits innervating IBAT based on the demonstration of doubly-infected neurons (*i.e.*, possible SNS-SS neural feedback loop neurons) and that these IBAT afferents are sensitive to β_3 -adrenoceptor stimulation/IBAT thermogenesis.

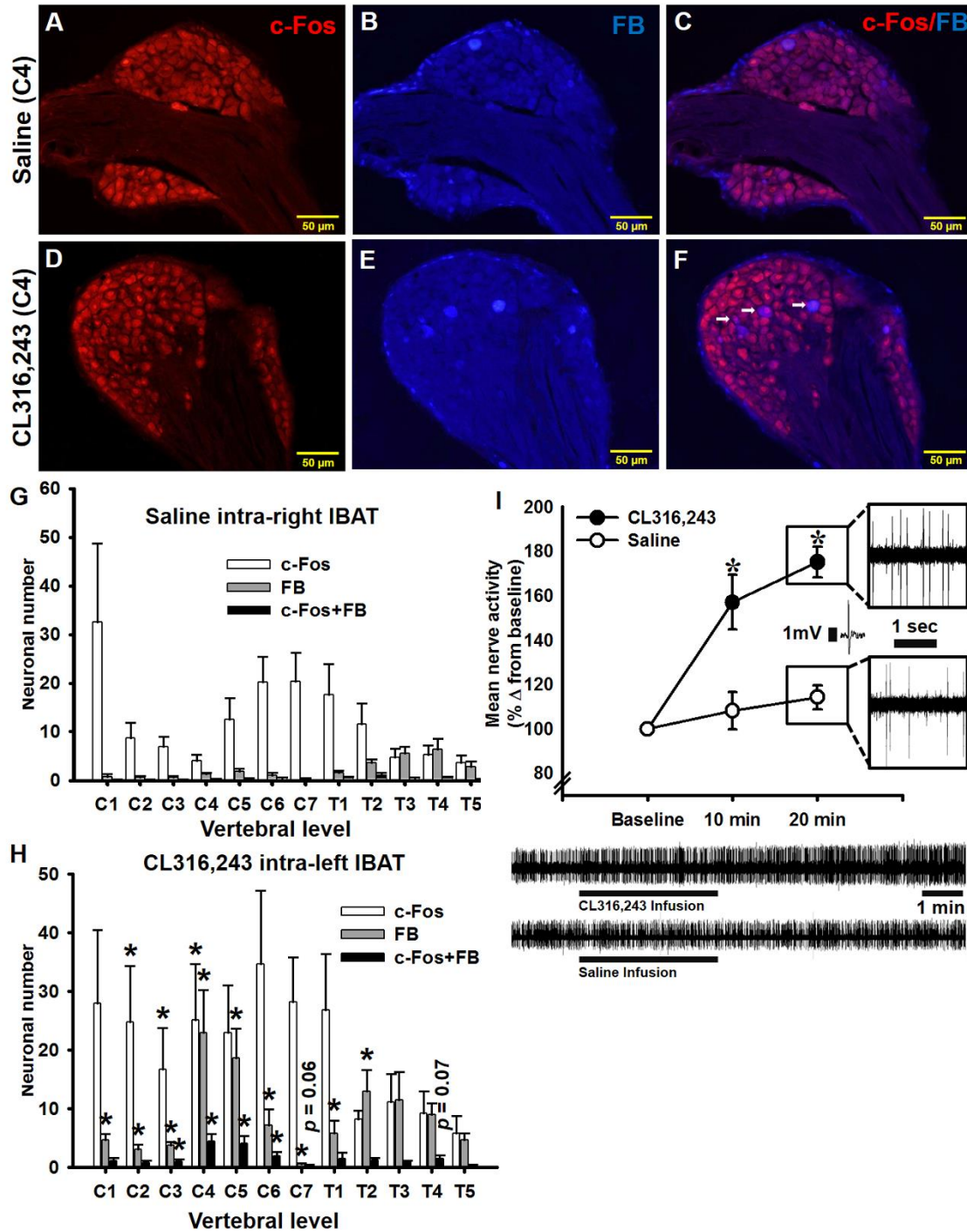


Figure 5. Activation of spinal afferents innervating BAT.

Representative microphotographs of DRG at C4 vertebral level showing c-Fos immunostaining (A, D), FB labeling (B, E) and c-Fos+FB colocalization (C, F; arrows) after CL316,243 microinjections intra-left and saline intra-right IBAT. Distribution of c-Fos-ir and FB-labeled neurons in IBAT innervating DRG at C1-T4 vertebral levels contralateral (G) and ipsilateral (H) to CL316,243 microinjections. The total number of positively-stained neurons per ganglion can be estimated by multiplying the number per section by 24. $n=12$; * $P<0.05$ vs. saline counter-mate. Scale bar=50 μm . (I) Mean nerve activity from IBAT afferent fibers before (baseline), at 10 min and at 20 min after CL316,243 or saline microinjections $n=5$ per group. CL316,243-evoked increase in IBAT sensory nerve activity. (Below) 10 min sample traces of IBAT afferent fibers before and after infusion of either CL316,243 (top) or saline (bottom). * $P<0.05$ vs. saline.

We found overlap of SNS-SS IBAT-innervating circuits across the neuroaxis. Specifically, the highest overlap of dually-infected PRV152+H129 neurons was in the LPGi (~13%), ROb (~13%), MPB (~13%) and RPa (~13%) in the hindbrain; LPAG (~12%), VLPAG (~10%) in the midbrain and SubZI (~14%), PVH (~11%), PH (~11%) and DM (~10%) in the forebrain. All these regions previously were reported to be involved in the control of BAT thermogenesis [(Richard et al., 2010; Ulhoa et al., 2013); for review see: (Morrison et al., 2014; Bartness et al., 2010b)]. Note that the number of double-labeled neurons likely was underestimated because infection of a neuron with one virus can, in principle, reduce the susceptibility to infection by a second virus [phenomenon of exclusion (Kim, Enquist, & Card, 1999)]. Due to the unpredictable time interval for each virus to reach each specific area, the neurons on both ascending and descending pathways to IBAT may not have necessarily showed dual infections despite the selection of inoculation/post-inoculation time points that optimized the double-virus technique by matching viral progression rates through the neural axis as closely as possible [for review see: (ter Horst, 2000)].

Despite predominantly equal SNS and SS representation in many brain regions, several brain regions had differing amounts of SNS efferent output/SS afferent input to and from IBAT. That is, the LPAG, DLPAG and DR in the midbrain had largely SNS output compared with SS input. The PAG receives afferent fibers not only from the parabrachial nucleus and RPa (Mantyh, 1982), which are critical for the proper thermoregulatory IBAT function [(Kobayashi & Osaka, 2003); for review see: (Morrison et al., 2014)], but also from the spinal cord (Pechura & Liu, 1986). We previously reported that the PAG sends SNS efferents ultimately to white adipose tissue (WAT) in Siberian hamsters (Bamshad, Aoki, Adkison, Warren, & Bartness, 1998; Nguyen et al.,

2014; Song, Jackson, Harris, Richard, & Bartness, 2005) as did others in laboratory rats (Adler, Hollis, Clarke, Grattan, & Oldfield, 2012). Moreover, we recently found that the dorsomedial PAG was among several other sites with predominantly SNS efferent output to the inguinal WAT (IWAT) as compared with SS input from IWAT (Ryu & Bartness, 2014) suggesting differential SNS nodes to different fat pads within the PAG. Regarding the DR, a profound IBAT thermogenic response is triggered with DR electrical stimulation (Dib, Rompre, Amir, & Shizgal, 1994); thus, it is not surprising to

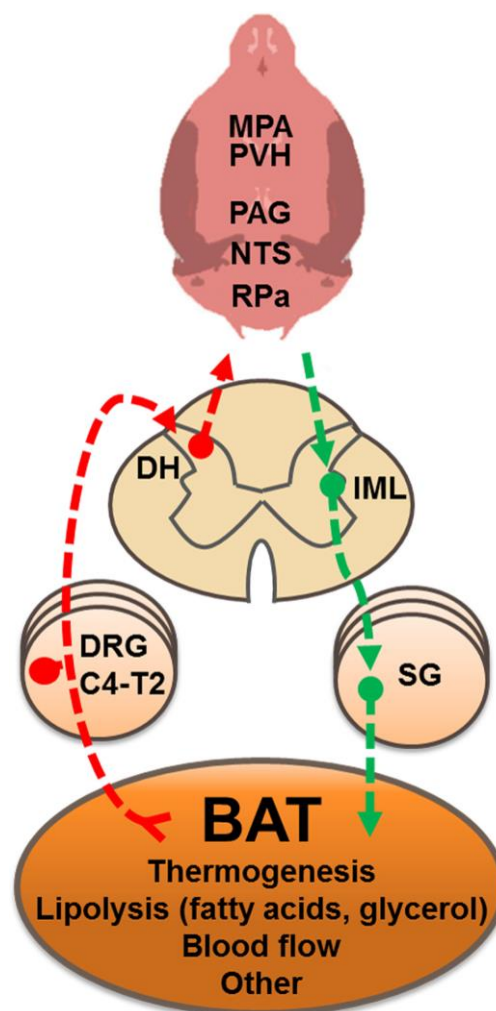


Figure 6. Diagram of BAT SS-SNS feedback loops.

A diaphragmatic representation of the efferent sympathetic (green arrows) and afferent sensory (red arrows) brain-IBAT neural feedback circuit for control of IBAT functions. BAT, brown adipose tissue; C4-T2, cervical and thoracic vertebral level; DH, dorsal horn; DRG, dorsal root ganglia; IML, intermediolateral cell column; MPA, medial preoptic area; NTS, nucleus of the solitary tract; PAG, periaqueductal gray; PVH, paraventricular hypothalamic nucleus; RPa, raphe pallidus nucleus; SG, sympathetic ganglia.

see the DR as a component of the SNS outflow to IBAT with our viral neurocircuit labeling method.

We found the MPA, MPO and MnPO were mostly involved with the SNS outflow to, but not the SS inflow from, IBAT and these sites are involved in the IBAT thermoregulatory SNS responses to skin cooling (Nakamura & Morrison, 2008a). This greater SNS outflow from the MPA than SS inflow supports our previous finding of relatively sparse MPA H129-infected neurons from IBAT compared with many other areas (Vaughan & Bartness, 2012), but impressive PRV152-infected neurons (Bamshad et al., 1999; Leitner & Bartness, 2009; Song et al., 2008). Despite the relatively small number of MPA-MPO-MnPO SS circuit neurons, this by no means necessarily lessens its contribution to thermoregulatory signaling from the skin (Nakamura & Morrison, 2008a, 2008b) as the MPA-SS innervation in the present study mainly reflects the SS pathway originating from the IBAT. IBAT increases thermogenesis in response to cold exposure in decerebrate rats. However, where most of the midbrain and all of the forebrain are surgically separated from the hindbrain/peripheral nervous systems (Nautiyal et al., 2008), the necessity of SS input to the MPA or other rostral brain sites combined with the presence of PRV152+H129 dually-infected neurons in the hindbrain indicates that, unlike some of the models proposed for the BAT SNS thermoregulatory control with the MPA as the 'origin' of the descending signals and recipient of the ascending afferent information [*e.g.*, (Morrison, Madden, & Tupone, 2012)], SS input may crosstalk with central SNS outflow across the neuroaxis including the hindbrain (Nautiyal et al., 2008). Indeed, this notion is supported by thermal sensory inputs to the midbrain and caudal hindbrain implicated in the thermal response to skin cooling and thermal control in general [*e.g.*, (Uno et al., 2003)].

Table 1. Distribution of sympathetic (PRV152) and sensory (H129) neurons across the neuraxis

	PRV152	H129	PRV152+H129	Percentage of PRV152+H129
Hindbrain				
7N	67.4±12.1	57.6±19.5	11.8±3.0	10.4±1.3
10N	16.0±8.2	14.5±1.2	2.0±1.6	5.7±4.7
12N	24.3±5.2	17.0±8.0	0.7±0.3	1.9±1.0
PnO	38.0±16.0	27.4±9.6	6.4±2.5	11.3±1.1
PnC	51.4±15.1	42.6±8.1	9.2±2.5	10.6±1.9
SuVe	74.2±20.8	59.6±16.1	13.2±2.4	12.1±1.8
MPB	36.6±10.3	40.5±8.4	7.6±1.5	12.7±1.1
LPBI	6.3±2.9	5.3±1.6	1.7±0.8	7.3±4.7
LPBC	23.6±7.1	13.4±5.3	3.0±1.2	9.5±4.3
MPBE	11.3±5.6	11.3±4.7	2.0±0.7	8.0±2.6
LC	29.8±9.9	28.3±5.7	5.0±1.5	8.5±2.4
Bar	16.3±6.6	9.7±4.6	3.8±1.2	11.6±4.8
Pr5	29.0±13.3	26.8±9.6	5.5±2.3	11.3±0.8
LDTg	13.3±4.6	4.3±0.7	1.7±0.7	12.3±7.0
Mo5	18.7±3.3	20.7±1.1	3.7±0.5	10.2±1.0
RMg	83.8±25.9	87.2±17.7	17.2±4.1	11.4±1.2
RPa	159.2±34.0	148.8±41.6	36.2±9.2	12.6±1.1
ROb	154.5±55.9	116.0±14.1	30.5±5.0	12.9±1.4
Gi	52.8±28.8	39.0±13.5	6.2±3.0	6.4±2.2
LPGi	31.0±6.6	29.0±6.8	7.0±1.3	13.0±1.2
DPGi	42.0±17.3	42.3±16.5	7.3±2.8	8.5±1.0
GiV	108.0±19.7	127.2±32.4	19.0±3.0	9.2±1.0
PCRT	14.0±4.1	10.7±3.9	1.3±0.5	4.6±2.0
IO	152.7±41.6	129.3±15.0	25.7±6.1	9.8±1.8
LRt	120.7±36.1	96.0±24.0	18.7±2.9	9.4±1.0
MdV	59.3±39.9	43.0±18.0	9.0±5.9	6.8±3.4
NTS	275.7±60.4	201.2±58.9	33.4±4.2	7.3±1.4
SolC	28.3±5.2	21.0±4.7	5.2±1.1	10.5±2.1
SolCe	7.2±2.8	5.3±2.0	1.3±0.4	9.3±2.6
SolDL	31.8±15.2	27.9±14.8	4.7±1.9	7.7±1.7
SolG	21.7±10.9	15.3±4.5	2.8±0.4	7.1±2.3
SolI	7.4±3.0	4.8±1.5	1.2±0.2	9.3±3.1
SolIM	25.3±8.8	19.5±4.1	3.7±1.3	7.9±2.2
SolM	97.3±12.0	66.0±14.5	12.7±4.3	7.2±2.0
SolV	11.7±3.4	10.8±3.5	2.0±0.2	8.6±1.3
SolVL	45.8±18.3	32.1±10.2	6.0±2.8	7.5±2.4
Pr	25.5±11.2	15.0±6.6	3.8±2.8	6.2±3.1
Midbrain				

PAG	260.6±51.3	109.2±28.8	32.0±5.8	9.6±1.5
DMPAG	32.4±9.3	12.2±4.7	2.8±1.11	6.3±1.2
DLPAG	26.0±6.1	8.4±2.6*	1.8±0.7	5.1±1.6
LPAG	60.0±11.5	30.0±6.9*	8.8±1.3	11.5±2.1
VLPAG	54.8±11.6	18.2±6.0	6.4±1.4	10.3±1.8
DR	23.6±6.7	7.0±2.2*	2.4±0.6	7.7±2.4
DpMe	54.3±20.3	19.0±6.4	6.0±1.9	8.5±3.1
R	18.0±5.5	9.6±2.9	2.6±0.2	9.4±3.3
VTA	32.5±12.7	13.5±4.6	3.5±1.2	7.6±2.8
Forebrain				
MPA	79.8±8.9	6.4±3.0*	2.2±1.0	3.0±1.7
MPO	36.4±13.8	6.8±2.6*	1.4±0.9	5.0±3.0
MnPO	17.4±5.2	0.8±0.8*	0.2±0.2	2.0±2.0
LPO	23.8±10.5	1.5±0.8	0.8±0.4	1.7±1.0
AVPO	32.6±9.5	7.8±5.9	1.4±1.0	2.8±1.7
AVPe	23.5±7.9	3.3±1.8	1.3±0.8	3.3±2.3
SCh	13.5±6.9	4.5±1.7	0.5±0.4	1.2±1.0
AHA	7.4±2.2	3.8±2.2	1±0.4	9.2±4.3
AHP	22.8±9.1	9.8±5.5*	2.4±1.3	5.8±2.4
PVH	277.4±55.5	237.8±58.7	48.8±8.7	11.2±1.8
PaAP	15.0±4.9	14.8±7.2	3.5±1.7	10.7±3.2
PaDC	30.6±7.3	36.4±11.3	6.2±1.7	8.9±3.1
PaMP	137.8±22.1	129.8±32.8	23.6±4.2	10.4±1.7
PaMM	12.2±4.9	7.2±2.3	1.8±1.1	6.8±4.5
PaLM	36.0±6.8	35.3±10.7	5.8±1.7	8.5±1.4
PaV	16.7±2.5	16.3±4.2	3.3±1.4	12.6±5.8
PaPo	22.7±12.0	25.4±12.5	7.6±5.2	8.4±2.3
Arc	19.6±7.1	8.2±2.1	2.0±0.9	5.9±2.6
LH	101.6±20.8	40.0±3.9	11.8±1.7	9.3±0.6
VMH	6.4±4.1	0	0	0
DM	83.3±31.8	30.3±5.8	8.7±1.7	9.8±2.3
PH	39.8±12.9	15.8±1.5	5.0±1.1	11.1±1.5
ZI	18±11.0	8.6±4.5	1.2±0.8	2.6±1.7
SubZI	31.6±4.6	22.4±8.9	6.8±2.0	13.5±3.9

Data are expressed as mean number of neurons per brain region ± SEM (n=5), *p<0.05 vs. PRV152. 7N, facial nucleus; 10N, dorsal motor nucleus of the vagus nerve; 12N, hypoglossal nucleus; AHA, anterior hypothalamic area, anterior part; AHP, anterior hypothalamic area, posterior part; Arc, arcuate nucleus; AVPe, anteroventral periventricular nucleus; AVPO, anteroventral preoptic nucleus; Bar, Barrington's nucleus; DLPAG, dorsolateral periaqueductal gray; DM, dorsomedial hypothalamic nucleus; DMPAG, dorsomedial periaqueductal gray; DPGi, dorsal paragigantocellular nucleus; DpMe, deep mesencephalic nucleus; DR, dorsal raphe nucleus; Gi, gigantocellular reticular nucleus; GiV, gigantocellular reticular nucleus, ventral part; IO, inferior olive; LC, locus coeruleus; LDTg, laterodorsal tegmental nucleus; LH, lateral hypothalamic area; LPAG, lateral periaqueductal gray; LPBC, lateral parabrachial nucleus, central part; LPGi, lateral paragigantocellular nucleus; LPO, lateral preoptic area; LPBI, lateral parabrachial nucleus, internal part; LRt, lateral reticular nucleus; MdV, medullary reticular nucleus, ventral part;

MnPO, median preoptic nucleus; Mo5, motor trigeminal nucleus; MPA, medial preoptic area; MPB, medial parabrachial nucleus; MPBE, medial parabrachial nucleus external part; MPO, medial preoptic nucleus; NTS, nucleus of the solitary tract; PaAP, paraventricular hypothalamic nucleus, anterior parvicellular part; PaDC, paraventricular hypothalamic nucleus, dorsal cap; PAG, periaqueductal gray; PaLM, paraventricular hypothalamic nucleus, lateral magnocellular part; PaMM, paraventricular hypothalamic nucleus, medial magnocellular part; PaMP, paraventricular hypothalamic nucleus, medial parvicellular part; PaPo, paraventricular hypothalamic nucleus, posterior part; PaV, paraventricular hypothalamic nucleus, ventral part; PCRT, parvicellular reticular nucleus; PH, posterior hypothalamic area; PnC, pontine reticular nucleus, caudal part; PnO, pontine reticular nucleus, oral part; Pr, prepositus nucleus; Pr5, principal sensory trigeminal nucleus; PVH, paraventricular hypothalamic nucleus; R, red nucleus; RMg, raphe magnus nucleus; ROb, raphe obscurus nucleus; RPa, raphe pallidus nucleus; Sch, suprachiasmatic nucleus; SolC, nucleus of the solitary tract, commissural part; SolM, nucleus of the solitary tract, medial part; SolVL, nucleus of the solitary tract, ventrolateral part; SubZI, sub zona incerta; SuVe, superior vestibular nucleus; VLPAG, ventrolateral periaqueductal gray; VMH, ventromedial hypothalamic nucleus

The highest percentage of double-labeled neurons reached ~13.0 % in several hindbrain, midbrain and hypothalamic regions. Compared with more than half of double-labeled SNS-SS feedback neurons in many of the same and other brain areas following injections of PRV152 and H129 into the IWAT (Ryu & Bartness, 2014), this lower rate of double-labeled neurons could reflect a lesser feedback from BAT versus WAT and/or may reflect a lesser number of BAT functions requiring neural feedback compared to WAT. That is, the SNS and SS innervations of BAT may primarily reflect its function in thermogenesis, whereas a neural feedback for its role in lipid and glucose clearance has not been, to our knowledge, tested and may not require neural feedback [for review see: (Cannon & Nedergaard, 2004b)]. By contrast, WAT stores/releases lipid and adipokines and has afferents sensitive to both increases in SNS drive (Bartness, Shrestha, Vaughan, Schwartz, & Song, 2010) and to leptin (Murphy et al., 2013), that latter perhaps conveying the amounts of stored lipid via this neural conduit (Bartness, Liu, Shrestha, & Ryu, 2014b).

We previously demonstrated that an intact SS innervation of BAT is necessary for normal acute cold exposure-induced IBAT thermogenic increases (Vaughan & Bartness, 2012). To our knowledge, no biochemical signal from BAT responsible for the activation of local SS nerve terminals has been identified at this time. In this regard, we previously reported (Song et al., 2009) that the firing frequency of decentralized SS nerve fibers

innervating IWAT was markedly increased when anesthetized hamsters were injected with the glucoprivic agent 2-deoxy-D-glucose known to drive SNS outflow and lipolysis (Brito et al., 2008). Those findings suggest that factors associated with activation of β_3 -adrenoceptors, such as fatty acids and glycerol, might activate BAT afferents. The necessity of lipolysis for the full effect of SNS/NE-induced BAT thermogenesis is demonstrated in brown adipocytes harvested from mice where ablation of all protein kinase A phosphorylation sites on the adipocyte intracellular protein perilipin A result in an abolished NE-induced lipolytic response and these mice exhibit a severely blunted (~70%) decrease in NE-induced thermogenesis *in vivo* (Souza et al., 2007). Other plausible functions for BAT SNS-SS feedback loops include IBAT afferents directly sensing changes in T_{IBAT} due to increases in SNS drive and/or to SNS-mediated marked increases in IBAT blood flow seen in cold-exposed Siberian hamsters, and laboratory rats and mice [\sim 15-100 fold or more; (Baron et al., 2012; Foster & Frydman, 1978; Puchalski, Bocker, Heldmaier, & Langefeld, 1987)]. Such a role for SS feedback in the control of local blood flow has been repeatedly proposed [*e.g.*, (Holzer, 2006; Loesch, 2002)]. Therefore, given that our FB tracing revealed several DRG (C4, C5 and T2) with the highest numbers of projections to IBAT, this may suggest contribution of more than one population of SS nerve bundles with heterogeneous capacity to sense the changes in local temperature, as observed in other organs (Borzan, LaGraize, Hawkins, & Peng, 2005), in blood flow and/or lipolysis-related factors.

In order to further understand both the functional and neuroanatomical basis underlying SNS-SS interaction relative to IBAT thermogenesis, we injected CL316,243, a highly selective and potent β_3 -adrenoceptor intra-IBAT to determine the vertebral levels at which DRG sensory neurons innervating IBAT are activated by β_3 -adrenoceptor

stimulation. Our goal was to approximate the naturally-occurring stimulation of these receptors by the SNS release of NE parenchymally, but do so specifically to β_3 -adrenoceptors using CL316,243. CL316,243 significantly increased T_{IBAT} within 10 min after injection, activated C2-C4 DRG as evidenced by significantly increased c-Fos immunolabeling in DRG neurons pre-labeled with FB ipsilateral to the injection compared with the contralateral control side. Functionally, CL316,243 intra-IBAT injections significantly increased T_{IBAT} and afferent nerve activity within the same 20 min time frame.

Collectively, our results show persuasive evidence of the BAT SNS-SS neural feedback loops with a coordinated or multiple redundant controls of thermoregulatory functions. In addition, we demonstrated that sympathetic stimulation directly activates BAT-associated DRG, and hence sensation, perhaps in relation to its thermogenic and/or lipolytic response. Finally, the approach of direct, intra-IBAT injection combined with c-Fos-ir in DRGs and/or electrophysiologic assessment of BAT afferent activity provides a model system with which to determine BAT sensory nerve activators analogous to our study of WAT afferents using the same methodologies (Murphy et al., 2013).

2.6 Author contributions

T.J.B, V.R., Y.L., and C.V. designed the neuroanatomical tracing experiments. V.R. performed the tracing, the BAT temperature recording, and DRG immunostaining experiments. T.J.B. and J.G. designed and J.G. performed the neurophysiological BAT afferent recording experiments.

3 LIPOLYSIS SENSATION BY WHITE ADIPOSE TISSUE AFFERENTS TRIGGERS BROWN FAT THERMOGENESIS

John T. Garretson^{1,3}, Laura A. Szymanski², Gary J Schwartz⁴, Bingzhong Xue^{1,2,3}, Vitaly Ryu^{2,3}, Timothy J. Bartness^{1, 2, 3}

¹Neuroscience Institute, Georgia State University, Atlanta GA 30303, USA.

²Department of Biology, Georgia State University, Atlanta GA 30303, USA.

³Center for Obesity Reversal, Georgia State University, Atlanta GA 30303, USA.

⁴Department of Medicine and Neuroscience Albert Einstein College of Medicine, Bronx NY 10461, USA.

Published in *Molecular Metabolism* on June 6th 2016

3.1 Abstract

Objective: Metabolic challenges, such as a cold environment, stimulate sympathetic neural efferent activity to white adipose tissue (WAT) to drive lipolysis, thereby increasing the availability of free fatty acids as one source of fuel for brown adipose tissue (BAT) thermogenesis. WAT is also innervated by sensory nerve fibers that network to metabolic brain areas; moreover, activation of these afferents is reported to increase sympathetic nervous system outflow. However, the endogenous stimuli sufficient to drive WAT afferents during metabolic challenges as well as their functional relation to BAT thermogenesis remain unknown. **Method:** We tested if local WAT lipolysis directly activates WAT afferent nerves, and then assessed whether this WAT sensory signal affected BAT thermogenesis in Siberian hamsters (*Phodopus sungorus*). **Results:** 2-deoxyglucose, a sympathetic nervous system stimulant, caused β -

adrenergic receptor dependent increases in inguinal WAT (IWAT) afferent neurophysiological activity. In addition, direct IWAT injections of the β_3 -AR agonist CL316,243 dose-dependently increased: 1) phosphorylation of IWAT hormone sensitive lipase, an indicator of SNS-stimulated lipolysis, 2) expression of the neuronal activation marker c-Fos in dorsal root ganglion neurons receiving sensory input from IWAT, and 3) IWAT afferent neurophysiological activity, an increase blocked by antilipolytic agent 3'5-dimethylpyrazole. Finally, we demonstrated that IWAT afferent activation by lipolysis triggers interscapular BAT thermogenesis through a neural link between these two tissues. **Conclusions:** These data suggest IWAT lipolysis activates local IWAT afferents triggering a neural circuit from WAT to BAT that acutely induces BAT thermogenesis.

3.2 Introduction

Adipose tissue is connected to the CNS via afferent and efferent nerve fibers directly innervating each fat depot. While adipose efferents are entirely catecholaminergic (Youngstrom & Bartness, 1995), adipose afferents are primarily unmyelinated c-fibers—positive for substance p and calcitonin gene-related peptide (CGRP)—and receptive to a variety of stimuli (Giordano et al., 1996). Although the anatomical reality of WAT afferents was initially discovered by Fishman and Dark (Fishman & Dark, 1987), the first functional role of neural afferents arising from white adipose tissue (WAT) was demonstrated by Nijima (Nijima, 1998) by injecting the adiposity hormone leptin directly into WAT then measuring neurophysiological activity in decentralized (sensory) nerve fibers connected to the tissue. These results have been interpreted to suggest that local leptin, secreted by WAT in proportion to adipocyte size

and number, is transduced as a neural signal proportional to the amount of stored energy (Caro, Sinha, Kolaczynski, Zhang, & Considine, 1996). However, WAT afferents also increase their neurophysiological activity in response to adenosine and bradykinin—indicating an active role of these afferents in blood pressure sensation (Shi et al., 2012). Despite the variety of signals sensed by WAT afferents, each neurophysiologically effective stimulus similarly increases sympathetic nervous system (SNS) drive to WAT and other tissues in a positive feedback WAT-brain-SNS reflex circuit termed the “adipose afferent reflex” (AAR) (Nijima, 1999; Shi et al., 2012). Indeed, our viral tracing studies expose the neuroanatomical framework for this AAR wherein WAT afferents are networked to WAT efferents throughout metabolically relevant CNS nuclei (*e.g.* intermediolateral nucleus of the spinal cord, nucleus of the solitary tract, periaqueductal gray, dorsomedial, lateral, arcuate and paraventricular hypothalamus). (Bartness & Song, 2007b). In addition, these studies reveal a high degree of neuroanatomical overlap between neuronal populations at multiple peripheral and central levels of the neuraxis including WAT sensory and brown adipose tissue (BAT) SNS innervation (Song et al., 2009; Vaughan et al., 2011). Thus, functional and neuroanatomical sensory-motor links between WAT and the SNS have been established (Murphy et al., 2013; Ryu & Bartness, 2014); however, the sensitivity of WAT afferents to local lipolytic activity of the tissue and the potential for these afferents to induce heat production in BAT have not been fully investigated.

Among all functions of WAT, its catabolism and subsequent efflux of stored energy is a rapid and necessary process for the release of fuels when energy demand is high with an evolutionarily highly conserved mechanism across species including non-mammals (Bartness et al., 2014a; Migliorini et al., 1992). During an energetic challenge

such as cold exposure, norepinephrine released by axon terminals of post ganglionic SNS neurons binds β_3 -adrenoreceptors (β_3 -AR)—present on adipocytes (Lafontan et al., 1997)—initiating a lipolytic cascade that is dependent on the phosphorylation of hormone sensitive lipase (HSL) and leads to the preferential release of long-chain free-fatty acids (FFAs) and glycerol as useable energy (Bartness & Song, 2007a; Belknap et al., 1981). Peripheral injection of 2-deoxyglucose (2DG), a glucoprivic and thus sympathomimetic drug, causes SNS dependent mobilization of triglycerides from WAT and also increases WAT afferent activity within minutes (Song et al., 2009). This efflux of substrates from WAT occurs locally first, then is circulated throughout the body/brain and oxidized as fuel when glucose is not readily available/sufficient for energy demand (Lass, Zimmermann, Oberer, & Zechner, 2011) or converted to heat via uncoupled oxidative phosphorylation by BAT, a tissue similarly dependent on SNS innervation to trigger thermogenesis. Thus, we hypothesize that WAT afferents activated by glucoprivation may be sensing locally released lipolytic products thereby transducing lipolysis into rapid neural signals communicated to the CNS (Song et al., 2009). If this is true, then lipolysis sensation by WAT afferents likely induces BAT thermogenesis because 1) lipolysis provides substrates that are required for BAT thermogenesis (Haemmerle et al., 2006; Labbé et al., 2015) and 2) the strikingly similar patterns of WAT afferent and BAT efferent neural connectivity (Song et al., 2009; Vaughan et al., 2011). To investigate these hypotheses, we first tested if WAT lipolysis and/or its products were sufficient to drive spinal afferent nerves receiving sensory input from subcutaneous inguinal WAT (IWAT), then we tested whether stimulation of lipolysis sensing IWAT afferents triggers interscapular BAT (IBAT) thermogenesis.

3.3 Methods and Materials

3.3.1 Animals

Adult male Siberian hamsters (*Phodopus sungorus*; ~3-4 months old) from our breeding colony were individually housed in a long day photoperiod (16h:8h light:dark cycle; at 22 ± 2 °C) with free access to water and rodent chow. Siberian hamsters were used because of the expanding literature characterizing the anatomy of their neuro-adipose axis (Bartness et al., 2014a) and the apparent conservation of adipocyte catabolism among mammalian species (Migliorini et al., 1992). All procedures were approved by the Georgia State University Institutional Animal Care and Use Committee and are in accordance with Public Health Service and United States Department of Agriculture guidelines.

3.3.2 Neurophysiological recordings of IWAT afferent nerve activity

Siberian hamsters ($n=13$, unilateral recordings; $n=16$, bilateral recordings) were anesthetized with ketamine (100 mg/kg)/xylazine (10 mg/kg, i.p.), then dissected by a 2 cm dorsal ventral incision. IWAT and connective tissue were resected and isolated from surrounding tissue, after which the nerves innervating right and/or left IWAT were exposed. Single nerve bundles from these WAT nerves were isolated and severed proximal to the electrode placement site to disconnect efferent fibers, finally the afferent ends of decentralized nerves were placed on platinum-iridium (32-gauge) hook electrodes. A petroleum jelly mineral oil mixture (1:1) was applied to the sites to completely surround the electrode/nerve connection, then warm mineral oil was pooled into the recording area to insulate electrical noise, prevent aqueous infusions from leaking to other tissue, secure the nerve on the electrode, and reduce drying of tissue. A

steady anesthetic plane was maintained with supplemental ketamine (50 mg/kg, s.c.) by examining toe pinch and eye blink responses throughout the recordings.

For unilateral recordings, baseline neurophysiological spike activity in IWAT afferents was recorded for 5 min as reported (Song et al., 2009), then hamsters received either propranolol (40 mg/kg, i.p.) or sterile saline vehicle (i.p.) and spikes were recorded for an additional 5 min. Finally, 2DG (500 mg/kg, s.c.) was administered and IWAT afferent activity was measured for an additional 10 min.

For bilateral recordings, decentralized nerves from left and right IWAT were each placed on electrodes then three sharp stainless steel needles connected with Silastic tubing to Hamilton microsyringes (Hamilton Company, Reno, NV) were inserted into left and right IWAT along the lateral-coronal plane spaced 4-5 mm apart at a depth of approximately 4-5 mm each (diagram of procedure, Fig. 8a). Ten minutes of basal electrical activity was measured followed by 15 μ l of the β 3 adrenergic receptor agonist CL316,243 (CL, 0.2 ng/kg or 0.1 ng/kg) and saline vehicle was infused simultaneously into the opposite IWAT pad at a rate of 3.0 μ l/min for 5 min. CL stimulation is commonly used to simulate SNS activity to adipose tissue and reliably induces lipolysis *in vivo* and *in vitro* (Atgie, Faintrenie, Carpenne, Bukowiecki, & Geloan, 1998b; Umekawa, Yoshida, Sakane, & Kondo, 1997). A separate cohort of animals was pretreated with the antilipolytic drug 3'-dimethylpyrazole (DMP, 12 mg/kg, i.p.) (Gerritsen & Dulin, 1965; Locci-Cubeddu & Bergamini, 1983; Masiello et al., 2002) 20 min before IWAT infusions of CL (0.2 ng/kg) and saline. Eicosapentanoic acid (EPA) and arachidonic acid (AA) are both highly mobilized from adipose tissue during stimulated-lipolysis at ratios to other mobilized FAs seemingly conserved across species (Conner, Lin, & Colvis, 1996; Raclot & Groscolas, 1993). Thus, EPA and AA were

used as representative FAs—of potentially many more FA species—that may signal acute and local lipolysis to WAT afferents. Doses for EPA[2.94 μ M in 15 μ l Tocrisolve, ~8.91 mg/kg] and AA[0.27 μ M in 15 μ l Tocrisolve, ~0.81 mg/kg] were calculated from studies that measured net output of lipolytic products from adipose fragments in rats (Raclot & Groscolas, 1993; Raclot et al., 1995); accordingly, physiologically relevant levels of EPA and AA were injected into WAT to assess whether lipolytic products stimulate WAT afferents directly. Infusions of drug or vehicle were counterbalanced by side to control for possible side bias of IWAT afferent innervations.

Extracellular signals were amplified 10000 times with a differential AC amplifier set to low pass filter 100 Hz and high pass filter 1000 Hz (Model 1700; A-M Systems, Sequim, WA). Analog signals were visualized on an oscilloscope (Model 2530, BK Precision, Yorba Linda, CA), audio analyzer (Model 74-30-1; FHC, Bowdoin, ME), and digitized through a Digidata data acquisition system (Model 1440a; Molecular Devices, Sunnyvale, CA) at a 20,000 Hz sampling rate. Recordings were captured with accompanying Clampex 10.3 software and analyzed for the number of spikes based on a voltage threshold two standard deviations above mean non-signal noise via Clampfit 10.3 data analysis software package. All counted waveforms were visually screened, and non-physiological noise detected with the set threshold was easily identified and removed from analysis. Percentage change from baseline nerve activity was calculated for 10 min bins for each nerve recording session, then the difference between IWAT afferent activities from CL injected pads and saline injected pads was calculated and used for statistical analysis.

3.3.3 Western blot analysis of lipolysis induced by CL

Using an identical infusion protocol to bilateral electrophysiology experiments, but without IWAT afferent dissection/dissociation from the CNS, CL (0.1 ng/kg or 0.2 ng/kg) was infused into one IWAT pad simultaneously, while saline vehicle was infused into the contralateral IWAT pad. Animals receiving a high dose of CL (0.2 ng/kg) were pretreated with either DMP (20 min prior, 12 mg/kg, i.p.) or saline vehicle, and animals receiving a lower dose of CL (0.1 ng/kg) received no pretreatment. Fifteen minutes after the start of bilateral infusions (15 μ l each pad, 3 loci, 3.0 μ l/min for 5 min), ~100 mg of each IWAT pad was quickly removed, snap frozen in liquid nitrogen to preserve protein, then stored at -80 °C until analysis by Western blot.

Frozen adipose tissue samples were homogenized using microcentrifuge tubes containing 0.5 mm zirconium oxide beads homogenization buffer containing 50 mM HEPES, 100 mM NaCl, 10 % SDS, 2 mM EDTA, 0.5 mM DTT, 1 mM benzamidine, protease inhibitor cocktail (Calbiochem, EMD Chemicals, Gibbstown, NJ), and phosphatase inhibitor cocktail (Thermo Fischer Scientific, Rockford, IL) at a ratio of 1:2 tissue weight (mg): homogenization buffer (μ l). The samples were agitated 2 X 1 min using a bullet blender tissue homogenizer and then centrifuged at 13,000 g for 10 min at 4 °C. The infranatant was collected, aliquoted and stored at -80 °C until protein content was determined. Samples were diluted 1:10 in dH₂O and the protein content of the tissue extract was determined using the bicinchoninic acid protein assay kit (Thermo Fisher Scientific, Rockford, IL). Samples containing 10 μ g of protein were mixed with loading buffer and heated at 95 °C for 5 min, electrophoresed on a low-bis SDS-PAGE[10 %: 0.08 % acrylamide:bis] and transferred to polyvinylidene difluoride membranes. Membranes were cut in half so that immunoblotting could be done on

duplicate lanes with different antibodies from the same gel. Cut membranes were incubated in Tris buffered-saline (TBS) with 4 % nonfat dry milk and 0.3 % Tween blocking solution for 2 h, then incubated in primary antibody at 4 °C (anti-ATGL, anti-HSL, anti-phospho-HSL, anti-beta-actin, 1:1000; Cell Signaling Technology, Danvers, MA) in TBS-4 %milk-0.3 % Tween for 2 days. Immunoblots were rinsed 4 X 5 min in TBS-Tween (TBST) and then incubated with secondary antibody (Anti-rabbit IgG HRP-linked antibody, 1:1000; Cell Signaling Technology, Danvers, MA) for 2 h at room temperature. The immunoblots were rinsed 3 X 10 min in TBST and then incubated with LumiGLO chemiluminescent kit (Cell Signaling Technology, Danvers, MA) to reveal bands.

3.3.4 Fast Blue (FB) labeling and CL administration

Siberian hamsters ($n = 10$) were anesthetized with ketamine/xylazine (100 mg/kg, 10 mg/kg; i.p.) and ventral lateral 2 cm incisions were made to expose both IWAT pads. The neuronal tracer FB (1.0 %; EMS-CHEMIE GmbH, Gross-Umstadt, Germany) was injected with a microsyringe into eight separate loci (2 μ l/locus) of the left and right IWAT. After the last injection, the incision was closed with sterile wound clips and ketofen (5 mg/kg, s.c.; Fort Dodge Animal Health, Fort Dodge, IA) was administered for 3 d postinjection to minimize postoperative discomfort.

One week later, CL (0.2 ng/kg in 0.9 % sterile saline) was injected into one IWAT pad across eight separate loci with nearly simultaneous intra-contralateral IWAT injections of the saline vehicle (2 μ l/locus for a total of 16 μ l) served as a within animal control. Injections of drug or vehicle were counterbalanced by side to control for possible side bias of IWAT afferent innervations. The skin was gently pinched closed,

and sterile saline-soaked gauze was laid over top of the incision site for 60 min until hamsters were sacrificed and DRGs processed for c-Fos immunohistochemistry.

3.3.5 Tissue fixation and c-Fos immunostaining on DRGs

Hamsters were overdosed with pentobarbital sodium (Sleep Away; 300 mg/kg) and transcardially perfused with 75 ml of 0.9 % heparinized saline followed by 150 ml 4.0 % paraformaldehyde in 0.1 M PBS, pH 7.4, directly into the aorta. The DRGs (T12-L2) were extracted, the epineurium debrided and postfixed in the same fixative for 15 min at 4 °C, then transferred to a 18.0 % sucrose solution in 0.1 M PBS with 0.1 % sodium azide and stored at 4 °C until they were sectioned at 20 μ m on a freezing microtome. Sections were received directly onto slides (Superfrost Plus, VWR International) in three series with every fourth section on the same slide. This procedure yielded ~24 sections with each slide containing eight sections. Thus, an estimated total neuronal number per ganglion could be obtained by multiplying the number per section by 24 or averages here by 8.

For DRG c-Fos immunostaining on slides, sections were rinsed in 0.1 M PBS (2 x 15 min) followed by 1 h blocking in 5.0 % normal horse serum (NHS; Vector Laboratories) and 0.3 % Triton X-100 in 0.1 M PBS. Sections were then incubated in primary rabbit anti-c-Fos (1:500; sc-52; Santa Cruz Biotechnology) antibody with 10.0 % NHS and 0.3 % Triton X-100 in 0.1 M PBS overnight. Next, the sections were incubated in secondary donkey anti-rabbit Cy3 (1:200; Jackson ImmunoResearch) for 3 h, rinsed with 0.1 M PBS (3 x 15 min) and coverslipped with ProLong Gold Antifade Reagent (Life Technologies). All steps were performed at room temperature.

3.3.6 Brown fat transponder implantation, temperature recordings, and acute surgical denervation of IWAT

Siberian hamsters ($n = 36$) were anesthetized with ketamine/xylazine (100 mg/kg, 10 mg/kg, i.p.) and a dorsal 2 cm interscapular incision was made to expose IBAT. One electronic transponder (Bio Medic Data Systems) with a built-in temperature sensor was gently implanted under one IBAT pad of each hamster, the temperature of which was read with a handheld DAS-7007R scanner (Bio Medic Data Systems) as we have used successfully previously (Brito et al., 2007; Ryu, Garretson, Liu, Vaughan, & Bartness, 2015a; Song et al., 2008). The incision was closed with sterile wound clips.

After two weeks of recovery, hamsters were again anesthetized with ketamine/xylazine (100 mg/kg, 10 mg/kg, i.p.) then a ventral lateral 3 cm incision was made to expose right IWAT. Nerves innervating the ventral portion of IWAT were either left intact, or surgically destroyed (Vaughan et al., 2014) to test whether WAT lipolysis sensed by local afferents could drive BAT thermogenesis (diagram of procedure, Fig. 12a). CL (0.2 ng/kg) or saline vehicle, was injected intra-right ventral IWAT exactly as above at three loci (5 μ l/locus for a total of 15 μ l). This dose was chosen based on neurophysiological recordings demonstrating dose-dependent IWAT afferent activation, Western blot data confirming increased lipolysis by significant pHSL/HSL increases of the pad delivered, and previous studies that determined CL microinjections of 0.2 ng/kg into IBAT did not affect core body temperature (Ryu et al., 2015). The incision was immediately covered with a warm saline-soaked gauze pad, animals were then moved to a circulating water warming pad set to 37 ° C and remained there under heat lamp with ambient air surrounding the animals stable at ~35-36 ° C. Temperature recordings from

IBAT were started immediately after the animal reached the warming pad then monitored every 5 min for 1 h postinjection as done previously (Ryu et al., 2015a). Core body temperature in these anesthetized animals was measured using a rectal temperature sensor connected to BAT-10 Thermometer (Physitemp Instruments).

3.3.7 Data analysis

3.3.7.1 Neurophysiological recordings

The numbers of WAT afferent action potentials occurring as a function of time were integrated into either 30 sec bins and compared across treatments for unilateral recordings, or 10 min bins for bilateral recordings, where the onset of infusion up to 20 min post infusion were compared against the pre-infusion 10 min baseline recordings. Percent change mean nerve activity from contralateral (vehicle-infused) IWAT was compared using one-way ANOVA for each treatment from baseline nerve activity. Nerve activity at individual time points across experiments were compared using Student's *t* tests with Bonferroni correction via SigmaPlot (v12.3; Systat Software Inc., San Jose, CA). Results were considered significant if mean nerve activity in unilateral recordings—or percent change from baseline activity in bilateral recordings—differed from vehicle control, $p < 0.05$.

3.3.7.2 Western blot protein analysis

Band intensity was quantified based on optical densitometry measurements using ImageJ (US National Institutes of Health, Bethesda, MA). The values for HSL/actin, and pHSL/actin were collected and ratios of pHSL/HSL were compared using paired samples *t*-tests between ipsilateral and contralateral IWAT within animals via SigmaPlot (v12.3; Systat Software Inc., San Jose, CA). Data are displayed (Fig. 9) as

arithmetic change in pHSL/HSL for clarity of presentation. Results were considered significant if mean pHSL/HSL from CL-infused pads differed from their contralateral vehicle-infused control, $p < 0.05$.

3.3.7.3 *c-Fos-ir and FB colocalization*

All labeled cells from three central sections of each DRG were counted from captured images by experimenters blind to treatment conditions. Raw totals for each label (*e.g.*, c-Fos and FB) as well as c-Fos+FB colocalized cells were compared between drug treatments using multiple Mann-Whitney U tests at each ganglionic level. In addition, the percentage of FB labeled cells expressing c-Fos was compared between drug treatments at each ganglionic level and combined across all ganglia to demonstrate the specificity of CL infusion to individual IWAT afferent neurons. Comparisons were considered statistically different when DRG labeling ipsilateral to CL infusion differed from the contralateral vehicle-infused counterpart, $p < 0.05$.

3.3.7.4 *BAT and rectal temperature recordings*

Temperature and change in temperature from the “0 min” time point were each analyzed by repeated measures two-way ANOVA by drug treatment and the state of IWAT neural connectivity. Preplanned comparisons between treatments at each time point were conducted using multiple Student’s t test with Bonferroni correction. Comparisons were considered statistically different when temperature or change in temperature from baseline differed from animals whose IWAT was injected with saline and innervating nerves intact, $p < 0.05$.

3.4 Results

2DG significantly increased neurophysiological activity of IWAT afferents in both 0-5 min and 5-10 min post-stimulus time intervals (Student's t test with Bonferroni correction; $n = 13$; baseline, $p = 0.143$; pretreatment, $p = 0.448$; 0-5 min, $p = 0.050$; 5-10 min, $p = 0.009$, Fig. 7), and the 2DG-induced increase was blocked by pretreatment with propranolol relative to saline infusions.

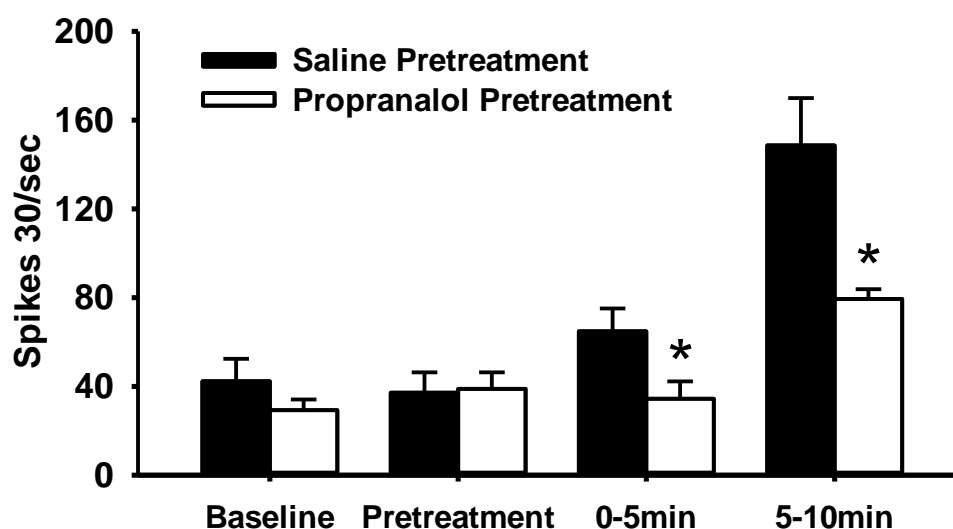


Figure 7. Glucoprivation increases IWAT multiunit nerve spiking in a β -AR dependent fashion. 2DG (500 mg/kg, i.p.) increased IWAT multiunit spiking, an effect blocked by pretreatment with β -AR antagonist propranolol. Bars represent number of spikes per 30 sec of IWAT afferents in hamsters that received either propranolol (40 mg/kg, s.c.) or saline vehicle (s.c.) pretreatment prior to 2DG application. * $p < 0.05$.

IWAT administration of the high dose of CL (0.2 ng/kg, Fig. 8b, c) also significantly increased neurophysiological spike activity beginning 5-10 min after the CL infusion, and lasting until the end of the recording session. IWAT neurophysiological spike activity was not increased in vehicle-injected contralateral IWAT or when CL was infused at a dose insufficient to induce lipolysis (0.1 ng/kg, Fig. 8b, c, Fig. 9). DMP blocked the ability of a high dose of CL to stimulate WAT afferents, and interestingly inhibited their activity from 10-20 min post-infusion (repeated measures ANOVA; CL 0.2 ng/kg, $n = 7$, $p = 0.002$; CL 0.1 ng/kg, $n = 4$, $p = 0.964$; CL 0.2 ng/kg + 12 mg/kg

DMP, $n = 5$, $p = 0.158$; Student's t test with Bonferroni correction; CL 0.2 ng/kg, $n = 7$, 0-10 min, $p = 0.022$, 10-20 min, $p = 0.002$; CL 0.1 ng/kg, $n = 4$, 0-10 min, $p = 0.779$, 10-20 min, $p = 0.968$; CL 0.2 ng/kg + 12 mg/kg DMP, $n = 5$, 0-10 min, $p = 0.979$, 10-20 min, $p < 0.001$).

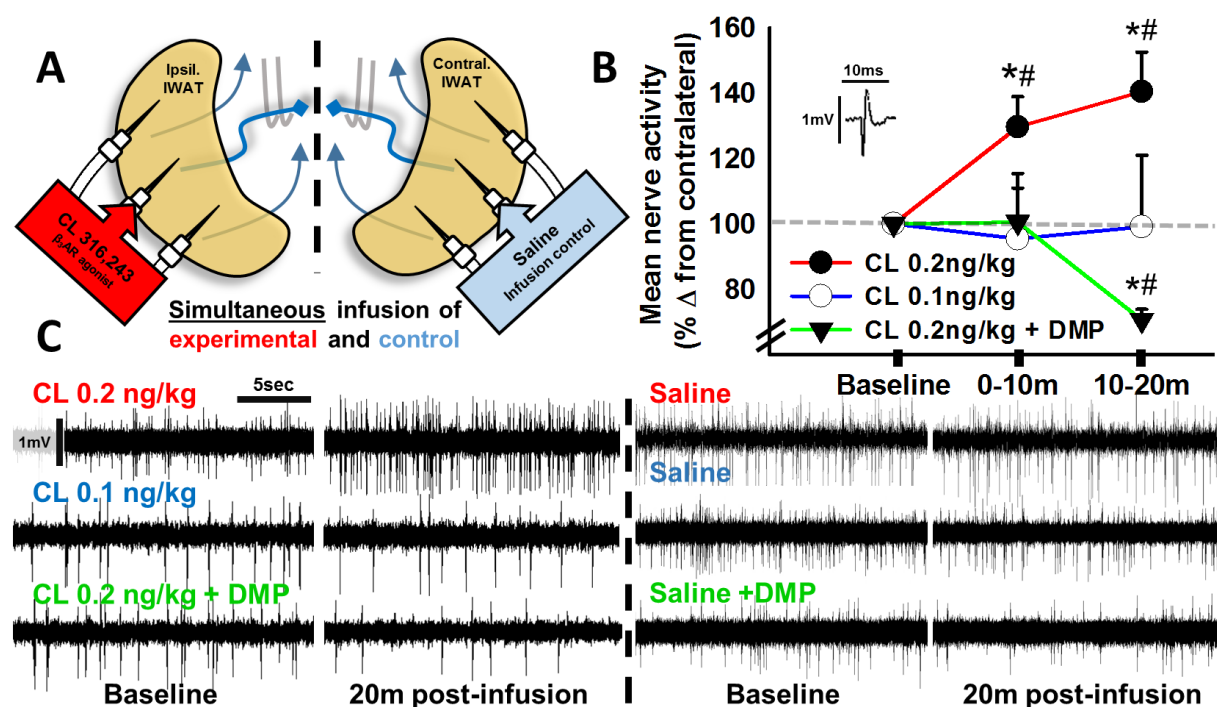


Figure 8. Intra-adipose β_3 -AR agonism increases IWAT multiunit nerve activity.

(a) Diagrammatic representation of real-time *in vivo* bilateral multiunit electrophysiology of WAT afferent nerves. Afferent nerves resected from ventrally exposed IWAT (blue curved lines), cut proximal to electrodes (gray hook pairs) to eliminate efferent interference, and analyzed for multiunit spike frequency over time. Symmetrically placed infusion needles indicate bilateral simultaneous infusion of lipolytic drug CL316,243 (CL, β_3 -AR agonist) and its sterile saline vehicle (no drug) in the contralateral negative control pad. (b) CL dose-dependently increased IWAT multiunit spiking, an effect blocked by pretreatment with the antilipolytic drug 3,5-dimethylpyrazole (DMP, 12 mg/kg, i.p). Data are expressed as a percentage change of activity from CL-infused pad over contralateral to eliminate whole animal IWAT nerve variability caused by the recording/injection procedure. Inset is a representative single spike to display acquired waveforms. (c) Representative (20 sec) traces from IWAT afferents and contralateral counterparts at baseline and 20 min post-infusion where the ipsilateral IWAT was infused with CL at either 0.2 ng/kg (top), 0.1 ng/kg (middle), or 0.2 ng/kg 20 min after pretreatment with antilipolytic drug DMP (bottom). Scale bars on first trace apply to all traces. Dotted line separates ipsilateral vs contralateral IWAT afferent recordings from each of the three representative animals. * $p < 0.05$.

CL-induced lipolysis was confirmed by examining the change in ratios between pHSL and HSL using Western blot as a well-established marker for fat-pad-specific sympathetically dependent lipolysis (Bartness et al., 2014a; Buettner et al., 2008). CL infusion (0.2 ng/kg) increased pHSL:HSL after 15 min but did not affect pHSL:HSL

when animals had been pretreated with DMP (12 mg/kg, CL 0.2 ng/kg) or CL only at a lower dose (0.1 ng/kg, Fig. 9) (paired t tests; CL 0.2 ng/kg, $n = 17$, $p = 0.015$; CL 0.1 ng/kg, $n = 5$, $p = 0.193$; CL 0.2 ng/kg + 12 mg/kg DMP, $n = 5$, $p = 0.515$). ATGL did not differ among treatment groups ($p > 0.05$).

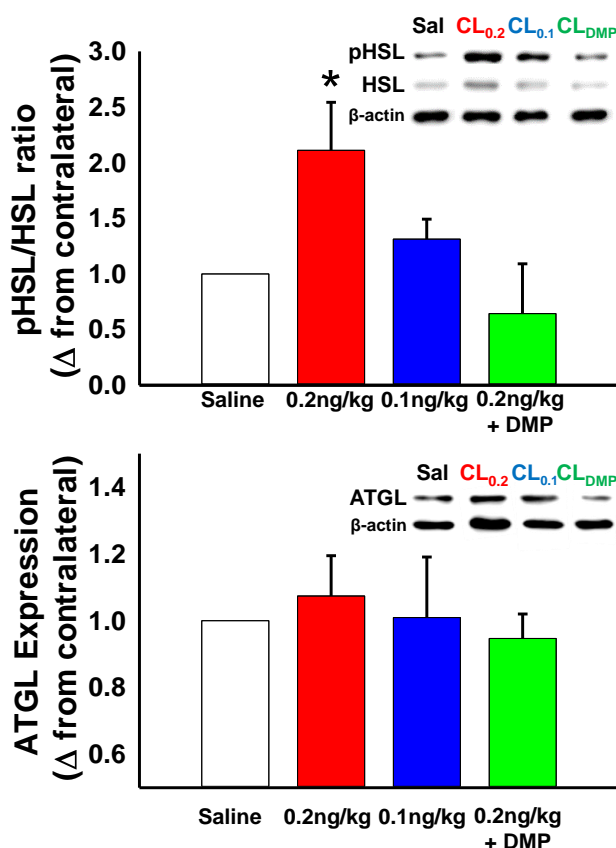


Figure 9. Intra-adipose CL increases pHSL/HSL indicating β_3 -AR induced lipolysis.

(a-b) Western blot analysis of the ratio of pHSL to HSL and ATGL reveals increased stimulated lipolysis with 0.2 ng/kg but not 0.1 ng/kg CL 15 min after infusion. In addition, pretreatment with DMP (i.p.) blocked CL stimulatory effects. Colored bars indicate (a) the mean ratio of pHSL to HSL and (b) ATGL in CL-injected IWAT compared with their saline-injected contralateral control IWAT (white bar). Error bars indicate SEM. Representative blots are provided as the inset with the label color and order of the bars used to indicate treatment (all units in ng/kg). * different from contralateral saline injected pad, $p < 0.05$.

FB neurotracing and c-Fos colocalization revealed a specific activation of DRG neurons connected directly to IWAT on the side ipsilateral to the high dose of CL infusion (0.2 ng/kg, Fig. 10a-f, j) despite nearly identical neurotracer labeling (Fig. 10h) and only a trend toward higher overall c-Fos-ir (Fig. 10i) (Mann-Whitney Rank Sum Tests; FB, T12, $n = 7$, $p = 0.905$; T13, $n = 7$, $p = 0.571$; L1, $n = 7$, $p = 0.556$; L2, $n = 7$, $p =$

0.486; L3, $n = 7$, $p = 0.286$; c-Fos-ir, T12, $n = 7$, $p = 0.556$; T13, $n = 7$, $p = 0.250$; L1, $n = 7$, $p = 0.111$; L2, $n = 7$, $p = 0.686$; L3, $n = 7$, $p = 0.905$; Colocalized, T12, $n = 7$, $p = 0.190$; T13, $n = 7$, $p = 0.502$; L1, $n = 7$, $p = 0.032$; L2, $n = 7$, $p = 0.030$; L3, $n = 7$, $p = 0.041$). In addition, the percent of FB labeled cells expressing c-Fos tended to increase in L3 but was significantly higher at ganglionic levels L1, L2, and overall across T12-L3 (Mann-Whitney Rank Sum Tests, T12, $n = 7$, $p = 0.215$; T13, $n = 7$, $p = 0.442$; L1, $n = 7$, $p = 0.032$; L2, $n = 7$, $p = 0.029$; L3, $n = 7$, $p = 0.063$; Total, $n = 35$, $p = 0.001$).

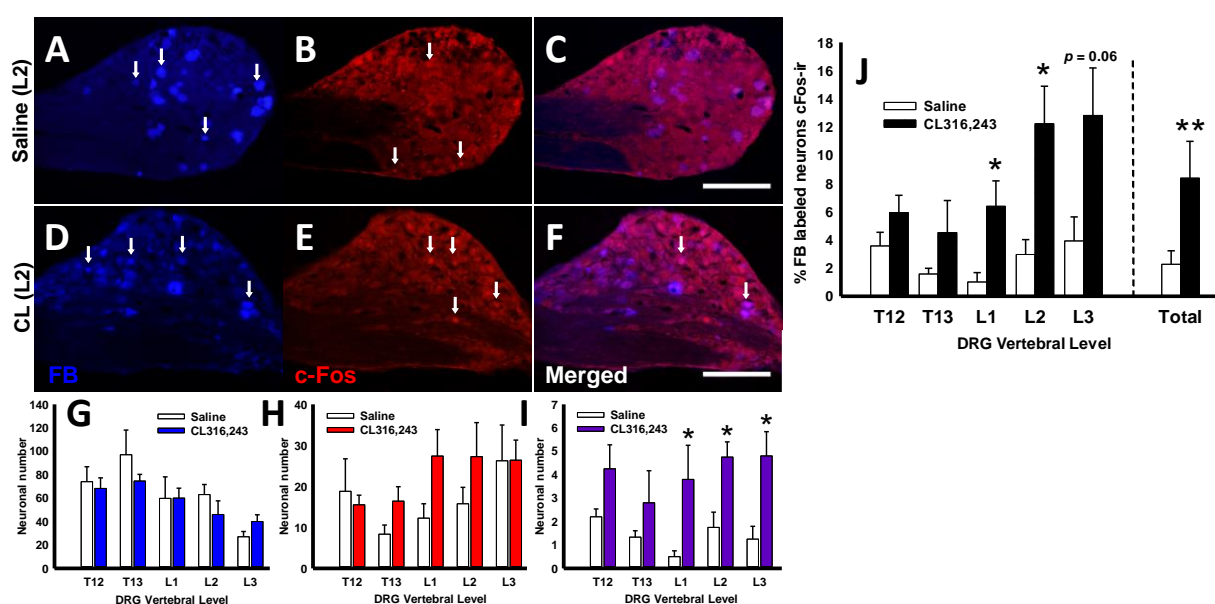


Figure 10. Intra-adipose β_3 -AR agonism increases c-Fos-ir in DRG neurons connected to IWAT. (a-f) Representative images of Fast Blue (FB, a, d) positive, c-Fos (b, e)-ir, and colocalized (c, f) neurons in DRG at the L2 vertebral level from the same animal both contralateral (top) and ipsilateral (bottom) to CL injections. Scale bar = 100 μ m. White arrows indicate some but not all labeled cells of interest and rows are separated by treatment. (g-i) Neuronal number counted from three central-most sections of each DRG, each animal, and both treatments positive for FB (g), c-Fos-ir (h), or both (i). (j) Percentage of FB labeled neurons expressing c-Fos at each vertebral level (T12-L3) from animals injected with CL into their ipsilateral IWAT and saline vehicle into their contralateral IWAT. * $p < 0.05$, ** $p < 0.001$.

EPA, AA, and a cocktail of both together each significantly increased neurophysiological activity of IWAT afferent nerves (Fig. 11a, b) (repeated measures ANOVA; EPA, $n = 6$, $p = 0.013$; AA, $n = 3$, $p = 0.003$; EPA+AA cocktail, $n = 4$, $p = 0.005$). Post hoc analysis revealed lipolytic products EPA and AA each increased multiunit activity to a similar magnitude and latency of effect as the high dose of CL.

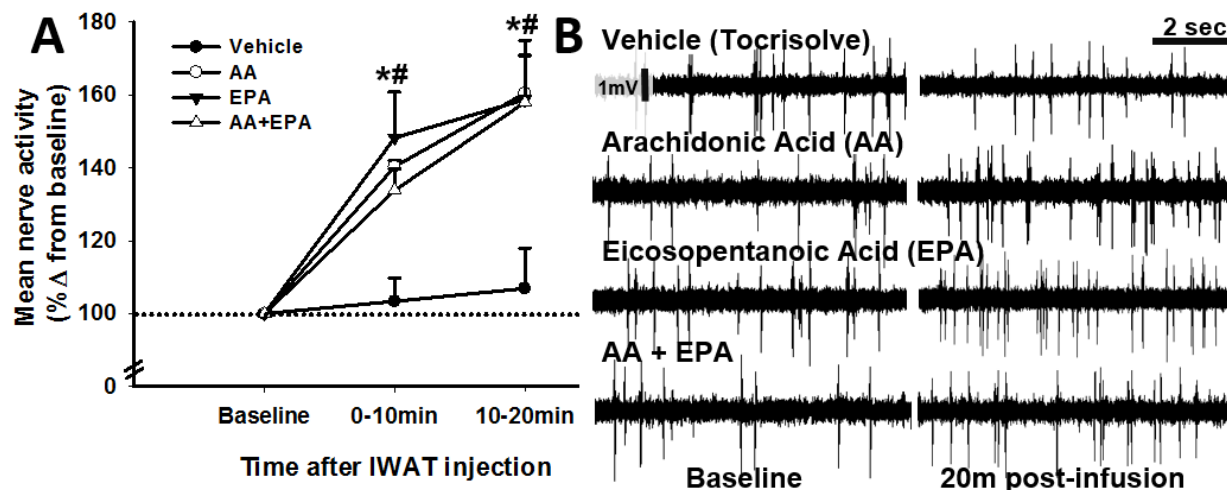


Figure 11. Intra-IWAT eicosopentanoic acid (EPA) and arachidonic acid (AA) increases IWAT multiunit nerve activity.

(a) EPA, AA, and a mixture of EPA + AA all increased IWAT multiunit spiking with a similar magnitude and latency to effect. Data are expressed as a percentage change of activity from baseline nerve activity. (b) Representative (8 sec) traces from IWAT afferents and contralateral counterparts at baseline and 20 min post-infusion. Scale bars on first trace apply to all traces. Dotted line separates ipsilateral vs contralateral IWAT afferent recordings from each of the three representative animals. * $p < 0.05$.

(Student's t test with Bonferroni correction; 0-10 min: EPA, $n = 6$, $p = 0.047$; AA, $n = 3$, $p = 0.019$; 10-20 min: EPA, $n = 6$, $p = 0.015$; AA, $n = 3$, $p = 0.003$).

IBAT temperature change from baseline was significantly increased after CL infusion in WAT pads with intact neural innervation (repeated measures ANOVA; $n = 36$, $p < 0.001$) as early as 5 min post infusion and persisted for every time point measured (Fig. 12c). This effect was abolished when WAT was denervated before CL infusion and did not increase when saline was infused into denervated WAT (Fig. 12c). Anesthetized hamsters experienced mild post anesthesia-induced hypothermia (Shimizu & Saito, 1991) after which IBAT (repeated measures ANOVA; $n = 36$, $p < 0.001$) and rectal raw temperatures (repeated measures ANOVA; $n = 36$, $p < 0.001$) slowly increased over time throughout the experiment (Fig. 12b, d); however, neither IBAT (repeated measures ANOVAs; $n = 36$, $p < 0.183$) nor rectal (repeated measures ANOVA;

$n = 36, p = 0.922$) raw temperatures differed among treatment groups at baseline or any subsequent time point measured (Fig. 12b, d).

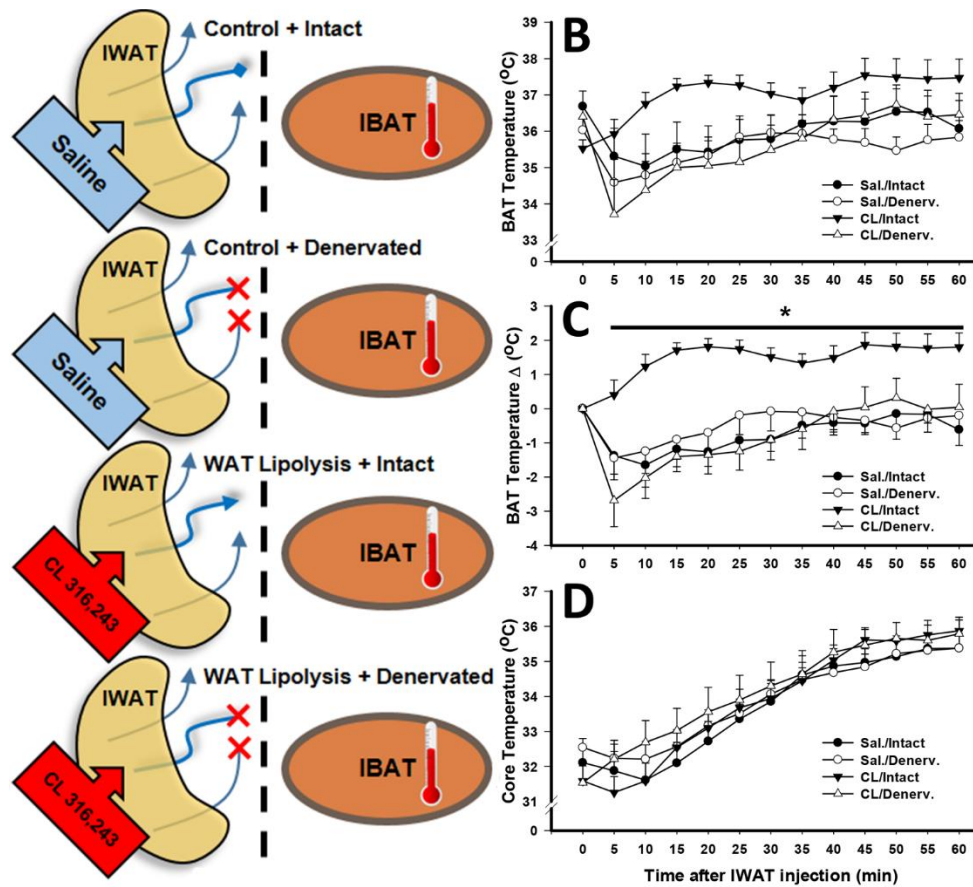


Figure 12. CL-induced IWAT afferent stimulation is sufficient to increase BAT thermogenesis. (a) Diagrammatic representation of the experimental setup. IWAT was either denervated or nerves left intact then injected with saline or a dose of CL 316,243 (0.2ng/kg) shown to increase IWAT afferent activity. (b) BAT temperature, (c) change in BAT temperature from baseline and (d) rectal temperature over the 60 minute recording period all demonstrate WAT afferent activation specifically increases BAT thermogenesis, * $p < 0.05$.

3.5 Discussion

IWAT afferents are activated by 2DG-induced glucoprivation (Song et al., 2009) and the present results show that this effect is attenuated by propranolol pretreatment, suggesting that β -AR-dependent lipolysis drives IWAT afferent spiking (Fig 8b, c). IWAT afferent activation appears to be reliant on local CL-induced lipolysis, as evidenced by increases in: 1) WAT HSL phosphorylation, 2) neurophysiological spike activity of WAT afferents, and 3) c-Fos immunoreactivity in adipose tissue-connected

sensory spinal neurons in the DRG. Furthermore, blocking CL-induced lipolysis with DMP pretreatment attenuated WAT CL-induced HSL phosphorylation (Fig. 9a) and blocked IWAT afferent activation (Fig. 8b, c). Although we did not observe increases in WAT ATGL protein content 15 min after CL injections, pHSL was significantly higher (Fig. 9a, b) demonstrating enhanced β_3 AR stimulation as a proxy for WAT lipolysis. To further support the hypothesis that lipolysis activates WAT afferents, we then tested two fatty acids known to be highly released during norepinephrine-induced lipid mobilization (Raclot & Groscolas, 1993) and both EPA and AA were sufficient to drive WAT afferent neurophysiological activity in the absence of CL. These data together suggest that lipolysis products are sufficient to drive WAT afferent spiking, perhaps relating the amount and types of released lipid to the CNS.

Sensory nerves identified within adipose tissue—using immunohistochemistry for CGRP and substance P as afferent nerve markers—are predominantly located around major blood vessels and less commonly innervate the parenchymal adipose depot (De et al., 1998). This observation is further illustrated by electron micrographs of the adipose cellular architecture (Cinti, 1999; Giordano et al., 1996). It is unlikely then that WAT afferents activated by CL infusions circumvent adipocytes at their cellular borders and most immediate site of efflux, but rather might serve as lipid sensors from WAT at the entry point to the bloodstream. The possible role of WAT afferent lipid sensors around major blood vessels may be to inform the CNS about the quantity and types of lipid species entering circulation. Furthermore, the functional association between WAT afferents and SNS outflow may exist to sense and potentially regulate released lipid and/or adipokines from individual fat depots to the rest of the body. Because of the variety of signals sensed, and potential for WAT to control SNS outflow

to other tissues, perhaps the primary role of WAT afferents is to distinguish these WAT depot-specific contributions to the bloodstream from lipid and adipokines accumulated in the bloodstream from other WAT depots and elsewhere.

To help understand the physiological context of this newfound sensory signal, we tested for the existence of a functional WAT to BAT neural link and for the first time demonstrate acute sufficiency of the neural connectivity from WAT to BAT to drive BAT thermogenesis (Fig. 12a-d). The general connectivity between WAT afferents and BAT is not novel to these present experiments because others have measured diminished BAT thermogenic capacity (Giordano et al., 1998) and atrophy of the BAT after the destruction of afferents by sensory excitotoxic denervation (Cui & Himms-Hagen, 1992b; Cui et al., 1990). Albeit chronic and loss of function methods to test the necessity of WAT afferents for healthy BAT function, these afferent lesion studies demonstrate that our findings are not solitary but together reiterate the likely neural interaction from WAT to BAT. Because surgical denervation blocked BAT temperatures in CL-infused WAT (Fig. 12a-d), this WAT to BAT neural circuitry likely induces BAT thermogenesis by either causing the adrenal release of norepinephrine or more likely the increase of efferent neural activity to BAT directly (Bartness & Ryu, 2015). Despite the anatomical pathway by which WAT CL infusion triggers BAT thermogenesis, we have measured an acute and robust thermogenic response by BAT—in line with other evidence—as a novel SNS output of the adipose afferent reflex (AAR) supported by others (Xiong et al., 2014).

Earlier reports by us and others (Murphy et al., 2013; Nijima, 1998) suggest WAT afferents activated by leptin presumably relay an inventory signal to the brain but also increase blood pressure via the AAR (Xiong et al., 2014), whereas we now provide evidence that WAT afferents are activated by the local release of lipid and are sufficient

to increase BAT temperature. Taken together, these reports identify heterogeneity among WAT afferents. It is still unclear, however, whether single WAT afferent neurons are receptive to both leptin and lipids or perhaps there are distinct neurons that sense and generate these seemingly different reflexive outputs. Additionally, peripheral afferent nerves also presumably release CGRP into their innervating tissue to which it is unclear how decentralizing afferent fibers in this study have affected subsequent afferent activity or adipose sensitivities to CL. Interestingly, CGRP injected directly into BAT attenuates norepinephrine-induced thermogenesis and is innately released by BAT afferent activation. This suggests that afferents possibly regulate adipose function via negative feedback (Osaka et al., 1998). Despite these effects in BAT, we believe that our within-animal design employed during neurophysiological recordings mitigates the confounding effects of WAT afferent neuropeptide release in this study. Clearly, further and more refined investigation is needed to interrogate WAT afferent functions to potentially discover bidirectionally active labeled-lines of opposing or parallel metabolic functions. The existence of apparently distinct AAR outputs suggests that lipolysis-activated WAT afferents also increase blood pressure and thereby facilitate newly released lipid distribution throughout the body, to fuel BAT thermogenesis. Such a system may allow us to better understand mechanisms of SNS dysregulation in human obesity (*i.e.*, wherein SNS is overactive and stimulated-lipolysis is high) (Bartness et al., 2014a).

Altogether, these results provide evidence that WAT afferents—shown by us and others to be involved in 1) SNS feedback regulation to multiple tissues (Nijijima, 1998, 1999), 2) SNS-induced hypertension (Xiong et al., 2014), 3) neural SNS feedback loops that are sensitive to insulin (Ding et al., 2015c), 4) regulation of fat deposition

throughout the body (Shi & Bartness, 2005), and 5) food intake regulation (Yamada et al., 2006)—increase their activity in response to the basic biological process of stimulated lipolysis (*i.e.*, simulated SNS outflow). In addition, one function of these lipolysis-activated WAT afferents is to increase BAT temperature in an acute fashion: a circuit which perhaps exists to correctly time the release of FFAs from WAT with the engagement of thermogenic machinery in BAT. This novel sensory signal has implications for many past and present studies examining the neural control of energy balance during physiological challenges where SNS-induced lipolysis is high (*e.g.*, food deprivation, cold exposure, and glucoprivation) (Dunn & Adams, 2014); therefore, we must continue to consider this synchrony of organ systems to more wholly understand homeostatic mechanisms of survival during energy challenges.

3.6 Author contributions

T.J.B., J.T.G., and G.J.S. designed and performed the neurophysiological recording experiments, L.A.S., J.T.G. performed the western blot lipolysis assays. J.T.G., V.R. performed the neurotracing experiments. J.T.G. performed the lipolysis induced brown adipose tissue temperature experiments. J.T.G., V.R., L.A.S., B.X. and G.J.S. wrote the paper. Supported by NIH R37DK035254 to T.J.B., NIH DK105441-01 to G.J.S., and NIH R01DK035254 to B.X.

3.7 Acknowledgements

We thank Dr. Chun Jiang (Georgia State University) for his technical assistance and advise, Rachel Stanford for her help with data collection and analysis, and GSU Department of Animal Resources for maintaining the health and wellness of our laboratory animals.

4 CHEMOGENETIC CONTROL OF ADIPOSE AFFERENT NERVES

John T. Garretson^{1, 3}, Emily Bruggeman^{1, 3}, Yogendra B. Shrestha⁴, Bingzhong Xue^{1,2,3}, Liana Artinian^{2,3}, M. Alex Thomas^{2,3}, Vitaly Ryu^{2,3}, Timothy J. Bartness^{1, 2, 3}

¹ Neuroscience Institute, Georgia State University, Atlanta GA 30303, USA.

² Department of Biology, Georgia State University, Atlanta GA 30303, USA.

³ Center for Obesity Reversal, Georgia State University, Atlanta GA 30303, USA.

⁴ NIDDK, National Institutes of Health, Rockville, MD 20851

4.1 Introduction

WAT afferent functions have been examined by two primary approaches: 1) Loss of function experiments using surgical denervation (which also removes efferent output to WAT) or excitotoxic chemical denervation using high dose capsaicin (Jancso et al., 1984) or resinerfertoxin (Acs et al., 1997) surgically injected into WAT of anesthetized rodents. Results of these experiments establish the necessity of chronic WAT afferent activity but the approaches employed have two shortcomings: the former completely removes afferent but also efferent SNS projections into WAT, while the latter is afferent specific but not complete, as it only targets capsaicin sensitive fibers and is believed to decrease sensory innervation by only approximately 40-50%. Each type relies on a surgical recovery period before function can be measured wherein nerve regrowth and compensatory mechanisms that compensate for afferent nerve destruction may occur. The second approach 2) is extracellular neurophysiological recordings in anesthetized animals beginning with Nijijima's (1998) discovery that leptin activates WAT afferents (Nijijima, 1999) and used more recently with understanding mechanisms of the AAR

(Shi et al., 2012; Xiong et al., 2012; Xiong et al., 2014). These methods—similar to that described in chapters 2 and 3 above—are used to identify WAT afferent sensation. Although valuable, this second approach cannot well characterize the role of WAT afferents in metabolic and behavioral responses of awake behaving animals. It is clear that a novel approach capable of testing real-time physiological consequences of WAT afferent activity is needed, which would markedly impact the field of integrative physiology.

In order to target WAT afferents specifically, we explored transgenic mouse models that employ afferent nerve specific promoters. Advillin—transcribed by the *AVIL* gene—is expressed only within neurons and is important for ganglionic development; moreover, advillin expression is primarily peripheral and entirely limited to afferent but not efferent neurons (Zurborg et al., 2011). Our collaborator (Y.B.S., NIH) has supplied mice (*AVIL*^{cre+}) wherein *cre-recombinase* is coexpressed with *AVIL* on afferent but not efferent peripheral neurons (Fig. 13 from (Zurborg et al., 2011)). These mice are viable and exhibit no metabolic deficits or observable phenotypic differences compared with wild-type mice. As such, the *AVIL*^{cre+} mice are ideal tools for *cre*-dependent strategies of adipose afferent control.

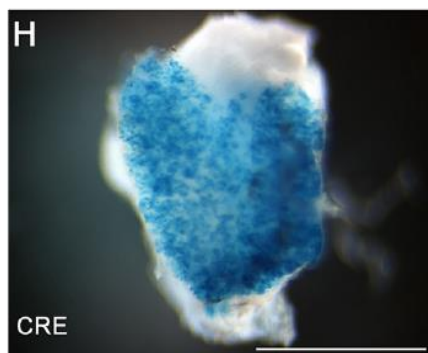


Figure 13. *AVIL*^{cre+} expression in mouse (modified from Zurborg et al., 2011). X-gal staining in whole-mount spinal DRG from adult mice. Cre mediated recombination was detected in adult *AVIL*^{cre+}. Figure from (Zurborg et al., 2011).

This *AVIL^{cre+}* combinational transgenic mouse model permits conditional genetic modifications in adulthood for the first time. *Cre*-dependent adeno-associated viral vectors (AAVs) that insert activation/inactivation receptors (*e.g.* Designer Receptors Explicitly Activated by Designer Drugs [DREADDs]) can be utilized to test WAT afferent control of energy balance and feeding behavior. Thus, we have designed a strategy to infect WAT afferents with *cre*-dependent AAVs carrying DREADDs (Gq [excite WAT afferents], or Gi [inhibit WAT afferents]) (Krashes, Shah, Koda, & Lowell, 2013), using this *AVIL^{cre+}* model for a novel, highly specific, and reversible chemogenetic control of WAT afferents *in vivo*. Using this approach, we will measure behavioral and metabolic consequences of WAT afferent activation/inhibition to test the effects of WAT afferent activity on energy balance and feeding behavior.

4.2 Method and Results

This section is organized chronologically to best represent the logical improvements to study design as new developments unfold during the assessment of this unique chemogenetic approach of WAT afferent nerve control. As this work is in a preliminary stage, the developing methodology and results in the following three sections (*i.e.* Pilot, Experiment 1, Experiment 2) are outlined in general form.

4.2.1 Pilot experiment using AAV2 transduction of excitatory

DREADDs

AVIL^{cre+} (n=2) mice and a wild type mouse were anesthetized and then surgically injected with AAV2-hSyn-DIO-hM3D(q)-mCherry (10 x 1 μ l injections totaling 2.0×10^{10} viral particles per loci) into IWAT to drive expression of excitatory (hM3D[q]) receptors in IWAT afferent nerves. This viral construct and ones used in future experiments were

all produced by Bryan Roth (Krashes et al., 2011) and deposited into the University of North Carolina Viral Vector Core for commercially available distribution. This family of viral constructs are packaged into a variety of AAV serotypes and designed for *cre*-dependent translation of DREADD-mCherry fusion proteins by cells that express the neuronal-specific synapsin promoter (hSyn). Furthermore, DREADDs-mCherry fusion translation is *cre*-dependent due to the double-floxed inverted open reading frame (DIO) flanking the target sequence. Thus, AAV2-hSyn-DIO-hM3D(q)-mCherry injected into IWAT of *AVIL*^{cre+} should cause hM3D(q)-mCherry (excitatory DREADD) translation in *cre-recombinase* positive *AVIL* neurons (*i.e.* IWAT afferents). Two weeks after AAV infection, mice were food deprived for 12 hr then WAT afferent nerves were activated with clozapine-*N*-oxide (CNO, 0.5mg/kg i.p., DREADD agonist). Food deprivation-induced food intake was measured at 1 and 2 hr after refeeding. Mice were sacrificed by sodium pentobarbital overdose, transcardially perfused, and DRGs (T12-L3) extracted for histological verification of mCherry in Fast Blue labeled neurons.

4.2.1.1 Pilot experiment: Results

This initial examination revealed a measurable attenuation of food deprivation-induced refeeding (Fig. 14a) as well as likely infection of adipose afferents evidenced by mCherry visualization on Fast Blue labeled neurons from IWAT (Fig. 14b). Given these data, sample sizes were increased for future experiments and to more thoroughly characterize the effects of WAT afferent nerve activity on metabolism.

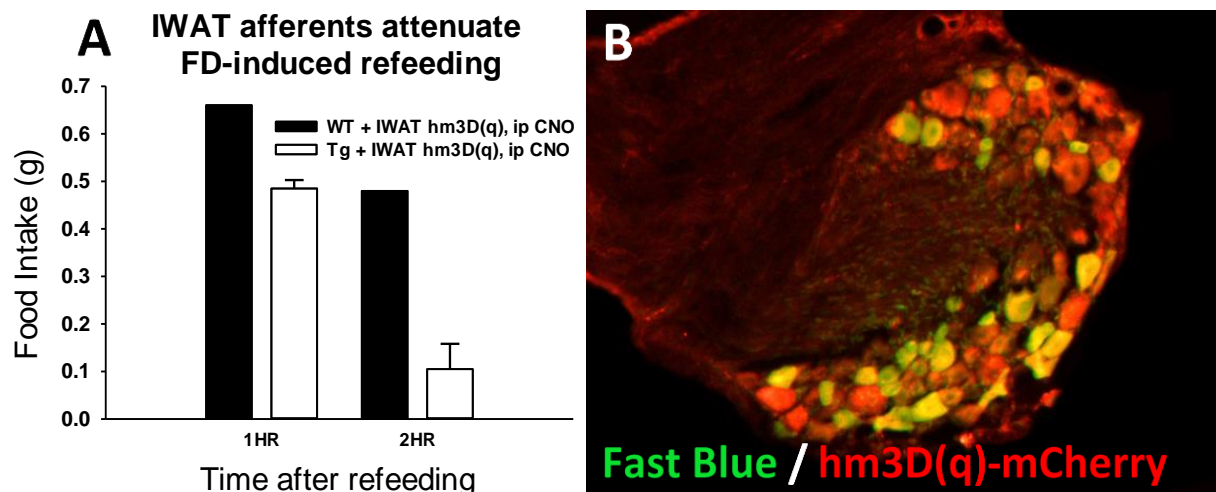


Figure 14. Pilot experiment demonstrating probable DREADD control of IWAT afferents.

Food intake of *AVIL^{cre+}* transgenic (Tg, n=2) and one wild type littermate. Mice were food deprived for 12 hours and administered CNO upon refeeding. B) DRG (T13) hm3D(q)-mCherry visualization on *AVIL^{cre+}* mouse injected with AAV2/hSyn-DIO-hm3D(q)-mCherry dissolved in fast blue neurotracer (pseudocolored green). Animals were sacrificed then perfused 3 weeks after infection into bilateral IWAT.

4.2.2 Experiment 1: Chemogenetic control of WAT afferents 2 weeks after AAV2 injection into IWAT.

Using a similar approach to pilot experiments with the addition of a new group of mice injected with AAV2-hSyn-DIO-hM4D(i)-mCherry (inhibitory DREADD), we submitted all mice (n=16) to our experimental model (Fig. 15). *AVIL*^{cre+} and wild type mice were injected with AAVs, and were then analyzed two weeks later for baseline body mass, fat mass, and lean mass using time-domain nuclear magnetic resonance technology (TD-NMR) by a MiniSpec machine (Bruker; Spring, TX). Mice were then assigned to individual TSE PhenoMaster metabolic chamber cages (TSE Systems; Chesterfield, MO) where energy expenditure, respiratory exchange ratio (RER), food intake, and locomotor activity were measured. After 3 days of acclimation, cages were cleaned and fresh bedding was given. All mice were given 0.5 mg/kg CNO twice daily for the remaining 4 days in metabolic chambers. On Day 1 and Day 2 after acclimation, mice were fed *ad libitum*, followed by a 24 hr food deprivation, then refeed with continuous measurements for the remaining 16 hr (Fig. 15). After 7 days, all mice were removed from metabolic chambers, reanalyzed for their body composition, and then returned to their home cages. One week later, all mice were euthanized for histological verification of viral transfection.

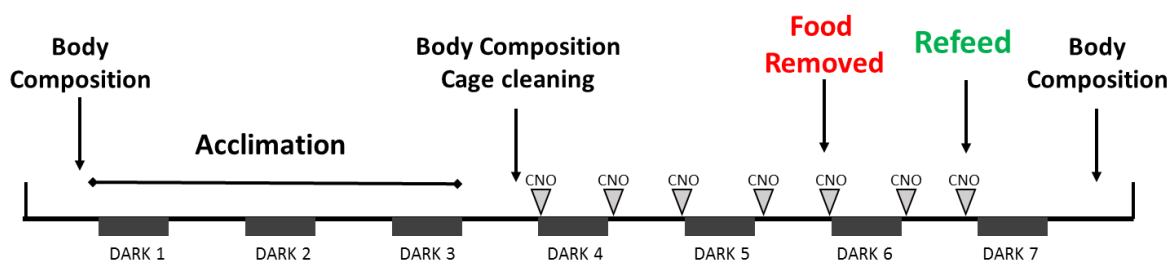


Figure 15. Timeline for metabolic chamber experiments using AAV2 transfection of DREADDs. Metabolic chamber characterization of *ad libitum* fed mice given twice daily CNO for 3 days.

4.2.2.1 Experiment 1: Results

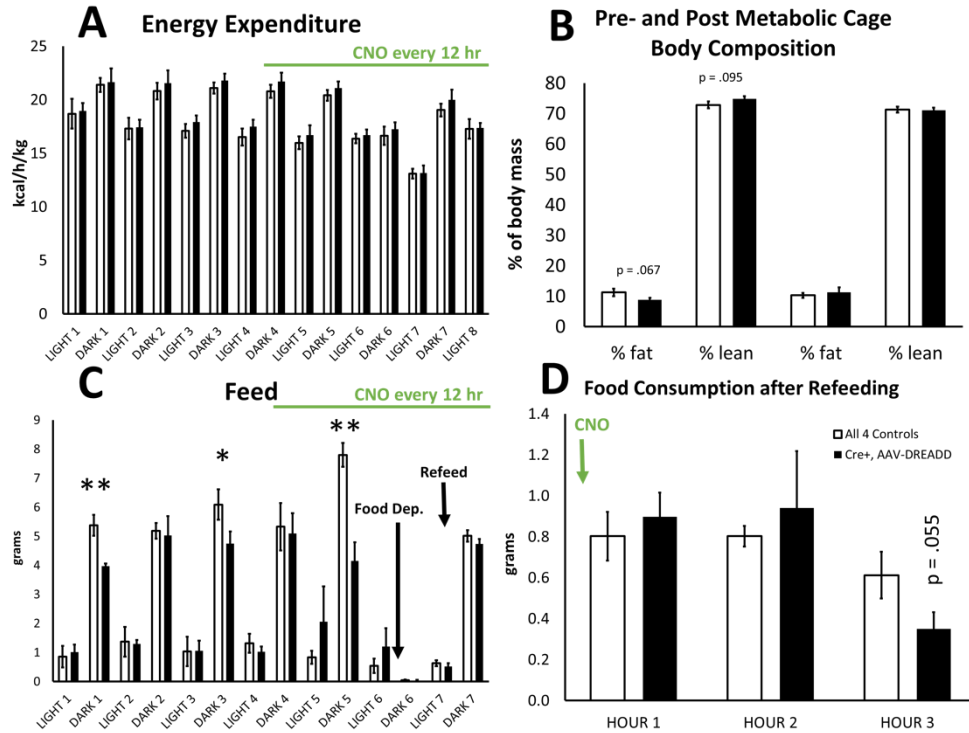


Figure 16. Experiment 1: Metabolic consequences of hm3d(q) activation of IWAT afferent nerves. Food intake was significantly lower in *AVIL*^{cre+} mice before and after CNO was administered. * $p < .05$, ** $p < 0.01$.

Unlike the pilot data acquired at the onset of this study, we observed no or trivial differences among treatment groups across all measures (Figs. 16, 17). In addition, confounding food intake differences between *AVIL*^{cre+} and wild type mice were present

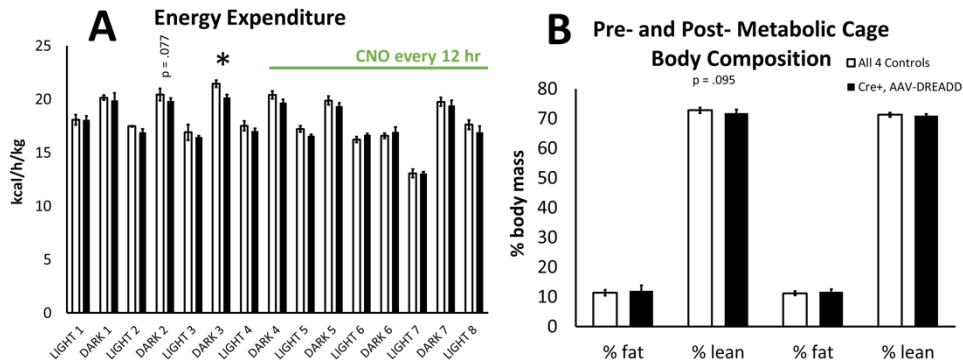


Figure 17. Experiment 1: hm4d(i) inhibition of IWAT afferent nerves does not produce a robust phenotype. Energy expenditure was significantly lower in *AVIL*^{cre+} mice before and after CNO was administered. * $p < .05$, ** $p < 0.01$.

during acclimation before CNO was administered (Fig. 16c). No differences in energy expenditure were detected on days where CNO was administered. Of note, the only difference in energy expenditure was between hm4D(i) *AVIL*^{cre+} and wild type mice during acclimation before any exposure to CNO (Fig. 17a). Postmortem assessment of AAV2 transduction of mCherry revealed that previous pilot characterization of endogenous mCherry (viral-mediated mCherry fluorescence) may have been nonspecific fluorescence apparent also in wild type mice (Fig. 18, top). We were able to confirm transduction of mCherry only after IHC in fixed DRG sections. Robust and specific mCherry fluorescence was observed in *AVIL*^{cre+} mouse neurons, suggesting that AAV2-

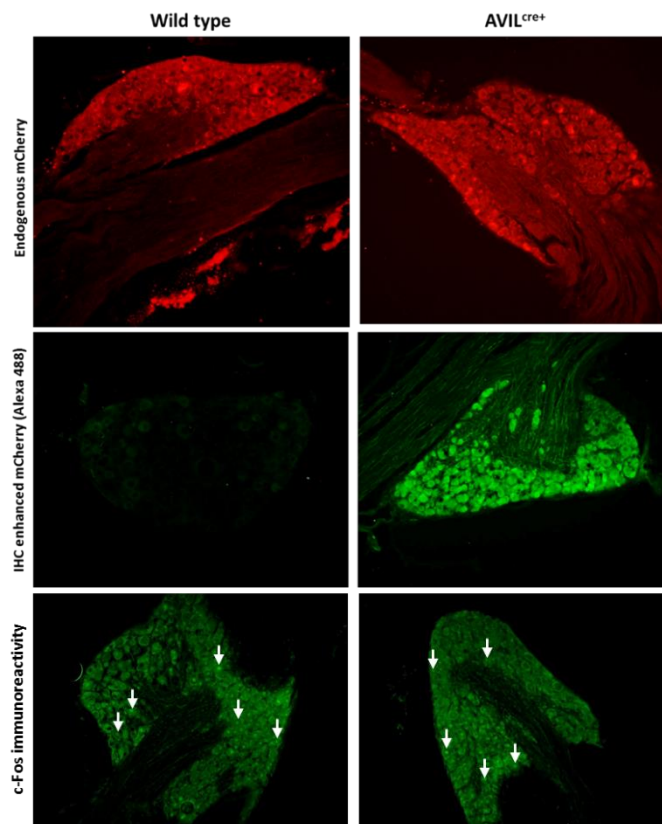


Figure 18. AAV2 translation of mCherry and c-Fos response to CNO.

Top) mCherry fluorescence without IHC amplification in wild type (left) and *AVIL*^{cre+} mice (right). Middle) IHC amplification of mCherry with Alexa 488 (green). Bottom) c-fos immunoreactivity 60 min after CNO 0.5mg/kg.

hSyn-DIO viruses successfully infect and sufficiently transduce mCherry-hm3D and mCherry-hm4D expression (Fig. 18, middle).

Due to 1) the ambiguous endogenous mCherry fluorescence in DRGs, 2) equivalent CNO-induced c-fos between groups (Fig. 18, bottom), 3) underwhelming phenotype from what theoretically should be a vigorous and chronic activation of IWAT afferents, and 4) differences between the pilot data and data acquired in this experiment, we conclude that DREADD control of these nerves was not effectively accomplished. In Experiment 2, we define particular strategies we used to enhance the likelihood of AAV transfection, effective measurement, and assessment of this WAT afferent nerve chemogenetic approach.

4.2.3 Experiment 2: Chemogenetic control of WAT afferents 6 weeks after AAV8 injection into IWAT and GWAT.

Viral trafficking efficiency of AAVs is not contiguous among the variety of serotypes (Castle, Gershenson, Giles, Holzbaur, & Wolfe, 2014). Correspondence with L. Vulchanova (Schuster et al., 2014; Schuster et al., 2013) and examination of the retrograde/trafficking efficiency of various serotypes discriminates against the use of AAV2 as a highly efficient virus for viral uptake/trafficking from neural process, but rather suggests AAV8 and AAV9 as more robust alternatives. Commercial availability of AAV8-hSyn-DIO-hm3/4D (UNC Vector Core; Chapel Hill, NC) allows efficient access to a more robust transduction agent to target sensory terminals. The enhanced efficiency of AAV8 compared with AAV2 likely will improve the efficiency of mCherry-DREADD translation by WAT afferents and thus their activity induced by CNO (Zheng et al., 2010). Although AAV8 is less efficient for retrograde transport than is AAV9 (Schuster

et al., 2014), its cost and immediate availability makes it preferred over AAV2 in order to improve endogenous mCherry expression and likely DREADD translation. Also in an effort to improve AAV8-induced translation of mCherry and DREADDs, we increased the duration of time after infection from two weeks to six.

Activation of adipose afferents only from IWAT may be insufficient to drive a reproducible behavioral and/or physiological phenotype. Considering this possibility, we also infected bilateral GWAT to control adipose afferents from four total fat pads simultaneously. We believe that if any effect is to be achieved by adipose afferent control, increasing the number of infected adipose afferent neurons may improve the likelihood of producing a discernable phenotype. Because both GWAT and IWAT afferents are leptin sensitive (Murphy et al., 2013; Shi et al., 2012), produce similar SNS increases in anesthetized rats, and connect with similar level DRGs (T12-L3), it is likely that that GWAT and IWAT afferent activation together produces a stronger cohesive effect rather than two conflicting/counteracting effects.

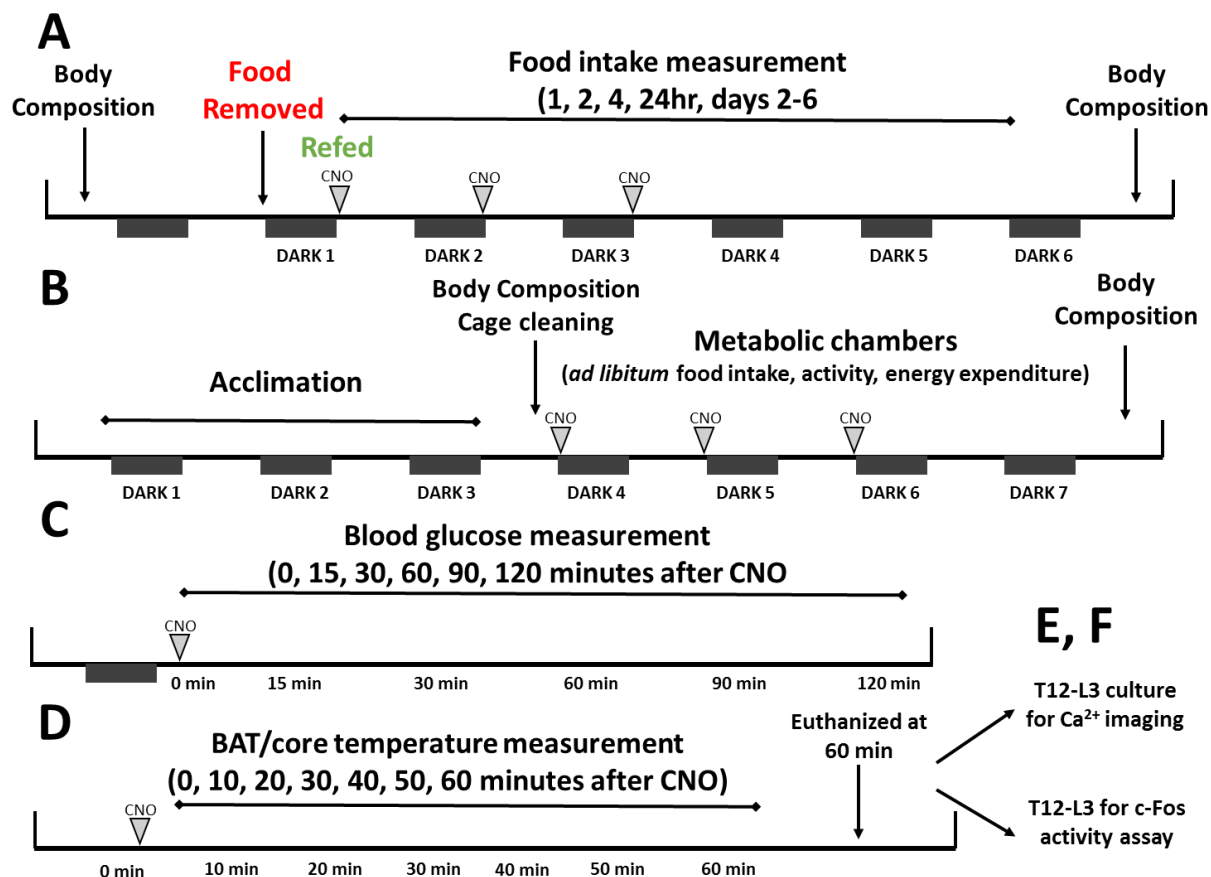


Figure 19. Timeline for Experiment 2a-f using AAV8 DREADD 6wks after infection.

Experiment 2a-f in chronological order. The same *AVIL^{Cre+}* and wild type mice were subjected to four experiments (a-d) between 6-10 weeks after viral infection then sacrificed at the end of BAT/core temperature measurements. a) Food deprivation-induced refeeding experiment conducted by manual food weight measurement 1, 2, 4 hr up to 6 days after CNO+refeeding. b) Metabolic chamber characterization of *ad libitum* fed mice given daily CNO for 3 days. c) Blood glucose measurements in response to CNO. d) BAT and body temperature in response to CNO of anesthetized mice. e-f) postmortem assessment of mCherry expression and neuronal activity of dissociated cultured DRG neurons (e) and fixed DRG histological sections (f).

CNO is used throughout the literature in the context of hm3D(q) stimulation at doses ranging from 0.3 mg/kg (Krashes et al., 2011) to 3.0 mg/kg (Nicoleau, Nation, Kinsman, Browning, & Stocker, 2016). The dose of 0.5 mg/kg was in the pilot study and Experiment 1, it is unclear if this dose is sufficient to induce WAT afferent nerve control given this unique strategy using peripheral DREADDs. Thus, we have increased the CNO dose to 3.0 mg/kg as this has still been shown to be inert in wild type mice metabolism and imbues greater confidence that DREADDs will be stimulated even after low viral efficiency. Importantly, there is little evidence to suggest sensitization of

animals to CNO based on high and/or multiple doses (Roman, Derkach, & Palmiter, 2016).

Automated metabolic chamber food intake measurements do not account for food spillage (*i.e.* food removed from automated hoppers that remains in soiled bedding and not eaten) and could explain differences in measured food intake between the pilot and Experiment 1. Therefore, we first food deprived animals for 12 hr then manually weighed food 1, 2, 4, 24 hr, and each day for 6 days after refeeding. This was performed to best mimic the pilot experimental design. In addition to these measures and the use of metabolic chambers in Experiment 1, additional experiments were added in Experiment 2 to test the role of WAT afferent activity on blood glucose and BAT thermogenesis (Fig. 19c-f). These experiments were added to investigate known effects of WAT afferent activity on other systems (Ding et al., 2015b; Nijijima, 1998).

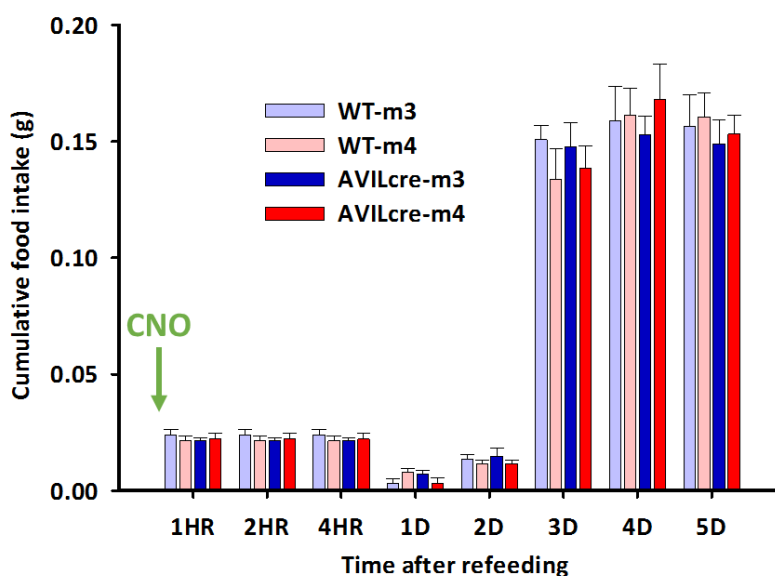


Figure 20. Experiment 2a: AAV8-hm3d(q) activation of IWAT and GWAT afferent nerves does not produce a food intake differences after food deprivation.

4.2.3.1 Experiment 2 results

Unlike the pilot data acquired at the onset of this study, we observed no or trivial differences among treatment groups in food deprivation-induced feeding (Figs. 19a, 20) or food intake and energy expenditure measures within metabolic chambers (Fig. 19b, 21). This was clear in all time points measured after food deprivation-induced refeeding (Fig. 19a, 20), but less clear in wild type and *AVIL*^{cre+} mice housed in metabolic cages

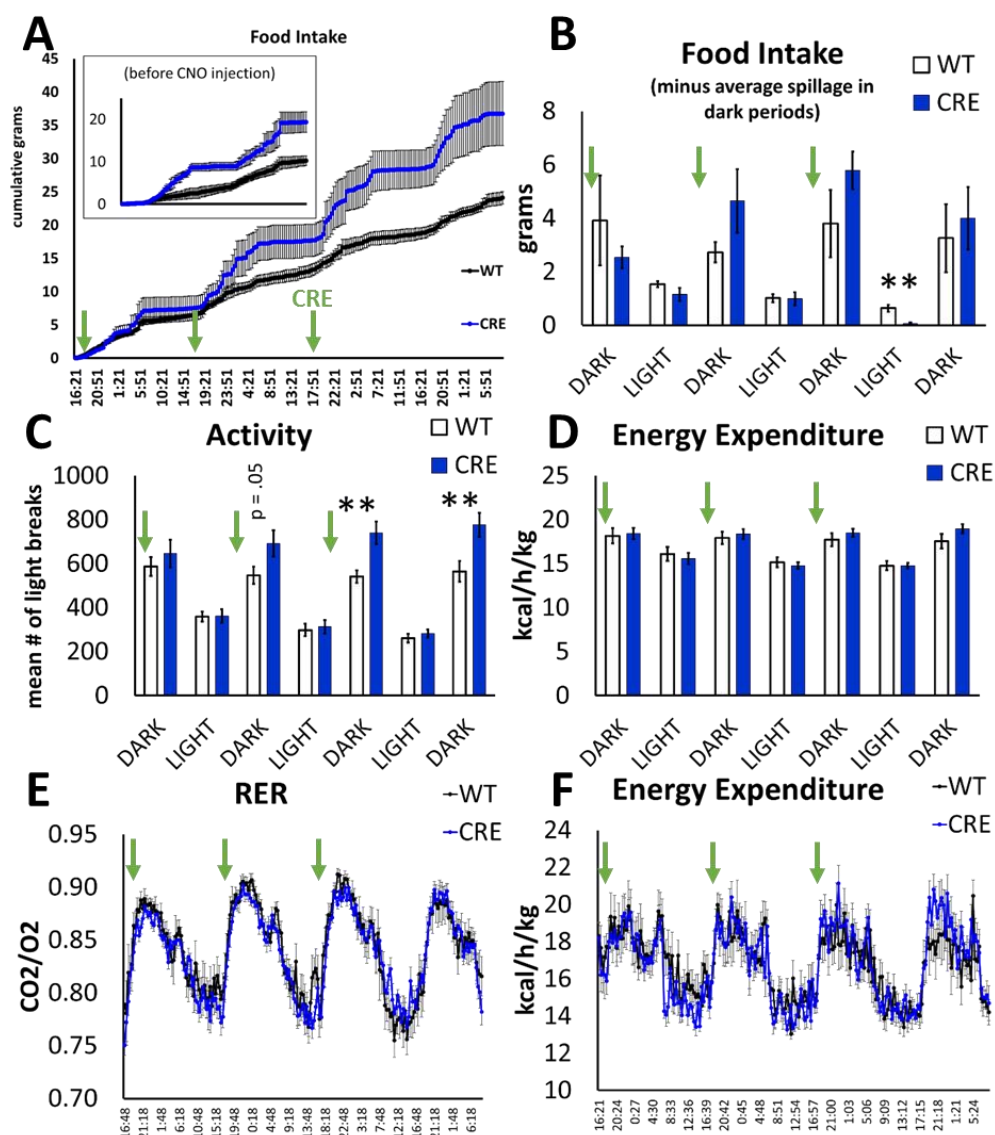


Figure 21. Experiment 2b: AAV8-hm3d(q) activation of IWAT and GWAT afferent nerves does not produce robust differences in metabolic measures.

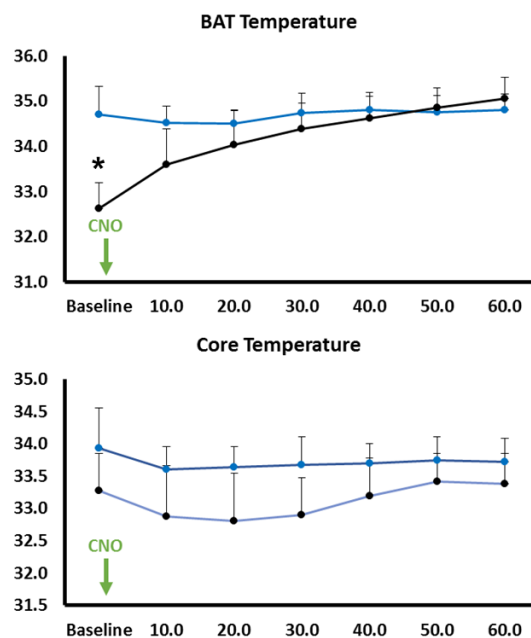


Figure 22. Experiment 2d: AAV8-hm3d(q) activation of IWAT and GWAT afferent nerves does not produce a differences in BAT or body temperature.

(Fig. 21a, b). Similar to Experiment 1, *AVIL*^{cre+} mice infected with AAV8-hm3D had different baseline food intake (Fig. 16c) during metabolic chamber acclimation before CNO was given compared with wild type mice (Fig. 21a, inset). Unlike Experiment 1, Experiment 2b *AVIL*^{cre+} ate more than wild type mice (Figs. 16a, 21a). This result could be due to the previous exposure to CNO which was given eight days prior in Experiment 2a (see timeline Fig. 19). Accordingly, CNO could be causing delayed or chronic feeding effects beginning with injections during Experiment 2a and continuing to affect baseline differences in feeding during Experiment 2b (Fig. 21b) conducted on the following week. However, the difference between *AVIL*^{cre+} mice in Experiment 1 and *AVIL*^{cre+} mice in Experiment 2b is unclear, but may be driven by higher food spillage of *AVIL*^{cre+} mice in Experiment 2b (data not shown). CNO treatment increased locomotor activity (Fig. 21c) but did not affect energy expenditure. Body composition at any time points measured was not different between treatment groups (data not shown). Metabolic chamber data

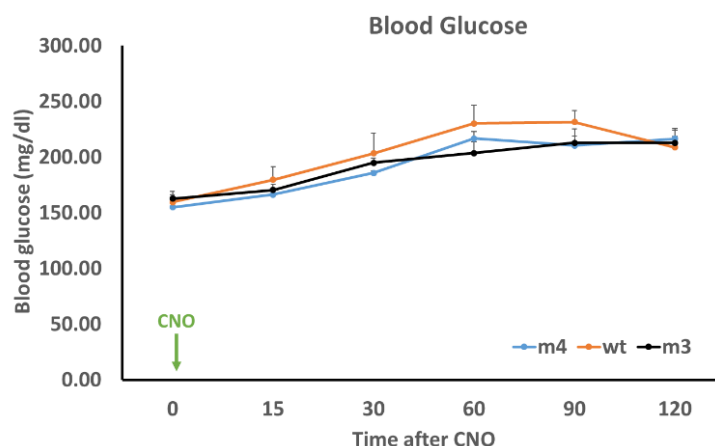


Figure 23. Experiment 2c: AAV8-hm3d(q) activation or AAV8-hm4d(i) inhibition of IWAT and GWAT afferent nerves does not produce a differences in blood glucose.

for AAV8 hm4D(i) injected *AVIL*^{cre+} and wild type mice were corrupted by non-stable reference CO₂ measurements and thus are inconclusive (data not shown).

Neither BAT temperature (Fig. 22) nor blood glucose (Fig. 23) was affected by CNO injection in *AVIL*^{cre+} or wild type mice. Reminiscent of baseline food intake differences in Experiment 2b, BAT temperature was higher in *AVIL*^{cre+} mice at baseline. Much like the above possibility, this baseline difference could be due to the prior administration of CNO from Experiments 2a-c (Fig. 19).

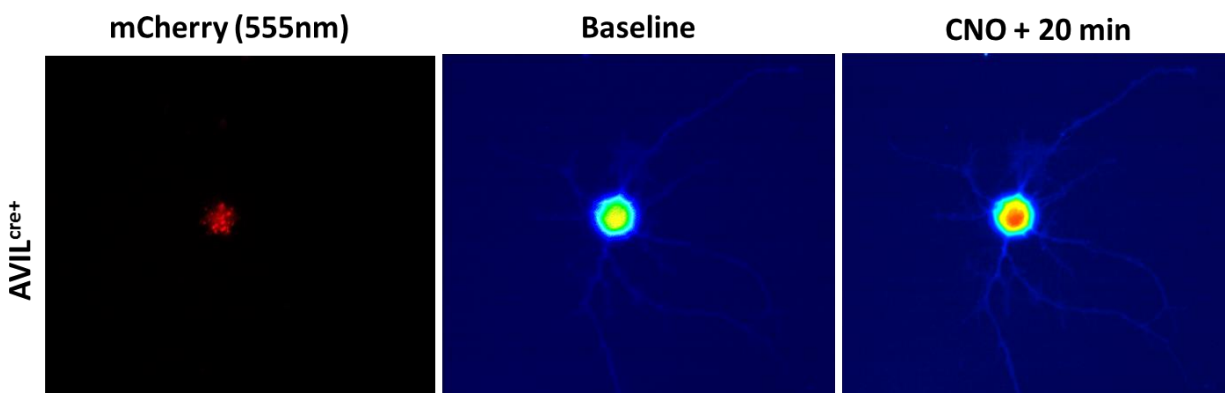


Figure 24. Experiment 2e: CNO applied to dissociated mCherry-positive DRG neurons from *AVIL*^{cre+} mice increases intracellular calcium.

Postmortem analysis revealed mCherry positive cultured DRG neurons from *AVIL^{cre+}* mice infected with AAV8-hm3D(q); furthermore, we identified intracellular calcium increases after CNO bath application (Fig. 24). DRG neurons positive for mCherry increased intracellular calcium after CNO application suggesting excitatory DREADDs [hm3D(q)] were present and functional on WAT afferents infected with AAV8. Similarly, CNO application modestly decreased intracellular calcium of mCherry positive neurons with inhibitory DREADDs [hm4D(i)] (data not shown). These data collectively indicate that DREADDs can be inserted on WAT afferents, and that endogenous mCherry expression can be detected in dissociated DRG neurons without the use of antibodies. This finding constitutes the largest degree of success for our approach thus far. These positive control experiments establish that our method for DREADD insertion is robust and infects approximately 80% of the neurons observed

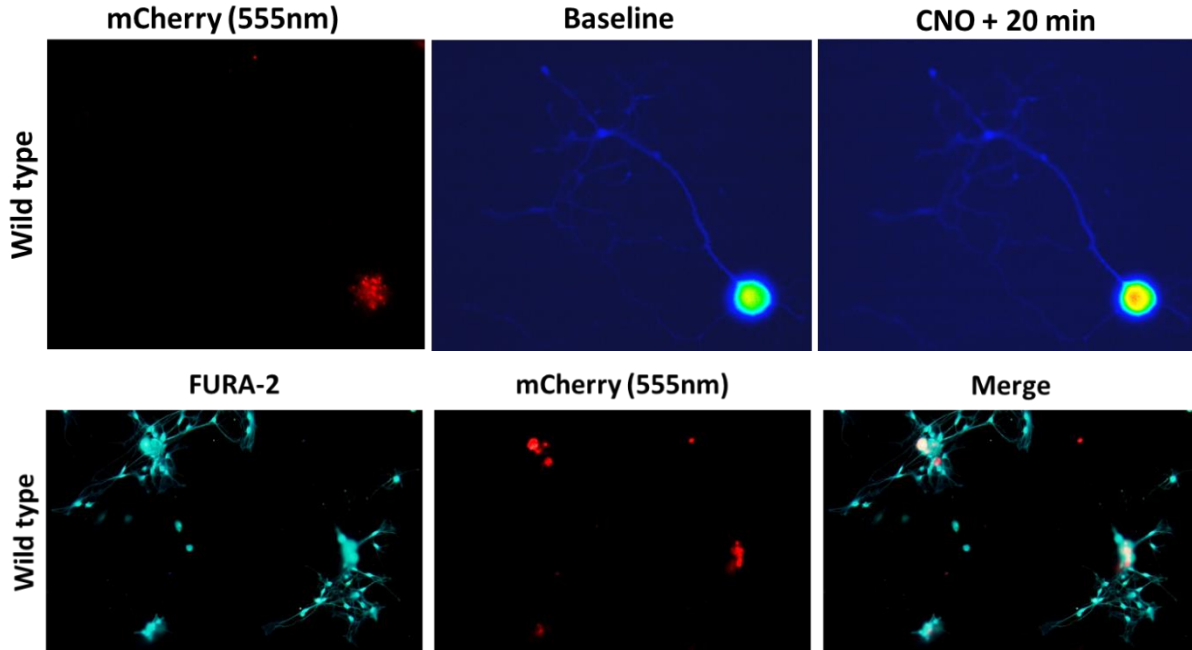


Figure 25. Experiment 2e: CNO applied to dissociated mCherry-positive DRG neurons from wild type mice injected with hm3d(q) increases intracellular calcium.

(J.T.G., unpublished observations), a percentage of total DRG neurons homologous to H129 transneuronal labeling efficiency of IWAT afferents (Song et al., 2009).

Unfortunately, we also have also accumulated evidence to suggest that either because of impure AAV8s obtained commercially, and due to the large volumes of total virus injected into each animal (~32 μ l across all four WAT pads), mCherry expression and CNO-induced calcium changes are observed in both *AVIL*^{cre+} and wild type mice. Indeed, DREADD expression using the viral construct delivered by AAV8 is non-specific. Our negative control groups [wild type injected with AAV8-hSyn-DIO-mCherry-hm3D(q)/hm4D(i)] robustly express mCherry in DRGs across all levels extracted T12-L3 and dissociated cultured neurons. Neurons from wild type injected with AAV8-hm3D(q) were activated by CNO application to the same magnitude and latency of *AVIL*^{cre+} neurons (Fig. 25). The exact problem that led to these results is still under investigation but appears to be driven both by inconsistency in the viral constructs as well as high viral injection titres/volumes used in these studies.

4.3 Discussion

The surprising findings of non-specific DREADD insertion in Experiment 2 pose two major problems for our novel approach to control adipose afferent nerve activity. If AAV8s are causing mCherry-hm3D(q) expression in neurons that are negative for *cre-recombinase* then 1) WAT afferents in our wild type negative control mice were activated to a similar degree as afferents in our *AVIL*^{cre+} experimental mice, and 2) SNS neurons in all animals injected are presumably being infected and activated as well. These two problems limit our ability to draw conclusions from any of the experiments using viral constructs delivered by AAV8 (*i.e.* Experiments 2a-f, Fig 19).

It is possible that AAV2 infection specifically caused mCherry-DREADD translation within *cre-recombinase* positive neurons, yet a reliable phenotype was not achieved due to shortcomings discussed above from Experiment 1 to Experiment 2 (*e.g.* CNO dose, number of fat depots injected, time after infection, added experiments, see Fig. 19). Thus, methods involving AAV2-induced DREADD expression may be replicated in the future in addition to assessing the validity of AAV9 retrograde transport (Schuster et al., 2014). Overall, refined control experiments must be conducted before meaningful conclusions can be reached as to the capacity of WAT afferents to affect physiology *in vivo*.

4.4 Author contributions

J.T.G. designed the chemogenetic approach to WAT afferent nerve control. Transgenic mice were supplied by Y.B.S. through collaboration with T.J.B.. J.T.G. performed the AAV injections and subsequent characterization of the CNO-induced phenotype at all levels. E.B. assisted with metabolic chamber assessment, M.A.T. with the blood glucose and BAT temperature experiments, L.A. with DRG culture and calcium imaging experiments, and V.R. with ganglia extraction. Supported by NIH R37DK035254 to T.J.B., NIH DK105441-01 to G.J.S., and NIH R01DK035254 to B.X.

5 CONCLUSIONS AND FUTURE DIRECTIONS

We have expanded the known sensitivities and capacities of adipose afferents by demonstrating their 1) within-BAT neural feedback circuits, 2) sensitivities to BAT thermogenesis, and 2) role as lipid sensors. We also have identified a functional neural link between WAT and BAT that drives thermogenesis. The novelty represented by this body of work lies within our particular strategy employed to test the effects of adipocyte-derived signals on adipose afferents rather than their sensitivity to exogenously injected ligands [*e.g.* leptin (Nijima, 1998), capsaicin (Shi et al., 2012)]. In addition, our bilateral simultaneous neurophysiological recording technique demonstrates that WAT afferents are able to distinguish local signals from circulated factors. Together, these data highlight an emerging role of these sensory fibers in their sensitivities and potential to exert control of basic adipocytes functions. Future explorations of this system seek to discover unique strategies to treat obesity by the specific neural control of WAT and BAT functions.

Taken together, the similar potential of WAT and BAT afferents to sense SNS-directed adipose activity reveals a novel signaling mechanism of energy depletion to the brain. Importantly, adipose afferents seem to be sensitive to many signals (*e.g.* leptin, adenosine, bradykinin, lipolysis, thermogenesis) but the precise segregation of these signals has not been explored. Because of the multiunit approach to measuring adipose sensitivities, we and others can only describe macro activation of entire peripheral nerves that knowingly contain many individual firing units. Future explorations with enhanced neuronal precision need to disentangle these signals to test whether these activators increase spiking in individual parallel pathways integrated at their point of convergence or whether all adipose afferents are each activated by these excitatory

events and transduce the milieu of signals beginning at the tissue level. Possibly, the adipose afferents share similar organization to vagal afferent innervation whereby specific neurons send parallel messages (*e.g.* stomach stretch, nutrient intake) from the gut to the brain for central processing (Williams et al., 2016).

Although many studies—including ours above—demonstrate adipose afferent activators, none have described a single ligand or process capable of inhibiting this neuronal population. Inhibitory mechanisms of this circuit are critical to elucidate because of the seemingly feed-forward capability of this SNS-induced lipolysis sensing circuit that promotes SNS increases (Nijima, 1999). Finding the anatomical level and process of adipose afferent inhibition may be key to discovering how obesity—a state where adipose afferent activators are high (*e.g.* leptin, lipolysis)—and hypertension (*i.e.* an output of the adipose afferent reflex) are interrelated.

Our unique chemogenetic approach to control WAT afferent activity, although largely inconclusive as to if these afferents affect *in vivo* metabolic processes, showed that AAV-induced translation of functional DREADDs on WAT afferents is possible. This positive result will guide future advancements into how we can discover the function of these and other adipose afferents. These principles cannot only be extended to measure functional effects of BAT afferents but also to test the necessity and sufficiency of afferents from other organs (*e.g.* muscle, gut, liver). In addition, specific control of adipose afferents could prove clinically beneficial given their dysregulation in obesity hypertension (Xiong et al., 2012). Stepwise and progressive experiments that test the potential capacities of WAT and BAT afferents will continue to deepen our understanding of the complex integration of adipose tissue physiology with energy balance.

REFERENCES

- Acs, G., Biro, T., Acs, P., Modarres, S., & Blumberg, P. M. (1997). Differential activation and desensitization of sensory neurons by resiniferatoxin. *J.Neurosci.*, *17*(14), 5622-5628.
- Adler, E. S., Hollis, J. H., Clarke, I. J., Grattan, D. R., & Oldfield, B. J. (2012). Neurochemical characterization and sexual dimorphism of projections from the brain to abdominal and subcutaneous white adipose tissue in the rat. *J.Neurosci.*, *32*(45), 15913-15921.
- Allison, M. B., & Myers, M. G., Jr. (2014). 20 years of leptin: connecting leptin signaling to biological function. *J Endocrinol*, *223*(1), T25-35.
- Atgie, C., Faintrenie, G., Carpene, C., Bukowiecki, L. J., & Geloën, A. (1998a). Effects of chronic treatment with noradrenaline or a specific beta3-adrenergic agonist, CL 316 243, on energy expenditure and epididymal adipocyte lipolytic activity in rat. *Comp Biochem.Physiol A Mol.Integr.Physiol*, *119*(2), 629-636.
- Atgie, C., Faintrenie, G., Carpene, C., Bukowiecki, L. J., & Geloën, A. (1998b). Effects of chronic treatment with noradrenaline or a specific beta3-adrenergic agonist, CL 316 243, on energy expenditure and epididymal adipocyte lipolytic activity in rat. *Comp Biochem Physiol A Mol Integr Physiol*, *119*(2), 629-636.
- Au-Yong, I. T., Thorn, N., Ganatra, R., Perkins, A. C., & Symonds, M. E. (2009). Brown adipose tissue and seasonal variation in humans. *Diabetes*, *58*(11), 2583-2587.
- Ballantyne, B. (1968). Histochemical and biochemical aspects of cholinesterase activity of adipose tissue. *Arch.Int.Pharmacodyn.Ther.*, *173*, 343-350.

- Bamshad, M., Aoki, V. T., Adkison, M. G., Warren, W. S., & Bartness, T. J. (1998). Central nervous system origins of the sympathetic nervous system outflow to white adipose tissue. *Am.J.Physiol.*, 275, R291-R299.
- Bamshad, M., Song, C. K., & Bartness, T. J. (1999). CNS origins of the sympathetic nervous system outflow to brown adipose tissue. *Am.J.Physiol.*, 276, R1569-R1578.
- Barnett, E. M., Evans, G. D., Sun, N., Perlman, S., & Cassell, M. D. (1995). Anterograde tracing of trigeminal afferent pathways from the murine tooth pulp to cortex using herpes simplex virus type 1. *Journal of Neuroscience*, 15(4), 2972-2984.
- Baron, D. M., Clerte, M., Brouckaert, P., Raher, M. J., Flynn, A. W., Zhang, H., . . . Scherrer-Crosbie, M. (2012). In vivo noninvasive characterization of brown adipose tissue blood flow by contrast ultrasound in mice. *Circ.Cardiovasc.Imaging*, 5(5), 652-659.
- Bartness, T., Liu, Y., Shrestha, Y., & Ryu, V. (2014a). Neural innervation of white adipose tissue and the control of lipolysis. *Frontiers in Neuroendocrinology*, 35(4), 473-493.
- Bartness, T., & Song, C. K. (2007a). Thematic review series: adipocyte biology. Sympathetic and sensory innervation of white adipose tissue. *Journal of lipid research*, 48(8), 1655-1672.
- Bartness, T. J., Liu, Y., Shrestha, Y. B., & Ryu, V. (2014b). Neural innervation of white adipose tissue and the control of lipolysis. *Frontiers in Neuroendocrinology*.
- Bartness, T. J., & Ryu, V. (2015). Neural control of white, beige and brown adipocytes. *Int J Obes Suppl*, 5(Suppl 1), S35-39.

- Bartness, T. J., Shrestha, Y. B., Vaughan, C. H., Schwartz, G. J., & Song, C. K. (2010). Sensory and sympathetic nervous system control of white adipose tissue lipolysis. *Mol.Cell Endocrinol.*, 318(1-2), 34-43.
- Bartness, T. J., & Song, C. K. (2007b). Brain-adipose tissue neural crosstalk. *Physiology and Behavior*, 91, 343-351.
- Bartness, T. J., & Song, C. K. (2007c). Sympathetic and sensory innervation of white adipose tissue. *Journal of Lipid Research*, 48(8), 1655-1672.
- Bartness, T. J., Song, C. K., Shi, H., Bowers, R. R., & Foster, M. T. (2005). Brain-adipose tissue cross talk. *Proceedings of the Nutrition Society*, 64, 53-64.
- Bartness, T. J., Vaughan, C. H., & Song, C. K. (2010). Sympathetic and sensory innervation of brown adipose tissue. *Int.J.Obes.(Lond)*, 34 Suppl 1, S36-S42.
- Belfrage, P., Fredrikson, G., Nilsson, N. O., & Stralfors, P. (1981). Regulation of adipose-tissue lipolysis by phosphorylation of hormone-sensitive lipase. *Int.J.Obes.*, 5(6), 635-641.
- Borzan, J., LaGraize, S. C., Hawkins, D. L., & Peng, Y. B. (2005). Dorsal horn neuron response patterns to graded heat stimuli in the rat. *Brain Res*, 1045(1-2), 72-79.
- Bourgeois, F., Alexiu, A., & Lemonnier, D. (1983). Dietary-induced obesity: Effect of dietary fats on adipose tissue cellularity in mice. *British Journal of Nutrition*, 49, 17-26.
- Bowers, R. R., Festuccia, W. T., Song, C. K., Shi, H., Migliorini, R. H., & Bartness, T. J. (2004). Sympathetic innervation of white adipose tissue and its regulation of fat cell number. *Am J Physiol Regul Integr Comp Physiol*, 286(6), R1167-1175.

- Brito, M. N., Brito, N. A., Baro, D. J., Song, C. K., & Bartness, T. J. (2007). Differential activation of the sympathetic innervation of adipose tissues by melanocortin receptor stimulation. *Endocrinology*, *148*(11), 5339-53347.
- Brito, N. A., Brito, M. N., & Bartness, T. J. (2008). Differential sympathetic drive to adipose tissues after food deprivation, cold exposure or glucoprivation. *Am.J.Physiol Regul.Integr.Comp Physiol*, *294*(5), R1445-R1452.
- Buettner, C., Muse, E. D., Cheng, A., Chen, L., Scherer, T., Poci, A., . . . Buettner, C. (2008). Leptin controls adipose tissue lipogenesis via central, STAT3-independent mechanisms. *Nat.Med.*, *14*(6), 667-675.
- Cannon, B., & Nedergaard, J. (2004a). Brown adipose tissue: function and physiological significance. *Physiol Rev*, *84*(1), 277-359.
- Cannon, B., & Nedergaard, J. (2004b). Brown adipose tissue: function and physiological significance. *Physiol Rev.*, *84*(1), 277-359.
- Carey, A. L., & Kingwell, B. A. (2013). Brown adipose tissue in humans: therapeutic potential to combat obesity. *Pharmacol Ther*, *140*(1), 26-33.
- Caro, J. F., Sinha, M. K., Kolaczynski, J. W., Zhang, P. L., & Considine, R. V. (1996). Leptin: The tale of an obesity gene. *Diabetes*, *45*(11), 1455-1462.
- Castle, M. J., Gershenson, Z. T., Giles, A. R., Holzbaur, E. L., & Wolfe, J. H. (2014). Adeno-associated virus serotypes 1, 8, and 9 share conserved mechanisms for anterograde and retrograde axonal transport. *Hum Gene Ther*, *25*(8), 705-720.
- Centers for Disease Control and Prevention (2009). *National Vital Statistics Report*.
- Cinti, S. (1999). *The Adipose Organ*. Milano: Editrice Kurtis.
- Conner, W. E., Lin, D. S., & Colvis, C. (1996). Differential mobilization of fatty acids from adipose tissue. *Journal of Lipid Research*, *37*(2), 290-298.

- Crahay, F. X., & Nizet, J. L. (2016). [Metabolic and cardiovascular consequences of suction-assisted lipectomy: Systematic review]. *Ann Chir Plast Esthet*.
- Cui, B. P., Li, P., Sun, H. J., Ding, L., Zhou, Y. B., Wang, J. J., . . . Zhu, G. Q. (2013). Ionotropic glutamate receptors in paraventricular nucleus mediate adipose afferent reflex and regulate sympathetic outflow in rats. *Acta Physiol (Oxf)*.
- Cui, J., & Himms-Hagen, J. (1992a). Long-term decrease in body fat and in brown adipose tissue in capsaicin-desensitized rats. *Am.J.Physiol.*, 262, R568-R573.
- Cui, J., & Himms-Hagen, J. (1992b). Rapid but transient atrophy of brown adipose tissue in capsaicin-desensitized rats. *Am.J.Physiol.*, 262, R562-R567.
- Cui, J., Zaror-Behrens, G., & Himms-Hagen, J. (1990). Capsaicin desensitization induces atrophy of brown adipose tissue in rats. *Am.J.Physiol.*, 259, R324-R332.
- Curanovic, D., & Enquist, L. (2009). Directional transneuronal spread of alpha-herpesvirus infection. *Future.Virol.*, 4(6), 591.
- Cypess, A. M., Chen, Y.-C., Sze, C., Wang, K., English, J., Chan, O., . . . Kahn, C. R. (2012). Cold but not sympathomimetics activates human brown adipose tissue in vivo. *Proceedings of the National Academy of Sciences of the United States of America*, 109(25), 10001-10005.
- Dag, Z. O., & Dilbaz, B. (2015). Impact of obesity on infertility in women. *J Turk Ger Gynecol Assoc*, 16(2), 111-117.
- Dankel, S. J., Loenneke, J. P., & Loprinzi, P. D. (2016). The Individual, Joint, and Additive Interaction Associations of Aerobic-Based Physical Activity and Muscle Strengthening Activities on Metabolic Syndrome. *Int J Behav Med*.

- Dattani, R. S., Swerner, C. B., Stradling, J. R., & Manuel, A. R. (2016). Exploratory study into the effect of abdominal mass loading on airways resistance and ventilatory failure. *BMJ Open Respir Res*, 3(1), e000138.
- De, M. R., Ricquier, D., & Cinti, S. (1998). TH-, NPY-, SP-, and CGRP-immunoreactive nerves in interscapular brown adipose tissue of adult rats acclimated at different temperatures: an immunohistochemical study. *Journal of Neurocytology*, 27(12), 877-886.
- Dib, B., Rompre, P. P., Amir, S., & Shizgal, P. (1994). Thermogenesis in brown adipose tissue is activated by electrical stimulation of the rat dorsal raphe nucleus. *Brain Research*, 650, 149-152.
- Ding, L., Gao, R., Xiong, X. Q., Gao, X. Y., Chen, Q., Li, Y. H., . . . Zhu, G. Q. (2015a). GABA in Paraventricular Nucleus Regulates Adipose Afferent Reflex in Rats. *PLoS One*, 10(8), e0136983.
- Ding, L., Tong, N., Feng, X. M., Chen, D., Wang, H. S., Wang, Y., . . . Zhou, Y. B. (2015b). Adipose afferent reflex response to insulin is mediated by melanocortin 4 type receptors in the paraventricular nucleus in insulin resistance rats. *Acta Physiol (Oxf)*, 214(4), 450-466.
- Ding, L., Tong, N., Feng, X. M., Chen, D., Wang, H. S., Wang, Y., . . . Zhou, Y. B. (2015c). Adipose afferent reflex response to insulin is mediated by melanocortin 4 type receptors in the paraventricular nucleus in insulin resistance rats. *Acta Physiol (Oxf)*.
- Ding, L., Zhang, L. L., Gao, R., Chen, D., Wang, J. J., Gao, X. Y., . . . Zhu, G. Q. (2013). Superoxide anions in paraventricular nucleus modulate adipose afferent reflex and sympathetic activity in rats. *PLoS ONE*, 8(12), e83771.

- Dogiel, A. S. (1898). Die sensiblen Nervenendigungen im Herzen und in den Blutgefassen der Säugethiere. *Arch.mikr.Anat.*, 52, 44-70.
- Dunn, T. N., & Adams, S. H. (2014). Relations between Metabolic Homeostasis, Diet, and Peripheral Afferent Neuron Biology. *Advances in Nutrition: An International Review Journal*, 5(4), 386-393.
- Dvorakova, M. C., Kruzliak, P., & Rabkin, S. W. (2014). Role of neuropeptides in cardiomyopathies. *Peptides*, 61, 1-6.
- Dyck, D. J., Heigenhauser, G. J., & Bruce, C. R. (2006). The role of adipokines as regulators of skeletal muscle fatty acid metabolism and insulin sensitivity. *Acta Physiol (Oxf)*, 186(1), 5-16.
- Edens, N. K., Moshirfar, A., Potter, G. M., Fried, S. K., & Castonguay, T. W. (1999). Adrenalectomy reduces adiposity by decreasing food efficiency, not direct effects on white adipose tissue. *Obes.Res.*, 7(4), 395-401.
- Ekstrand, M. I., Enquist, L. W., & Pomeranz, L. E. (2008). The alpha-herpesviruses: molecular pathfinders in nervous system circuits. *Trends Mol.Med.*, 14(3), 134-140.
- Enquist, L. W. (2002). Exploiting circuit-specific spread of pseudorabies virus in the central nervous system: insights to pathogenesis and circuit tracers. *J.Infect.Dis.*, 186 Suppl 2, S209-S214.
- Fedorenko, A., Lishko, P. V., & Kirichok, Y. (2012). Mechanism of fatty-acid-dependent UCP1 uncoupling in brown fat mitochondria. *Cell*, 151(2), 400-413.
- Festuccia, W. T., Blanchard, P. G., Richard, D., & Deshaies, Y. (2010). Basal adrenergic tone is required for maximal stimulation of rat brown adipose tissue UCP1

- expression by chronic PPAR-gamma activation. *Am.J Physiol Regul.Integr.Comp Physiol*, 299(1), R159-R167.
- Fishman, R. B., & Dark, J. (1987). Sensory innervation of white adipose tissue. *Am.J.Physiol.*, 253, R942-R944.
- Foster, D. O., & Frydman, M. L. (1978). Nonshivering thermogenesis in the rat II. Measurements of blood flow with microspheres point to brown adipose tissue as the dominant site of the calorogenesis induced by noradrenaline. *Canadian Journal of Physiology and Pharmacology*, 56, 110-122.
- Funakoshi, K., Goris, R., Kadota, T., Atobe, Y., Nakano, M., & Kishida, R. (2003). Prenatal development of peptidergic primary afferent projections to mouse lumbosacral autonomic preganglionic cell columns. *Developmental Brain Research*, 144(1), 107-119.
- Gabaldón, A. M., McDonald, R. B., & Horwitz, B. A. (1998). Effects of age, gender, and senescence on beta-adrenergic responses of isolated F344 rat brown adipocytes in vitro. *American Journal of Physiology*, 274(4), E726-E736.
- Gerritsen, G. C., & Dulin, W. E. (1965). Effect of a new hypoglycemic agent, 3,5-dimethylpyrazole, on carbohydrate and free fatty acid metabolism. *Diabetes*, 14, 507-515.
- Giordano, A., Frontini, A., Castellucci, M., & Cinti, S. (2004). Presence and distribution of cholinergic nerves in rat mediastinal brown adipose tissue. *Journal of Histochemistry and Cytochemistry*, 52(7), 923-930.
- Giordano, A., Frontini, A., Murano, I., Tonello, C., Marino, M. A., Carruba, M. O., . . . Cinti, S. (2005). Regional-dependent increase of sympathetic innervation in rat

- white adipose tissue during prolonged fasting. *Journal of Histochemistry and Cytochemistry*, 53(6), 679-687.
- Giordano, A., Morroni, M., Carle, F., Gesuita, R., Marchesi, G. F., & Cinti, S. (1998). Sensory nerves affect the recruitment and differentiation of rat periovarian brown adipocytes during cold acclimation. *J. Cell Sci.*, 111, 2587-2594.
- Giordano, A., Morroni, M., Santone, G., Marchesi, G. F., & Cinti, S. (1996). Tyrosine hydroxylase, neuropeptide Y, substance P, calcitonin gene-related peptide and vasoactive intestinal peptide in nerves of rat periovarian adipose tissue: an immunohistochemical and ultrastructural investigation. *Journal of Neurocytology*, 25, 125-136.
- Giordano, A., Song, C. K., Bowers, R. R., Ehlen, J. C., Frontini, A., Cinti, S., & Bartness, T. J. (2006). White adipose tissue lacks significant vagal innervation and immunohistochemical evidence of parasympathetic innervation. *Am.J.Physiol*, 291, R1243-R1255.
- Giordano, A., Song, C. K., Bowers, R. R., Ehlen, J. C., Frontini, A., Cinti, S., & Bartness, T. J. (2007). No sympathy for the claim of parasympathetic innervation of white adipose tissue. *Am.J.Physiol.*, 293., R550-R552.
- Grundy, S. M. (2016). Overnutrition, ectopic lipid and the metabolic syndrome. *J Investig Med*.
- Gunawardana, S. C., & Piston, D. W. (2012). Reversal of type 1 diabetes in mice by brown adipose tissue transplant. *Diabetes*, 61(3), 674-682.
- Haemmerle, G., Lass, A., Zimmermann, R., Gorkiewicz, G., Meyer, C., Rozman, J., . . . Zechner, R. (2006). Defective lipolysis and altered energy metabolism in mice lacking adipose triglyceride lipase. *Science*, 312(5774), 734-737.

- Halberg, N., Wernstedt-Asterholm, I., & Scherer, P. E. (2008). The adipocyte as an endocrine cell. *Endocrinol Metab Clin North Am*, 37(3), 753-768, x-xi.
- Himms-Hagen, J., Cui, J., Danforth, E., Taatjes, D. J., Lang, S. S., Waters, B. L., & Claus, T. H. (1994). Effect of CL-316,243, a thermogenic beta-3 agonist, on energy balance and brown and white adipose tissues in rats. *Am.J.Physiol.*, 266, R1371-R1382.
- Hoffman, G. E., Smith, M. S., & Verbalis, J. G. (1993). c-Fos and related immediate early gene products as markers of activity in neuroendocrine systems. *Frontiers in Neuroendocrinology*, 14, 173-213.
- Holt, S. J., Wheal, H. V., & York, D. A. (1988). Response of brown adipose tissue to electrical stimulation of hypothalamus centres in intact and adrenalectomized Zucker rats. *Neuroscience Letters*, 84, 63-67.
- Holzer, P. (2006). Efferent-like roles of afferent neurons in the gut: Blood flow regulation and tissue protection. *Auton.Neurosci.*, 125(1-2), 70-75.
- Horn, J. P., & Stofer, W. D. (1989). Preganglionic and sensory origins of calcitonin gene-related peptide-like and substance P-like immunoreactivities in bullfrog sympathetic ganglia. *The Journal of neuroscience*, 9(7), 2543-2561.
- Ishibashi, J., & Seale, P. (2010). Medicine. Beige can be slimming. *Science*, 328(5982), 1113-1114.
- Jancso, G., Karcsu, S., Kiraly, E., Szebeni, A., Toth, L., Bacsy, E., . . . Parducz, A. (1984). Neurotoxin induced nerve cell degeneration: possible involvement of calcium. *Brain Research*, 295(2), 211-216.
- Jansco, G., Kiraly, E., & Jansco-Gabor, A. (1980). Direct evidence for an axonal site of action of capsaicin. *Nauyn-Schmiedeberg's Arch.Pharmacol.*, 31, 91-94.

- Jansco, G., Kiraly, E., Joo, F., Such, G., & Nagy, A. (1985). Selective degeneration by capsaicin of a subpopulation of primary sensory neurons in the adult rat. *Neuroscience Letters*, *59*, 209-214.
- Johansson, S. M., Lindgren, E., Yang, J. N., Herling, A. W., & Fredholm, B. B. (2008). Adenosine A1 receptors regulate lipolysis and lipogenesis in mouse adipose tissue-interactions with insulin. *Eur.J.Pharmacol.*, *597*(1-3), 92-101.
- Kim, J. S., Enquist, L. W., & Card, J. P. (1999). Circuit-specific coinfection of neurons in the rat central nervous system with two pseudorabies virus recombinants. *J.Virol.*, *73*, 9521-9531.
- Kobayashi, A., & Osaka, T. (2003). Involvement of the parabrachial nucleus in thermogenesis induced by environmental cooling in the rat. *Pflugers Arch.*, *446*(6), 760-765.
- Koltzenburg, M. (2004). The role of TRP channels in sensory neurons. *Novartis.Found.Symp.*, *260*, 206-213.
- Krashes, M. J., Koda, S., Ye, C., Rogan, S. C., Adams, A. C., Cusher, D. S., . . . Lowell, B. B. (2011). Rapid, reversible activation of AgRP neurons drives feeding behavior in mice. *J Clin.Invest*, *121*(4), 1424-1428.
- Krashes, M. J., Shah, B. P., Koda, S., & Lowell, B. B. (2013). Rapid versus delayed stimulation of feeding by the endogenously released AgRP neuron mediators GABA, NPY, and AgRP. *Cell Metab*, *18*(4), 588-595.
- Kreier, F., Fliers, E., Voshol, P. J., Van Eden, C. G., Havekes, L. M., Kalsbeek, A., . . . Buijs, R. M. (2002). Selective parasympathetic innervation of subcutaneous and intra-abdominal fat - functional implications. *J.Clin.Invest*, *110*(9), 1243-1250.

- Krief, S., Bazin, R., Dupuy, F., & Lavau, M. (1989). Role of brown adipose tissue in glucose utilization in conscious pre-obese Zucker rats. *Biochemical Journal*, 263(1), 305-308.
- Kyle, U. G., & Pichard, C. (2006). The Dutch Famine of 1944-1945: a pathophysiological model of long-term consequences of wasting disease. *Curr Opin Clin Nutr Metab Care*, 9(4), 388-394.
- Labbé, S., Caron, A., Bakan, I., Laplante, M., Carpentier, A., Lecomte, R., & Richard, D. (2015). In vivo measurement of energy substrate contribution to cold-induced brown adipose tissue thermogenesis. *The FASEB Journal*, 29(5), 2046-2058.
- Lafontan, M., Barbe, P., Galitzky, J., Tavernier, G., Langin, D., Carpene, C., . . . Berlan, M. (1997). Adrenergic regulation of adipocyte metabolism. *Hum Reprod*, 12 Suppl 1, 6-20.
- Lafontan, M., & Berlan, M. (1993). Fat cell adrenergic receptors and the control of white and brown fat cell function. *Journal of Lipid Research*, 34, 1057-1091.
- Lass, A., Zimmermann, R., Oberer, M., & Zechner, R. (2011). Lipolysis - a highly regulated multi-enzyme complex mediates the catabolism of cellular fat stores. *Prog.Lipid Res.*, 50(1), 14-27.
- Lee, B., & Shao, J. (2014). Adiponectin and energy homeostasis. *Rev Endocr Metab Disord*, 15(2), 149-156.
- Leitner, C., & Bartness, T. J. (2009). Acute brown adipose tissue temperature response to cold in monosodium glutamate-treated Siberian hamsters. *Brain Res*, 1292, 38-51.
- Lewis, G. F. (2013). Devastating metabolic consequences of a life of plenty: focus on the dyslipidemia of overnutrition. *Clin Invest Med*, 36(5), E242-247.

- Li, P., Sun, H. J., Zhang, L. L., Ding, L., Han, Y., Zhu, G. Q., & Zhou, Y. B. (2013). Melanocortin 4 receptors in the paraventricular nucleus modulate the adipose afferent reflex in rat. *PLoS One*, *8*(11), e80295.
- Lidell, M. E., & Enerback, S. (2010). Brown adipose tissue--a new role in humans? *Nat Rev Endocrinol*, *6*(6), 319-325.
- Locci-Cubeddu, T., & Bergamini, E. (1983). Effects of antilipolytic agents on peroxisomal beta-oxidation of fatty acids in rat liver. *Biochem Pharmacol*, *32*(11), 1807-1809.
- Loesch, A. (2002). Perivascular nerves and vascular endothelium: recent advances. *Histol.Histopathol.*, *17*(2), 591-597.
- Lundberg, J. M., Terenius, L., Hokfelt, T., & Goldstein, M. (1983). High levels of neuropeptide Y in peripheral noradrenergic neurons in various mammals including man. *Neuroscience Letters*, *42*(2), 167-172.
- Mace, J., Bhatti, W., & Anand, S. (2016). Infrapatellar fat pad syndrome: a review of anatomy, function, treatment and dynamics. *Acta Orthop Belg*, *82*(1), 94-101.
- Mantyh, P. W. (1982). The ascending input to the midbrain periaqueductal gray of the primate. *J.Comp Neurol.*, *211*(1), 50-64.
- Masiello, P., Novelli, M., Bombara, M., Fierabracci, V., Vittorini, S., Prentki, M., & Bergamini, E. (2002). The antilipolytic agent 3,5-dimethylpyrazole inhibits insulin release in response to both nutrient secretagogues and cyclic adenosine monophosphate agonists in isolated rat islets. *Metabolism*, *51*(1), 110-114.
- Masters, R., Reither, E., Powers, D., Yang, Y. C., Burger, A., & Link, B. (2013). The impact of obesity on US mortality levels: the importance of age and cohort factors in population estimates. *American journal of public health*, *103*(10), 1895-1901.

- Mauer, M. M., & Bartness, T. J. (1994). Body fat regulation after partial lipectomy in Siberian hamsters is photoperiod dependent and fat pad specific. *Am J Physiol*, *266*(3 Pt 2), R870-878.
- Mauer, M. M., Harris, R. B. S., & Bartness, T. J. (2001). The regulation of total body fat: lessons learned from lipectomy studies. *Neurosci.Biobehav.Rev.*, *25*, 15-28.
- Melnyk, A., & Himms-Hagen, J. (1994). Leanness in capsaicin-desensitized rats one year after treatment. *International Journal of Obesity*, *18*(Suppl. 2), 130.
- Migliorini, R. H., Lima-Verde, J. S., Machado, C. R., Cardona, G. M., Garofalo, M. A., & Kettelhut, I. C. (1992). Control of adipose tissue lipolysis in ectotherm vertebrates. *Am J Physiol*, *263*(4 Pt 2), R857-862.
- Morrison, S. F., Madden, C. J., & Tupone, D. (2012). Central control of brown adipose tissue thermogenesis. *Front Endocrinol.(Lausanne)*, *3*(5).
- Mullen, K. L., Pritchard, J., Ritchie, I., Snook, L. A., Chabowski, A., Bonen, A., . . . Dyck, D. J. (2009). Adiponectin resistance precedes the accumulation of skeletal muscle lipids and insulin resistance in high-fat-fed rats. *Am J Physiol Regul Integr Comp Physiol*, *296*(2), R243-251.
- Murphy, K. T., Schwartz, G. J., Nguyen, N. L., Mendez, J. M., Ryu, V., & Bartness, T. J. (2013). Leptin-sensitive sensory nerves innervate white fat. *Am.J.Physiol Endocrinol.Metab*, *304*(12), E1338-E1347.
- Myers, M. G., Jr. (2015). Leptin Keeps Working, Even in Obesity. *Cell Metabolism*, *21*(6), 791-792.
- Myers, M. G., Jr., Heymsfield, S. B., Haft, C., Kahn, B. B., Laughlin, M., Leibel, R. L., . . . Yanovski, J. A. (2012). Challenges and opportunities of defining clinical leptin resistance. *Cell Metab*, *15*(2), 150-156.

- Nakamura, K., & Morrison, S. F. (2008a). Preoptic mechanism for cold-defensive responses to skin cooling. *J.Physiol*, *586*(10), 2611-2620.
- Nakamura, K., & Morrison, S. F. (2008b). A thermosensory pathway that controls body temperature. *Nat.Neurosci.*, *11*(1), 62-71.
- Nautiyal, K. M., Dailey, M. J., Brito, N. A., Brito, M. N., Harris, R. B. S., Bartness, T. J., & Grill, H. J. (2008). Energetic responses to cold temperatures in rats lacking forebrain-caudal brainstem connections. *Am.J.Physiol*, *295*(3), R789-R798.
- Nedergaard, J., Bengtsson, T., & Cannon, B. (2007). Unexpected evidence for active brown adipose tissue in adult humans. *Am.J.Physiol Endocrinol.Metab*, *293*(2), E444-E452.
- Nedergaard, J., Bengtsson, T., & Cannon, B. (2011). New powers of brown fat: fighting the metabolic syndrome. *Cell Metab*, *13*(3), 238-240.
- Ng, T. B. (1990). Studies on hormonal regulation of lipolysis and lipogenesis in fat cells of various mammalian species. *Comp Biochem.Physiol B*, *97*(3), 441-446.
- Nguyen, N. L., Randall, J., Banfield, B. W., & Bartness, T. J. (2014). Central sympathetic innervations to visceral and subcutaneous white adipose tissue. *Am.J.Physiol Regul.Integr.Comp Physiol*.
- Nicoleau, M. H., Nation, H., Kinsman, B., Browning, K., & Stocker, S. D. (2016). DREADD (Designer Receptors Exclusively Activated by Designer Drugs)-induced activation of subfornical organ neurons stimulates thirst and salt appetite. *The FASEB Journal*, *30*(1 Supplement), 751.753.
- Nijijima, A. (1998). Afferent signals from leptin sensors in the white adipose tissue of the epididymis, and their reflex effect in the rat. *J Auton.Nerv.Syst.*, *73*(1), 19-25.

- Nijima, A. (1999). Reflex effects from leptin sensors in the white adipose tissue of the epididymis to the efferent activity of the sympathetic and vagus nerve in the rat. *Neuroscience Letters*, 262(2), 125-128.
- Norman, D., Mukherjee, S., Symons, D., Jung, R. T., & Lever, J. D. (1988). Neuropeptides in interscapular and perirenal brown adipose tissue in the rat: a plurality of innervation. *Journal of Neurocytology*, 17, 305-311.
- Odegaard, J. I., & Chawla, A. (2013). Pleiotropic Actions of Insulin Resistance and Inflammation in Metabolic Homeostasis. *Science*, 339(6116), 172-177.
- Oldfield, B. J., Giles, M. E., Watson, A., Anderson, C., Colvill, L. M., & McKinley, M. J. (2002). The neurochemical characterisation of hypothalamic pathways projecting polysynaptically to brown adipose tissue in the rat. *Neuroscience*, 110(3), 515-526.
- Oliveira, A. L., Hydling, F., Olsson, E., Shi, T., Edwards, R. H., Fujiyama, F., . . . Meister, B. (2003). Cellular localization of three vesicular glutamate transporter mRNAs and proteins in rat spinal cord and dorsal root ganglia. *Synapse*, 50(2), 117-129.
- Omran, Z. (2016). Obesity, Current Treatment and Future Horizons. *Mini Rev Med Chem*.
- Osaka, T. (2004). Thermogenesis elicited by skin cooling in anaesthetized rats: lack of contribution of the cerebral cortex. *J.Physiol*, 555(Pt 2), 503-513.
- Osaka, T., Kobayashi, A., Namba, Y., Ezaki, O., Inoue, S., Kimura, S., & Lee, T. H. (1998). Temperature- and capsaicin-sensitive nerve fibers in brown adipose tissue attenuate thermogenesis in the rat. *Pflugers Arch*, 437(1), 36-42.
- Paxinos, G., & Franklin, K. B. J. (2007). *The Mouse Brain in Stereotaxic Coordinates* (2nd ed.). New York: Academic Press.

- Pechura, C. M., & Liu, R. P. (1986). Spinal neurons which project to the periaqueductal gray and the medullary reticular formation via axon collaterals: a double-label fluorescence study in the rat. *Brain Res.*, *374*(2), 357-361.
- Prentice, A. M. (2005). Early influences on human energy regulation: thrifty genotypes and thrifty phenotypes. *Physiol Behav.*, *86*(5), 640-645.
- Puchalski, W., Bocker, H., Heldmaier, G., & Langefeld, M. (1987). Organ blood flow and brown adipose tissue oxygen consumption during noradrenaline-induced nonshivering thermogenesis in the Djungarian hamster. *J.Exp.Zool.*, *242*, 263-271.
- Quintas-Neves, M., Preto, J., & Drummond, M. (2016). Assessment of bariatric surgery efficacy on Obstructive Sleep Apnea (OSA). *Rev Port Pneumol (2006)*.
- Raclot, T., & Groscolas, R. (1993). Differential mobilization of white adipose tissue fatty acids according to chain length, unsaturation, and positional isomerism. *Journal of Lipid Research*, *34*(9), 1515-1526.
- Raclot, T., Mioskowski, E., Bach, A. C., & Groscolas, R. (1995). Selectivity of fatty acid mobilization: a general metabolic feature of adipose tissue. *Am.J.Physiol.*, *269*, R1060-R1067.
- Reuss, S. (1993). Calcitonin gene-related peptide-like immunoreactivity in spinal cord and superior cervical ganglion of the Djungarian hamster (*Phodopus sungorus*). *J Chem.Neuroanat.*, *6*(6), 343-350.
- Reverchon, M., Ram, C., Bertoldo, M., & Dupont, J. (2014). Adipokines and the Female Reproductive Tract. *International Journal of Endocrinology*, *2014*, 10.
- Richard, D., & Picard, F. (2011). Brown fat biology and thermogenesis. *Front Biosci.*, *16*, 1233-1260.

- Rinaman, L., & Schwartz, G. J. (2004). Anterograde transneuronal viral tracing of central viscerosensory pathways in rats. *Journal of Neuroscience*, *24*(11), 2782-2786.
- Roman, C. W., Derkach, V. A., & Palmiter, R. D. (2016). Genetically and functionally defined NTS to PBN brain circuits mediating anorexia. *Nat Commun*, *7*, 11905.
- Ryu, V., & Bartness, T. J. (2014). Short and long sympathetic-sensory feedback loops in white fat. *Am.J.Physiol Regul.Integr.Comp Physiol*.
- Ryu, V., Garretson, J., Liu, Y., Vaughan, C., & Bartness, T. (2015a). Brown adipose tissue has sympathetic-sensory feedback circuits. *The Journal of neuroscience*, *35*(5), 2181-2190.
- Ryu, V., Garretson, J. T., Liu, Y., Vaughan, C. H., & Bartness, T. J. (2015b). Brown adipose tissue has sympathetic-sensory feedback circuits. *J Neurosci*, *35*(5), 2181-2190.
- Sacks, H. S., Fain, J. N., Bahouth, S. W., Ojha, S., Frontini, A., Budge, H., . . . Symonds, M. E. (2013). Adult Epicardial Fat Exhibits Beige Features. *J.Clin.Endocrinol.Metab*.
- Salazar, J., Luzardo, E., Mejias, J. C., Rojas, J., Ferreira, A., Rivas-Rios, J. R., & Bermudez, V. (2016). Epicardial Fat: Physiological, Pathological, and Therapeutic Implications. *Cardiol Res Pract*, *2016*, 1291537.
- Schafer, M. K., Eiden, L. E., & Weihe, E. (1998). Cholinergic neurons and terminal fields revealed by immunohistochemistry for the vesicular acetylcholine transporter. II. The peripheral nervous system. *Neuroscience*, *84*(2), 361-376.

- Scheller, E. L., Cawthorn, W. P., Burr, A. A., Horowitz, M. C., & MacDougald, O. A. (2016). Marrow Adipose Tissue: Trimming the Fat. *Trends Endocrinol Metab*, 27(6), 392-403.
- Scherer, P. E. (2006). Adipose tissue: from lipid storage compartment to endocrine organ. *Diabetes*, 55(6), 1537-1545.
- Schuster, D. J., Dykstra, J. A., Riedl, M. S., Kitto, K. F., Belur, L. R., McIvor, R. S., . . . Vulchanova, L. (2014). Biodistribution of adeno-associated virus serotype 9 (AAV9) vector after intrathecal and intravenous delivery in mouse. *Front Neuroanat*, 8, 42.
- Schuster, D. J., Dykstra, J. A., Riedl, M. S., Kitto, K. F., Honda, C. N., McIvor, R. S., . . . Vulchanova, L. (2013). Visualization of spinal afferent innervation in the mouse colon by AAV8-mediated GFP expression. *Neurogastroenterol Motil*, 25(2), e89-100.
- Seip, M., & Trygstad, O. (1996). Generalized lipodystrophy, congenital and acquired (lipoatrophy). *Acta Paediatr Suppl*, 413, 2-28.
- Shi, H., & Bartness, T. J. (2005). White adipose tissue sensory nerve denervation mimics lipectomy-induced compensatory increases in adiposity. *Am.J.Physiol.*, 289, R514-R520.
- Shi, H., Song, C. K., Giordano, A., Cinti, S., & Bartness, T. J. (2005). Sensory or sympathetic white adipose tissue denervation differentially affects depot growth and cellularity. *Am.J.Physiol*, 288, R1028-R1037.
- Shi, Z., Chen, W. W., Xiong, X. Q., Han, Y., Zhou, Y. B., Zhang, F., . . . Zhu, G. Q. (2012). Sympathetic activation by chemical stimulation of white adipose tissues in rats. *J.Appl.Physiol*, 112(6), 1008-1014.

- Shimizu, Y., & Saito, M. (1991). Activation of brown adipose tissue thermogenesis in recovery from anesthetic hypothermia in rats. *Am.J.Physiol*, *261*(2 Pt 2), R301-R304.
- Siebenhofer, A., Jeitler, K., Horvath, K., Berghold, A., Posch, N., Meschik, J., & Semlitsch, T. (2016). Long-term effects of weight-reducing drugs in people with hypertension. *Cochrane Database Syst Rev*, *3*, Cd007654.
- Song, C. K., Enquist, L. W., & Bartness, T. J. (2005). New developments in tracing neural circuits with herpesviruses. *Virus Res.*, *111*(2), 235-249.
- Song, C. K., Jackson, R. M., Harris, R. B., Richard, D., & Bartness, T. J. (2005). Melanocortin-4 receptor mRNA is expressed in sympathetic nervous system outflow neurons to white adipose tissue. *Am.J.Physiol Regul.Integr.Comp Physiol*, *289*(5), R1467-R1476.
- Song, C. K., Schwartz, G. J., & Bartness, T. J. (2009). Anterograde transneuronal viral tract tracing reveals central sensory circuits from white adipose tissue. *Am.J.Physiol Regul.Integr.Comp Physiol*, *296*(3), R501-R511.
- Song, C. K., Vaughan, C. H., Keen-Rhinehart, E., Harris, R. B., Richard, D., & Bartness, T. J. (2008). Melanocortin-4 receptor mRNA expressed in sympathetic outflow neurons to brown adipose tissue: Neuroanatomical and functional evidence. *Am.J.Physiol.*, *295*, R417-R428.
- Souza, S. C., Christoffolete, M. A., Ribeiro, M. O., Miyoshi, H., Strissel, K. J., Stancheva, Z. S., . . . Greenberg, A. S. (2007). Perilipin regulates the thermogenic actions of norepinephrine in brown adipose tissue. *J Lipid Res.*, *48*(6), 1273-1279.

- Stanford, K. I., Middelbeek, R. J., Townsend, K. L., An, D., Nygaard, E. B., Hitchcox, K. M., . . . Goodyear, L. J. (2013). Brown adipose tissue regulates glucose homeostasis and insulin sensitivity. *J.Clin.Invest*, *123*(1), 215-223.
- Strack, A. M., & Loewy, A. D. (1990). Pseudorabies virus: a highly specific transneuronal cell body marker in the sympathetic nervous system. *Journal of Neuroscience*, *10*(7), 2139-2147.
- Tandrup, T. (1995). Are the neurons in the dorsal root ganglion pseudounipolar? A comparison of the number of neurons and number of myelinated and unmyelinated fibres in the dorsal root. *J Comp Neurol*, *357*, 341-347.
- Tchkonia, T., Thomou, T., Zhu, Y., Karagiannides, I., Pothoulakis, C., Jensen, M. D., & Kirkland, J. L. (2013). Mechanisms and metabolic implications of regional differences among fat depots. *Cell Metab*, *17*(5), 644-656.
- Tharp, K. M., Jha, A. K., Kraiczy, J., Yesian, A., Karateev, G., Sinisi, R., . . . Stahl, A. (2015). Matrix-Assisted Transplantation of Functional Beige Adipose Tissue. *Diabetes*, *64*(11), 3713-3724.
- Tippins, J. R. (1986). CGRP: a novel neuropeptide from the calcitonin gene is the most potent vasodilator known. *J Hypertens Suppl*, *4*(5), S102-105.
- Umekawa, T., Yoshida, T., Sakane, N., & Kondo, M. (1997). Effect of CL316,243, a highly specific beta (3)-adrenoceptor agonist, on lipolysis of epididymal, mesenteric and subcutaneous adipocytes in rats. *Endocr.J.*, *44*, 181-185.
- van Marken, L. W. (2012). Brown adipose tissue and the regulation of nonshivering thermogenesis. *Curr.Opin.Clin.Nutr.Metab Care*, *15*(6), 547-552.

- Vaughan, C. H., & Bartness, T. J. (2012). Anterograde Transneuronal Viral Tract Tracing Reveals Central Sensory Circuits From Brown Fat and Sensory Denervation Alters Its Thermogenic Responses. *Am.J.Physiol*, 302, R1049--R1058.
- Vaughan, C. H., Shrestha, Y. B., & Bartness, T. J. (2011). Characterization of a novel melanocortin receptor-containing node in the SNS outflow circuitry to brown adipose tissue involved in thermogenesis. *Brain Res.*, 1411, 17-27.
- Vaughan, C. H., Zarebidaki, E., Ehlen, J. C., & Bartness, T. J. (2014). Analysis and measurement of the sympathetic and sensory innervation of white and brown adipose tissue. *Methods Enzymol.*, 537, 199-225.
- Vijgen, G. H., Bouvy, N. D., Teule, G. J., Brans, B., Hoeks, J., Schrauwen, P., & van Marken Lichtenbelt, W. D. (2012). Increase in brown adipose tissue activity after weight loss in morbidly obese subjects. *J.Clin.Endocrinol.Metab*, 97(7), E1229-E1233.
- W.H.O. (2014). *Global status report on noncommunicable diseases 2014*. Geneva, Switzerland: WHO Press.
- Williams, E. K., Chang, R. B., Storchlic, D. E., Umans, B. D., Lowell, B. B., & Liberles, S. D. (2016). Sensory Neurons that Detect Stretch and Nutrients in the Digestive System. *Cell*, 166(1), 209-221.
- Wu, J., Bostrom, P., Sparks, L. M., Ye, L., Choi, J. H., Giang, A. H., . . . Spiegelman, B. M. (2012). Beige adipocytes are a distinct type of thermogenic fat cell in mouse and human. *Cell*, 150(2), 366-376.
- Wu, J., Cohen, P., & Spiegelman, B. M. (2013). Adaptive thermogenesis in adipocytes: is beige the new brown? *Genes Dev.*, 27(3), 234-250.

- Xiong, X. Q., Chen, W. W., Han, Y., Zhou, Y. B., Zhang, F., Gao, X. Y., & Zhu, G. Q. (2012). Enhanced adipose afferent reflex contributes to sympathetic activation in diet-induced obesity hypertension. *Hypertension*, *60*(5), 1280-1286.
- Xiong, X. Q., Chen, W. W., & Zhu, G. Q. (2014). Adipose afferent reflex: sympathetic activation and obesity hypertension. *Acta Physiol (Oxf)*, *210*(3), 468-478.
- Yamada, T., Katagiri, H., Ishigaki, Y., Ogihara, T., Imai, J., Uno, K., . . . Oka, Y. (2006). Signals from intra-abdominal fat modulate insulin and leptin sensitivity through different mechanisms: neuronal involvement in food-intake regulation. *Cell Metab*, *3*(3), 223-229.
- Yamamoto, K., Senba, E., Matsunaga, T., & Tohyama, M. (1989). Calcitonin gene-related peptide containing sympathetic preganglionic and sensory neurons projecting to the superior cervical ganglion of the rat. *Brain Research*, *487*(1), 158-164.
- Youngstrom, T. G., & Bartness, T. J. (1995). Catecholaminergic innervation of white adipose tissue in the Siberian hamster. *Am.J.Physiol.*, *268*, R744-R751.
- Yuan, X., Hu, T., Zhao, H., Huang, Y., Ye, R., Lin, J., . . . Chen, Z. J. (2016). Brown adipose tissue transplantation ameliorates polycystic ovary syndrome. *Proc Natl Acad Sci U S A*, *113*(10), 2708-2713.
- Zhang, Y., Proenca, R., Maffei, M., Barone, M., Leopold, L., & Friedman, J. M. (1994). Positional cloning of the mouse obese gene and its human homologue. *Nature*, *372*(6505), 425-432.
- Zhao, J., Unelius, L., Bengtsson, T., Cannon, B., & Nedergaard, J. (1994). Coexisting beta-adrenoceptor subtypes: significance for thermogenic process in brown fat cells. *Am.J.Physiol*, *267*(4 Pt 1), C969-C979.

Zheng, H., Qiao, C., Wang, C. H., Li, J., Li, J., Yuan, Z., . . . Xiao, X. (2010). Efficient retrograde transport of adeno-associated virus type 8 to spinal cord and dorsal root ganglion after vector delivery in muscle. *Hum Gene Ther*, 21(1), 87-97.

Zurborg, S., Piszczek, A., Martinez, C., Hublitz, P., Al Banchaabouchi, M., Moreira, P., . . . Heppenstall, P. A. (2011). Generation and characterization of an Advillin-Cre driver mouse line. *Mol Pain*, 7, 66.